TECHNICAL NOTE

D-1091

FLIGHT-PATH CHARACTERISTICS FOR DECELERATING FROM SUPERCIRCULAR SPEED

By Roger W. Luidens

Lewis Research Center
Cleveland, Ohio

NATIONAL AERONAUTICS AND SPACE ADMINISTRATION
WASHINGTON

December 1961

NATIONAL AERONAUTICS AND SPACE ADMINISTRATION

TECHNICAL NOTE D-1091

FLIGHT-PATH CHARACTERISTICS FOR DECELERATING FROM SUPERCIRCULAR SPEED

By Roger W. Luidens

SUMMARY

Characteristics of the following six flight paths for decelerating from a supercircular speed are developed in closed form: constant angle of attack, constant net acceleration, constant altitude, constant free-stream Reynolds number, and "modulated roll." The vehicles were required to remain in or near the atmosphere, and to stay within the aerodynamic capabilities of a vehicle with a maximum lift-drag ratio of 1.0 and within a maximum net acceleration G of 10 g's. The local Reynolds number for all the flight paths for a vehicle with a gross weight of 10,000 pounds and a 60° swept wing was found to be about 0.7×10^{6}.

With the assumption of a laminar boundary layer, the heating of the vehicle is studied as a function of type of flight path, initial G load, and initial velocity. The following heating parameters were considered: the distribution of the heating rate over the vehicle, the distribution of the heat per square foot over the vehicle, and the total heat input to the vehicle. The constant G load path at limiting G was found to give the lowest total heat input for a given initial velocity. For a vehicle with a maximum lift-drag ratio of 1.0 and a flight path with a maximum G of 10 g's, entry velocities of twice circular appear thermodynamically feasible, and entries at velocities of 2.8 times circular are aerodynamically possible. The predominant heating (about 85 percent) occurs at the leading edge of the vehicle. The total ablated weight for a 10,000-pound-gross-weight vehicle decelerating from an initial velocity of twice circular velocity is estimated to be 5 percent of gross weight. Modifying the constant G load flight path by a constant-angle-of-attack segment through a flight- to circular-velocity ratio of 1.0 gives essentially a "point landing" capability but also results in an increased total heat input to the vehicle.

INTRODUCTION

Studies of interplanetary missions indicate that atmospheric braking can be markedly more efficient (in terms of weight requirements) than

propulsive braking (ref. 1). To apply atmospheric braking at the entry velocities associated with interplanetary trips, several problems must be studied. One of these is the question of whether the achievable aerodynamic entry corridors (e.g., refs. 2 and 3) are compatible with the corridor capability of the planet approach guidance system. A second problem is protecting the vehicle from the heat generated in decelerating from the entry velocity.

In terms of acceptable G loads, entry to Earth at velocities greater than circular appears feasible. The advent of ablation heat-protection systems, in contrast to radiation- and heat-sink systems, also makes possible the consideration of supercircular entry speeds from the thermodynamic point of view. To minimize the weight of the heat-protection system requires the use of "deceleration flight paths" that have inherently low total heat inputs. The deceleration flight path is defined as that segment of the total flight path in the atmosphere which is flown for the purpose of decelerating the vehicle from an initial velocity and altitude to a desired terminal condition. It is subsequent to the maneuver which determines the entry corridor. The velocity change during the entry maneuver may be small (ref. 3), so that to a first approximation the initial velocity for the deceleration flight is equal to the entry velocity.

A number of studies of the heat input and flight mechanics of deceleration flight paths have been made (refs. 4 to 7). The stagnation-point heat input per unit area nondimensionalized by functions of nose radius R_N, lift-drag ratio L/D, wing loading W/A, and drag coefficient C_D is the parameter usually presented. Items not considered in these studies which are dealt with in the present analyses are: (1) the interrelation among the parameters R_N, L/D, W/A, and C_D required by the vehicle geometry, (2) the heat input to the windward side of the vehicle, (3) the integration of the heat input per unit area over the vehicle area, and (4) the effect of differentiating between the vehicle maximum and operating lift-drag ratios. The parameter heat input per unit vehicle gross weight is used as a measure of the heat input to the vehicle. This parameter is closely related to the ablated weight as a fraction of the vehicle gross weight.

The present analysis yields closed-form results. The flight mechanical approximations made are less restrictive than the assumptions used to arrive at existing closed-form solutions. The characteristics of the following types of flight paths are derived: (1) constant angle of attack, (2) constant G load, (3) constant heat rate, (4) constant altitude, (5) constant free-stream Reynolds number, and (6) "modulated roll." The following constraints are imposed: that the vehicle (1) remain in or near the atmosphere, (2) stay within its aerodynamic capabilities, and (3) stay within the G load capabilities of the payload and

structure. A Reynolds number constraint is also discussed. The total heat input to the vehicle and the G load history are discussed as a function of the type of flight path, initial velocity, and the initial G load. Finally, a method of controlling landing location is discussed.

ANALYSIS

The general objective of this analysis is to develop closed-form solutions for the characteristics of the deceleration flight path.

Equations of Motion

The equations of motion including gravitation and aerodynamic forces in the directions tangent and normal to the flight path may be written in the nomenclature of figure 1 as

$$\frac{1}{g}\frac{dV}{d\tau} = \frac{-C_D\rho\bar{V}^2Ar}{2m} - \sin\varphi = \frac{-C_D\rho\bar{V}^2Agr}{2W} - \sin\varphi \qquad (1)$$

$$\frac{V}{g}\frac{d\varphi}{d\tau} = \frac{C_L\rho\bar{V}^2Ar}{2m} + (\bar{V}^2 - 1)\cos\varphi = \frac{C_L\rho\bar{V}^2Agr}{2W} + (\bar{V}^2 - 1)\cos\varphi \qquad (2)$$

The symbols are defined in appendix A.

The following assumptions are made: (1) that the flight-path angle relative to the local horizontal is always small, so that $\cos\varphi$ is approximately unity and $\sin\varphi$ is approximately φ, and (2) that $\sin\varphi$ is small compared with the nondimensional term representing the aerodynamic forces in equation (1).

Equations (1) and (2) then reduce to

$$\frac{1}{g}\frac{dV}{d\tau} = -G\frac{C_D}{C_R} \qquad (3)$$

$$\frac{V}{g}\frac{d\varphi}{d\tau} = G\frac{C_L}{C_R} + \bar{V}^2 - 1 \qquad (4a)$$

where G is defined as

$$G \equiv \frac{C_R\rho\bar{V}^2Ar}{2m} \equiv \frac{C_R\rho\bar{V}^2Agr}{2W} \qquad (5)$$

G represents the net force on the vehicle in terms of the planet g's, or is the net acceleration vector felt by the pilot in planet g's.

For future reference, equation (4a), with the aid of equation (5) and the definition of C_L (appendix A), may also be written as

$$\frac{L}{mg} \equiv \frac{L}{W} = 1 - \overline{V}^2 + \frac{V}{g}\frac{d\varphi}{d\tau} \tag{4b}$$

$$\rho\overline{V}^2 = \frac{2m\left(1 - \overline{V}^2 + \frac{V}{g}\frac{d\varphi}{d\tau}\right)}{C_L Ar} = \frac{2W\left(1 - \overline{V}^2 + \frac{V}{g}\frac{d\varphi}{d\tau}\right)}{C_L Agr} \tag{4c}$$

Also from figure 1, the component of lift in the vertical direction is related to the total aerodynamic lift $C_{L,a}$ and the roll angle θ by

$$C_L = C_{L,a} \cos\theta \tag{6}$$

Vehicle Aerodynamics

The vehicle aerodynamics (fig. 2) are calculated using the equations and assumptions given in appendix B. The vehicle design is specified by, or characterized by, its maximum lift-drag ratio $(L/D)_{max}$. In general, for a given lift coefficient these curves have double values of C_D, C_R, and α. In the present study the low range of angle of attack is used.

Flight Paths

Many possible flight paths can be considered; the present report considers six particular flight paths and a generalized flight path. The flight paths are defined as follows:

(1) Constant α: $\theta = 0$; C_R, C_D/C_R, and C_L/C_R are constant (see fig. 2).

(2) Constant h: $\theta = 0$; ρ is constant.

(3) Constant G: $\theta = 0$; $C_R\rho\overline{V}^2$ is constant (see eq. (5)).

(4) Constant Re: $\theta = 0$; $\rho\overline{V}$ is constant (see eq. (17)).

(5) Constant $\dot{q}$: $\theta = 0$; $\rho^{1/2}\overline{V}^3$ is constant (see eq. (10)).

(6) Modulated roll: θ is varied from 0° to 90° (or 180°) in a manner to satisfy equations (4) and (6); the vehicle angle of attack is defined to be constant, and hence C_R, C_D/C_R, and $C_{L,a}/C_R$ are constant.

Heat Transfer

The heat transfer for the present analysis is estimated assuming a laminar boundary layer. References 8 and 9 present a comprehensive review of heat-transfer theories. These have been found adequate up to Earth circular speeds and are assumed herein to be applicable also at supercircular speeds.

Reference 10 gives the following form for stagnation-point heat transfer:

$$\dot{q}_s = \frac{15.5\times10^{-9}\times2^{j/2}\rho^{1/2}V^3}{R_N^{1/2}}\left[1 - \frac{h_w}{h_{se}}\right] \tag{7a}$$

where $j = 0$ for the two-dimensional leading edge considered in the present analysis ($j = 1$ for a three-dimensional or spherical leading edge). For entry from high velocities $\frac{h_w}{h_{se}} \ll 1.0$ and with equation (7a) in a form using $\bar{V}$,

$$\dot{q}_s = 15.5\times10^{-9}\,\frac{\rho^{1/2}\bar{V}^3}{R_N^{1/2}}\,(gr)^{3/2} \tag{7b}$$

This equation may be modified to include the effect of sweep and nose radius angle by the relation suggested in reference 8 (pp. 19 and 22):

$$\frac{\dot{q}_l}{\dot{q}_s} = \cos^{\nu}\Lambda_c \cos\lambda = \left[1 - \sin^2\Lambda\cos^2\alpha\right]^{\nu/2}\cos\lambda \tag{8}$$

Combining equations (7) and (8) gives

$$\dot{q}_l = 15.5\times10^{-9}(gr)^{3/2}\,\frac{\rho^{1/2}\bar{V}^3}{R_N^{1/2}}\cos^{\nu}\Lambda_c\cos\lambda \tag{9}$$

The theory and experiments of reference 11 indicate that, for the high velocities of the present study, ν has a value of 1.5 for sweep angles from 0° to 60° and becomes less than 1.5 for sweeps greater than 60°.

(The theory and experiment of ref. 12 indicate that the value of ν may be as low as unity.)

The symbols defining the vehicle geometry and various flow components are illustrated in figure 3. In calculating the heating rates and total heat inputs, a family of vehicles was considered which are delta-wing configurations having a wing sweepback angle Λ, a constant thickness d, and a constant nose radius R_N. The configurations have no separate fuselage, and the volume in the wing is considered the usable volume.

The following analogously simple equation for the heat transfer to the windward side of the vehicle is developed in appendix C:

$$\dot{q}_w = 15.0\times10^{-9} k_c g r \sqrt{\frac{|L|}{Ax|\cos\theta|}}\,\bar{V}^2 = 10.2\, k_c \sqrt{\frac{|L|}{Ax|\cos\theta|}}\,\bar{V}^2 \qquad (10)$$

This result is independent of angle of attack between about 3° and 30° for a constant roll angle θ.

General Form of Equations for Flight-Path Characteristics

In addition to those characteristics involved directly with the equations of motion there are other flight-path characteristics of interest and these are given in general form here.

Altitude. - With the assumption of an exponential atmosphere, the flight-path altitude may be calculated if the flight-path density is known:

$$h = -\frac{1}{\beta} \ln \frac{\rho}{\rho_{SL}} \qquad (11)$$

For Earth the values $\beta^{-1} = 2.35\times10^4$ feet and $\rho_{SL} = 0.0027$ (slug)(ft^{-3}) are used as suggested in reference 4. Also for later use it is noted that

$$\frac{dh}{d\rho} = -\frac{1}{\beta\rho} \qquad (12)$$

Radiation equilibrium temperature. - With the flight path and vehicle design known, equations (9) and (10) give the heating rate per square foot $\dot{q}$. In some applications the radiation equilibrium temperature, determined by the heat rate, is of interest; it is given by

$$t_{\bar{w}} = \left(\frac{\dot{q}}{\sigma\epsilon}\right)^{1/4} \qquad (13)$$

Free-stream Reynolds number. - With the flight-path density ρ known as a function of $\bar{V}$ and the vehicle characteristic length, the free-stream Reynolds number may be calculated from

$$Re = \frac{\rho \bar{V} x}{\mu} \sqrt{gr} \tag{14}$$

By use of equation (5), equation (14) may alternatively be written as

$$Re = \frac{2G(W/A)x}{\mu \sqrt{gr}\, \bar{V} C_R} \tag{15}$$

The free-stream viscosity is assumed constant and independent of altitude for the present analysis, $\mu = 0.37 \times 10^{-6}$ slugs per foot-second, and x is taken as f plus the root chord c (see fig. 3).

Local Reynolds number. - Local Reynolds number is related to the free-stream Reynolds number by a function of the free-stream Mach number, the wing-sweep angle, and the angle of attack. The method of calculation of the ratio of local to free-stream Reynolds number Re_l/Re is given in appendix D and assumes $\gamma = 1.2$. The local Reynolds number is then

$$Re_l = Re\left(\frac{Re_l}{Re}\right) \tag{16}$$

The value of Re_l/Re depends on the value selected for γ, and more generally on the real gas properties. A more precise determination of the local Reynolds number than that of appendix D is of little value at present, because the transition Reynolds number is not accurately known.

Flight-path angle. - As mentioned previously, it is assumed that the flight-path angles are small, and hence

$$\sin \varphi \sim \varphi \sim \frac{V_v}{\bar{V}} \tag{17}$$

But

$$V_v = \frac{dh}{d\tau} = \frac{dh}{d\rho} \frac{d\rho}{d\bar{V}} \frac{d\bar{V}}{d\tau} \tag{18}$$

and by use of equations (3), (5), and (12)

$$\varphi = \frac{C_D g \bar{V}}{2\beta \frac{W}{A}} \frac{d\rho}{d\bar{V}} \tag{19}$$

The preceding characteristics are point functions along the flight path. The succeeding characteristics result from an integration along the flight path.

Time of flight. - The time of flight is obtained by integrating the time increment from equation (3) as follows:

$$\tau = \int_{\tau_1}^{\tau_2} d\tau = \frac{1}{g} \int_{V_2}^{V_1} \frac{dV}{G \frac{C_D}{C_R}} = \sqrt{\frac{r}{g}} \int_{\bar{V}_2}^{\bar{V}_1} \frac{d\bar{V}}{G \frac{C_D}{C_R}} \tag{20}$$

Range. - Using equation (3) for $d\tau$ and approximating $\cos \varphi$ by unity give the range traversed during the deceleration:

$$R = \int_{\tau_1}^{\tau_2} V \cos \varphi \, d\tau \approx r \int_{\bar{V}_2}^{\bar{V}_1} \frac{\bar{V} \, d\bar{V}}{G \frac{C_D}{C_R}} \tag{21}$$

Total heat input. - One of the important criteria of merit for a heat-protection system is its weight as a fraction of the vehicle gross weight. If, for example, the heat-protection system is of the ablation type and has a characteristic heat-absorbing capacity C in Btu per pound, then the ablated weight may be expressed as

$$\frac{W_p}{W} = \frac{1}{C} \frac{Q}{W} \tag{22}$$

The present analysis deals with the parameter Q/W which results from a double integration (along the flight path and over the vehicle). The integration along the flight path yields the total heat input per square foot, which is given by

$$q = \int_{\tau_1}^{\tau_2} \dot{q} \, d\tau = \sqrt{\frac{r}{g}} \int_{\bar{V}_2}^{\bar{V}_1} \frac{\dot{q} \, d\bar{V}}{G \frac{C_D}{C_R}} \tag{23}$$

where $\dot{q}$ is given by equations (9) and (10) and $d\tau$ is again given by equation (3).

The integration over the vehicle has the general form

$$\frac{Q}{W} = \frac{1}{W}\int_A q\, dA = \frac{1}{W}\iint_{A_w} q_w\, d\xi\, d\eta + \frac{1}{W}\iint_{A_l} q_l R_N\, d\lambda\, dl \qquad (24)$$

This integration is discussed in detail in appendix E.

Sample Development of Flight-Path Characteristics for a Constant Reynolds Number Path

The case of "constant free-stream Reynolds number" is considered here in detail. The velocity ratio $\bar{V}$ is taken as the independent variable. The free-stream Reynolds number is given by equation (14) or (15), if the vehicle is specified (i.e., f+c and W/A are constant and given). Then for Re to be constant, $\rho\bar{V}$ must be constant. Since G (eq. (5)) and all the terms collected on the left side of the equation

$$\frac{\rho\bar{V}A_{gr}}{2W} = \left\{\frac{G}{C_R\bar{V}}\right\} \qquad (25)$$

are defined as constants, the right side must also be a constant. This is the relation given in column 2 of table I. The first column identifies the type of flight path. The term in braces is a constant for the flight path and is specified if the path Reynolds number is specified.

Equation (25) may then be solved for ρ as a function of $\bar{V}$ to give column 3 in table I:

$$\rho = 2\,\frac{W}{A}\,\frac{1}{g_r}\left\{\frac{G}{C_R\bar{V}}\right\}\frac{1}{\bar{V}} \qquad (26)$$

Because $\{G/C_R\bar{V}\}$ is a constant along the flight path,

$$G = \left\{\frac{G}{C_R\bar{V}}\right\}C_R\bar{V} \qquad (27)$$

which is the result given in column 4. To determine the flight-path angle φ, the derivative $d\rho/d\bar{V}$ is required in equation (19). This may be obtained from equation (26):

$$\frac{d\rho}{d\bar{V}} = -2\,\frac{W}{A}\,\frac{1}{gr}\left\{\frac{G}{C_R\bar{V}}\right\}\frac{1}{\bar{V}^2} \tag{28}$$

Combining equations (19) and (28) leads to the result in column 5:

$$\varphi = -\frac{C_D}{\beta r}\left\{\frac{G}{C_R\bar{V}}\right\}\frac{1}{\bar{V}} \tag{29}$$

With φ having been determined, the term $\frac{V}{g}\frac{d\varphi}{d\tau}$ can be discussed. From equation (29)

$$\frac{V}{g}\frac{d\varphi}{d\tau} = \frac{C_D}{\beta r}\left\{\frac{G}{C_R\bar{V}}\right\}\frac{1}{\bar{V}}\,\frac{1}{g}\frac{dV}{d\tau} \tag{30}$$

where the term $\frac{1}{g}\frac{dV}{d\tau}$ is given by equation (3), and G in that equation is given by equation (27) (or column 4). With these substitutions equation (30) becomes

$$\frac{V}{g}\frac{d\varphi}{d\tau} = -\frac{1}{\beta r}\left\{\frac{G}{C_R\bar{V}}\right\}^2\left(\frac{C_D}{C_R}\right)^2 C_R^2 \equiv -k_{Re} \tag{31}$$

The term $\frac{V}{g}\frac{d\varphi}{d\tau}$ (column 6) is equal to $-k_{Re}$ (column 19). For C_D/C_R and C_R constant, an assumption required later, k_{Re} is constant.

Equation (4a) may now be solved for the lift coefficient, using the result of equation (31) and equation (27) for G, to arrive at the result in column 7:

$$C_L = \frac{1 - \bar{V}^2 - k_{Re}}{\left\{\frac{G}{C_R\bar{V}}\right\}\bar{V}} \tag{32}$$

The free-stream Reynolds number (column 8) is given by equation (14) and is a constant for this case. More generally it may be obtained from the relations of ρ to $\bar{V}$ like equation (26) or column 3 of table I.

Obtaining the local Reynolds number (column 9) requires knowledge of the wing sweep angle and the angle of attack. The wing sweep is part of the vehicle design specification. The angle of attack is determined by figure 2 using C_L from equation (32) and the vehicle $(L/D)_{max}$.

The heating rate to the leading edge $\dot{q}_l$ (eq. (9)) now depends only on the parameter ρ, which has been determined, and on the independent variable $\bar{V}$. This result is shown in column 10. The heating rate to the windward side $\dot{q}_w$ (eq. (10)) depends on L/A, which may be determined from equation (4b) and the result of equation (31) or column 6 as follows:

$$\frac{L}{A} = \frac{W}{A}\left(1 - \bar{V}^2 - k_{Re}\right) \tag{33}$$

Making this substitution in equation (10) gives the result listed in column 11 of table I.

The point functions have now all been determined, and it remains to determine the integrated functions. The time of flight may be obtained from equation (20) and the equation for G from column 4 (or eq. (27)), where the term in braces is a constant, so that

$$\tau = \sqrt{\frac{r}{g}}\,\frac{1}{\left\{\dfrac{G}{C_R\bar{V}}\right\}}\int_{\bar{V}_2}^{\bar{V}_1}\frac{1}{\dfrac{C_D}{C_R}\,C_R}\,\frac{d\bar{V}}{\bar{V}} \tag{34}$$

The variation of C_D/C_R and C_R (or just C_D) as a function of $\bar{V}$ required in equation (34) can be obtained from the curves of figure 2 and equation (32) for C_L. Hence, equation (34) can be integrated graphically or by numerical methods for the most general cases. The present report, however, deals only with the more simple cases where C_D/C_R and C_R can be approximated by constant values and closed-form solutions can be thus obtained. This assumption is different from the assumptions for the case of constant α for which C_L/C_R in addition to C_D/C_R and C_R is constant. With the assumptions of C_D/C_R and C_R constant,

which are noted in column 12, equation (34) becomes

$$\tau = \sqrt{\frac{r}{g}} \frac{1}{\left\{\frac{G}{C_R \bar{V}}\right\} \frac{C_D}{C_R} C_R} \int_{\bar{V}_2}^{\bar{V}_1} \frac{d\bar{V}}{\bar{V}} \tag{35}$$

which integrates to the result in column 13.

By similar substitutions and assumptions, equation (21) for this range becomes

$$R = \frac{r}{\left\{\frac{G}{C_R \bar{V}}\right\} \frac{C_D}{C_R} C_R} \int_{\bar{V}_2}^{\bar{V}_1} d\bar{V} \tag{36}$$

which integrates to the result in column 14.

Again with the similar substitutions and approximations, and by use of the result in column 10 or equation (9) for $\dot{q}_l$, equation (23) for q_l becomes

$$q_l = 14.9 \cos^{\nu}\Lambda_c \cos\lambda \sqrt{\frac{r}{g}} \sqrt{\frac{W}{R_N A}} \frac{1}{\sqrt{\left\{\frac{G}{C_R \bar{V}}\right\}}} \frac{1}{\frac{C_D}{C_R} C_R} \int_{\bar{V}_2}^{\bar{V}_1} \bar{V}^{1.5} \, d\bar{V} \tag{37}$$

which integrates to the result in column 15.

When column 11 or equation (10) with $\theta = 0$ is used for $\dot{q}_w$ in equation (23), the integral equation becomes

$$q_w = 10.2 \, k_c \sqrt{\frac{r}{g}} \sqrt{\frac{W}{Ax}} \frac{1}{\left\{\frac{G}{C_R \bar{V}}\right\}} \frac{1}{\frac{C_D}{C_R} C_R} \int_{\bar{V}_2}^{\bar{V}_1} \sqrt{|1 - \bar{V}^2 - k_{Re}|} \, \bar{V} \, d\bar{V} \tag{38}$$

which integrates to the result in column 16.

The integration over the vehicle to obtain Q/W indicated by equation (24) is carried out in detail in appendix E and gives the results shown in columns 17 and 18. Alternative forms for the denominator of columns 17 to 18 are shown in the bottom row.

The results for all the other flight paths except constant α can be derived in a similar manner. The case of constant angle of attack is discussed in appendix F.

RESULTS AND DISCUSSION

The results of the analysis for all the flight paths studied are summarized in tables I and II.

Tables of Equations

The first column of table I gives the name of the flight path. The term in braces in the second and subsequent columns is constant over the flight path. The equations with the exception of those in columns 10, 11, and 15 to 18 apply to any planet. The results in the aforementioned columns are given in table II in a form which is applicable to any planet that has an atmosphere with heat-transfer characteristics similar to Earth. The equations for G are in terms of planet g's, and $\overline{V}$ is the flight velocity divided by the planet circular velocity.

Three heating parameters are presented:

(1) Heating rate $\dot{q}$ (in Btu/(sq ft)(sec)). This is the parameter of interest, for example, for radiation cooling.

(2) Heat input per square foot of vehicle q, which depends on the location with respect to the stagnation point of the area being considered. (The stagnation point is not a fixed geometric point except for the cases of constant α and modulated roll.) The parameter q results from the integration over the flight path of the heat input to a given location.

(3) Heat input $Q = (Q_l + Q_w)$, which is related to the ablated weight and involves an integration over the vehicle surface as well as over the flight path.

The heating parameters are presented for two regions on the airplane: (1) the region in the vicinity of the leading edge or stagnation point, where the heating is a function of nose radius R_N, nose radius coordinate angle λ, and sweep angle Λ, and (2) the windward side of the vehicle, where the heat input is a function of the distance x from the stagnation point. The heat input to base and lee regions is not considered.

The term k_ζ (column 17) accounts for the reduction with angle of attack of both the effective sweepback angle and the area of the leading edge subject to heating. The value of k_ζ is approximately unity. The term k_c (columns 11, 16, and 18) accounts for the relative lift generated by the windward side and the leading edge. The term k_w accounts for the length of boundary layer ahead of the windward side. The term k with a subscript to designate the flight path (e.g., k_{Re}) accounts for the amount that the flight-path curvature differs from the planet surface curvature. Both k_c and k_w approach unity for slender (or high $(L/D)_{max}$) configurations and have a value of about 0.5 for the $(L/D)_{max} = 1.0$ configuration of this report.

In table I the heading "Modulated angle of attack" indicates the flight paths for which the lift vector is constrained to the vertical direction. For all but the constant α case, the assumption of constant C_D/C_R restricts the angle of attack to the vicinity of 0° or 90°, as may be seen from figure 2. The present results are for α near 0°.

"Modulated roll" in table I designates a specific case where angle of attack with respect to the free-stream direction is constant (hence, C_R, C_D/C_R, and $C_{L,a}/C_R$ are constant) and the variation of the roll angle θ with $\bar{V}$ is given by the equation in column 1. This relation between θ and $\bar{V}$ gives a constant G and $\theta = 0$ at $\bar{V}_1$.

Comparison with Other Analyses

To obtain closed-form solutions, a number of simplifying assumptions have been made. As an indication of the accuracy of the present analysis in the stagnation region, a comparison is made for the constant-angle-of-attack path with the results from machine integrations of the equations of motion and heating presented in reference 4. The procedure for reducing the results of the present report to the form of reference 4 is given in appendix G. Figure 4 presents the horizontal component of the G load G_H and the heating-rate parameter $\dot{q}$ as a function of velocity ratio $\bar{V}$ for an L/D of 0.1 and 1.0 and an initial velocity ratio $\bar{V}$ of 0.99. The heat-input parameter $\bar{q}$ for decelerating from $\bar{V} = 0.99$ to $\bar{V} = 0$ is given as a function of L/D. In the calculation of $\bar{q}$, the function F of table I was evaluated at the maximum value of $\bar{V}$. The present analysis generally gives the greater heat input. In all cases the agreement between the two analyses is considered satisfactory.

To indicate the accuracy of the present analysis in estimating the heat input to the windward side of the vehicle, a comparison is made with the results of reference 13 for the constant-angle-of-attack path. The results of reference 13 have been extrapolated to the condition of zero wall temperature and apply for the case of $F = 1$ in table I. Figure 5 compares the heating-rate parameter $\dot{q}(x/(W/A))^{1/2}$ and the heat input per unit span parameter $\dfrac{\int_0^{c'} q\,dx}{\frac{L}{D}\left(\frac{c'W}{A}\right)^{1/2}}$ as a function of velocity ratio $\overline{V}$ for an initial velocity $\overline{V}$ of 1.0. Also shown is the variation of heating rate with angle of attack for constant lift. In general, the agreement between the two analyses is satisfactory. Compared with reference 13, the present analysis indicates increasingly higher heat inputs with increasing angle of attack. The maximum angle of attack to which the present analysis is applicable depends on the degree of approximation considered acceptable. The present analysis is about 15 percent higher at $\alpha = 30^{\circ}$.

In general, the accuracy of the present analysis is adequate for preliminary studies.

Some General Considerations

For atmospheric braking it is desired to determine a combination of vehicle geometry and flight path which will result in a low heat input to the vehicle. Generally there is a substantial increase in convective heat input to the vehicle if the boundary layer on the vehicle is turbulent rather than laminar. Thus it is desirable to restrict the flight path to conditions for which laminar boundary layer can be maintained. An indication of the possible nature of the boundary layer is given by the magnitude of the Reynolds number. Two Reynolds numbers can be considered, the free-stream value, and a local value at the edge of the boundary layer. The free-stream Reynolds number depends on the vehicle design parameters W/A and c and on the flight-path parameter G (see eq. (17) or (18)). The local Reynolds number is further influenced by the vehicle design factors of leading-edge bluntness and sweep and the operating parameter of angle of attack. Both local and free-stream Reynolds number are presented in the section Point Functions.

The local Reynolds number is interrelated with the problem of hot-gas radiation. At entry velocity ratios $\overline{V}$ greater than 1.0, the heat input from hot-gas radiation can equal or become larger than the convective heat input to an unswept stagnation region. The lowest heat input to the vehicle will usually exist if hot-gas radiation is avoided

where possible. This requires that the vehicle surface angles be small with respect to the free-stream direction to avoid high air static temperatures. In general, unsweeping the wing leading edge decreases the local Reynolds number but tends to aggravate the problem of hot-gas radiation. The choice of wing sweep angle is, therefore, a compromise. The calculations for the present study were made for a sweep angle of 60°. Also to avoid hot-gas radiation the low-angle-of-attack rather than high-angle-of-attack region of aerodynamic operation was chosen. The choice of the low-angle-of-attack range and the 60° sweep is assumed to reduce the heat input from hot-gas radiation to a low value compared with the convective heat input. Only the convective heat input is considered subsequently in this report.

Point Functions

The evaluation of the various flight paths for decelerating in the Earth atmosphere is discussed with the aid of figures 6 to 11 in which is plotted the variation of the point functions of table I with $\overline{V}$. A second abscissa shows elapsed time in minutes with time equal to zero at $\overline{V} = 2.0$. To arrive at numerical results, a vehicle design defined by $\rho_f = 20$ pounds per cubic foot, $W = 10{,}000$ pounds, $\Lambda = 60^\circ$, and $(L/D)_{max} = 1.0$ was assumed. (Higher values of $(L/D)_{max}$ result in larger heat inputs.) For a vehicle like that of figure 3 and the above numerical values, the following vehicle characteristics may be determined by the equations given in appendix E: $W/A = 83$ pounds per square foot, $R_N = 2.06$ feet, and $c = 14.5$ feet. A length of 18.8 feet was used in the calculation of the Reynolds numbers. Vehicle operation is in the low-angle-of-attack range, and the assumptions are made that $C_D = C_{D,o}$ and $C_D/C_R = 1.0$, although for some cases more precise approaches to the calculation of the point functions are possible. All the flight paths have a common point, at $\overline{V} = 2.0$, $G = 10$ g's, and $\theta = 0.^\circ$ This results in approximately the same values of α and h, about 5.3° and 162,000 feet, respectively. When appropriate, the following physical limits are noted on the curves: $|C_{L,max}| = 0.9$, $G_{max} = 10$ g's, $h_{min} = 0$, and $\dot{q} = 190$ Btu/(ft^{-2})(sec), or $t_{\overline{w}} = 4460^\circ$ R for an emissivity of unity.

Flight-path angle. - The fact that for all cases the flight-path angle φ is small except in the vicinity of $\overline{V} = 0$ justifies the assumption of small angles. For all cases except constant α (fig. 6), φ is also continuous. For the constant α case, φ changes discontinuously from plus to minus near $\overline{V} = 1.0$ and the altitude becomes indefinite. This situation is physically approached by a shallow skip out of the atmosphere at $\overline{V} = 1.0$. In spite of this indefiniteness in the altitude, the heat input to the vehicle remains finite as is shown later (see also columns 17 and 18 of table I).

Altitude and lift coefficients. - For all cases except constant h (fig. 7) the altitude becomes less than zero for $\bar{V}$ approaching zero. On the constant h path excessive lift-coefficient requirements are encountered at $\bar{V}$'s approaching zero. The constant Re path (fig. 8) also requires excessive lift coefficients at low $\bar{V}$'s. In a practical flight these and other low-speed anomalies are usually precluded by specifying some terminal condition of velocity, lift coefficient, or altitude. The actual flight path may deviate from the specified path in the low-speed range with little effect on the total heat input calculated from an initially supercircular velocity, as is shown later.

The lift coefficient is negative; that is, lift force is directed toward the Earth for flight velocities greater than circular. This occurs fundamentally because the centrifugal force tending to "throw" the vehicle out of the atmosphere is greater than the gravity force and the difference in these forces must be counteracted by the lift. For all cases except constant G (fig. 9), constant $\dot{q}$ (fig. 10), and modulated roll (fig. 11), the lift coefficient is positive (directed away from the Earth) for subcircular velocities, because at subcircular speed the centrifugal force is less than the gravity force. However, to satisfy the assigned values of $\dot{q}$ and G for the cases of constant $\dot{q}$, constant G, and modulated roll, negative lift coefficients are required at subcircular speeds as well as at supercircular speeds (because of the term $(V/g)(d\varphi/dt)$ in eq. (4)).

G load. - For the constant G path (G = 10 g's), the abscissa of figure 9 shows that the time of deceleration in the region of strong heating, that is, from $\bar{V} = 2.0$ to $\bar{V} \sim 0.5$, is about 2 minutes. This combination of g's and time is about the presently accepted limit of human tolerance if useful functions are to be performed by the man. For this reason $G_{max} = 10$ g's was used in the present examples.

For all cases except constant $\dot{q}$ (fig. 10) the G load is at or below the initial G value at $\bar{V} = 2.0$. For the case of constant $\dot{q}$ the G increases with decreasing $\bar{V}$ to maintain $\dot{q}$ constant. At a $\bar{V}$ higher than 2 the C_L becomes excessive. These same characteristics exist if other values of constant $\dot{q}$ are specified. Thus it is concluded that the constant $\dot{q}$ path does not have application over a wide range of $\bar{V}$.

Angle of attack. - The angle of attack is shown as positive. For the flight paths where the lift coefficient varies from minus to plus along the flight path, one has the choice of permitting the sign of the angle of attack to change or of rolling the vehicle 180°. In the latter instance the same side of the vehicle remains the windward side. The vehicle angle of attack is for all cases equal to or less than the angle of attack at $\bar{V} = 2.0$, where α is about 5.3° (except for the very low $\bar{V}$'s). From figure 2 it can be seen that C_D, C_D/C_R, and C_R vary less

than ±5 percent from a mean value over the angle of attack range 0° to 5.3°. More generally, for G_i = 10 g's and $(C_L/C_R)_i = (1 - \overline{V}^2)/G_i$ (eq. (4a) with $\frac{d\varphi}{dt} = 0$), C_D, for example, varies less than ±7 percent from a mean value up to $\overline{V}_i = 2.25$ for $(L/D)_{max} = 1$ and 2, the values of $(L/D)_{max}$ examined. An increase in G_i will increase $\overline{V}_i$, for which the variation of the coefficients is small. Hence, for many problems of interest it is a good approximation to use constant values for C_D, C_D/C_R, and C_R as is required to arrive at some of the integrated functions.

Free-stream Reynolds number. - The free-stream Reynolds number Re is also shown in figures 6 to 11. The case of constant h shows a linearly decreasing Reynolds number with decreasing $\overline{V}$. The case of constant G for G = 10 g's shows increasing Reynolds number with decreasing $\overline{V}$ and values much larger than for the other cases in the lower $\overline{V}$ range. The various flight paths illustrated thus offer a choice of increasing, constant, or decreasing Reynolds number with decreasing $\overline{V}$.

Local Reynolds number. - The transition from laminar to turbulent flow in the boundary layer is more significantly related to the local Reynolds number than to the free-stream Reynolds number. The variation of the local Reynolds number Re_l with $\overline{V}$ is shown for the condition that the wing leading edge is blunt and swept 60°. All the flight paths except modulated roll (fig. 11) show a dip in Re_l in the vicinity of $\overline{V} = 1$ followed by a rise in Re_l for $\overline{V} < 1.0$. For the flight paths of constant G and constant Re, this dip is associated with a lower angle of attack in the vicinity of $\overline{V} = 1.0$. For the constant α case it is associated with a low air density (see fig. 6). In the vicinity of $\overline{V} = 1.0$, the local Reynolds number for both the constant α ($\alpha \sim 5.3°$) and constant G (G = 10) cases is substantially lower than for the modulated roll case (G = 10 g's and $\alpha = 5.3°$). This illustrates a disadvantage of using modulated roll. The high local Reynolds number for modulated roll is associated with the combination of the high air density and the 5.3° angle of attack at $\overline{V} = 1.0$. The effect of angle of attack on the ratio Re_l/Re is discussed in appendix D. In general, for the flight paths considered, it appears less difficult to achieve low local Reynolds number at supercircular than at subcircular speeds.

The constant α, constant h, constant Re, and constant G flight paths show rather small variation in Re_l with $\overline{V}$ and little variation among the several flight paths over the speed range from $\overline{V} = 3.0$ to 0.8. In this speed range the general level of the local Reynolds number, 0.7×10^6, suggests an extensive run of laminar boundary layer on the vehicle is possible.

Heating rate. - The values of the heating rate $\dot{q}$ shown are for a vehicle density $\rho_f = 20$ (lb)(ft^{-3}) and apply to the swept leading edge ($\Lambda = 60^\circ$) (note that, in column 10 of table I, $W/R_N A = 2\rho_f$). For all cases except constant $\dot{q}$, values of $\dot{q}$ increase with increasing $\overline{V}$. The temperature limits of presently known materials (e.g., ceramics) are about 4460° R. By equation (16) this corresponds to $\dot{q} = 190$ (Btu)(ft^{-2})(sec^{-1}). For this value the best case, constant α, shows that entry velocity ratios $\overline{V}$ up to 1.3 may be possible with radiation cooling, for the present vehicle and flight path. (The flight path and vehicle design shown do not yield the lowest possible radiation temperatures.) For entry velocity ratios greater than approximately 1.4 radiation cooling is probably not possible, and hence there is interest in the total heat input to the vehicle.

Maximum entry velocity. - From equation 4(a) for $G_1 = 10$ g's and the maximum values of C_L/C_R shown in figure 2, it can be determined that entry velocities of 2.8 times circular are aerodynamically possible with a vehicle with an $(L/D)_{max}$ of 1.0. Still higher entry velocities are possible with a vehicle with a higher $(L/D)_{max}$.

Summary of point functions. - The more important conclusions from the discussion of the point functions may be summarized as follows:

(1) All the flight paths considered except constant $\dot{q}$ are or approximate physically possible flight paths.

(2) For $G_1 = 10$ g's and $(L/D)_{max} = 1.0$ or 2.0 the assumption of C_R, C_D, and C_D/C_R constant is a valid approximation up to an entry velocity ratio $\overline{V}$ of about 2.25.

(3) With the vehicle designs and flight paths assumed, radiation cooling appears impossible for entries at supercircular speeds corresponding to $\overline{V} > 1.4$. Hence, the total heat input into the vehicle is important.

(4) The local Reynolds number for many of the flight paths of interest is about 0.7×10^6. This value suggests the possibility of a laminar boundary layer.

Total Heat Input

For the assumptions of laminar boundary layer and hot-gas radiation negligible because of low vehicle surface angles and with heat input to base and lee regions neglected, the total heat input to the vehicle is

given by the sum of columns 17 and 18 of table I or II. The total heat input depends on many factors, and these may be categorized as follows:

(1) Factors that depend on the flight plan: terms in braces or in column 2 that define the variation of G with $\overline{V}$ and the terms in brackets in columns 15 and 16 that depend on the initial and final velocity of the deceleration flight path.

(2) Factors that depend on the vehicle design: vehicle density, ρ_f; gross weight, W; wing loading, W/A; and wing sweep angle, Λ.

(3) Factors that depend on both vehicle design and flight plan: C_L and L/D or C_D/C_R and C_R. These depend on design through the configuration maximum lift-drag ratio and on the flight plan through the operating lift-drag ratio or angle of attack.

The heat input along families of flight plans related in two ways to the curves of figures 6 to 11 will be considered. For the first family the flight plans start at various points along the curves of figures 6 to 11 and the flight path then follows these curves. The second family is defined by the condition that, at the initial velocity V_i, the initial G load G_i is 10 g's.

Figure 12 considers the first family of flight paths, which have in common a net acceleration of 10 g's at V = 2.0, and presents the heat to the windward side of the vehicle Q_w and the total heat input Q (the sum of the heat inputs to the windward side and to the leading-edge region) as a function of $\overline{V}_i$. Though not shown by the curves, from the equation of tables I and II, the heat input Q equals zero for $\overline{V}_i = 0$.

Each point in figure 12 can be interpreted as giving the heat input for a complete "deceleration flight path" having a terminal velocity of zero and the initial velocity and initial G given by figures 6 to 11. The history of the flight is also given by figures 6 to 11. For the supercircular speed range the flight paths in order of increasing total heat input for a given $\overline{V}_i$ rank as follows: constant G, modulated roll, constant Re, constant h, and constant α. At $\overline{V}_i = 2$, the constant α case has about twice the heat input of the constant G case.

The curves of figure 12 can also be interpreted to show the distribution of heat input as a function of $\overline{V}$. For example, for a flight starting at any initial velocity, the contribution to the heat input in decelerating from $\overline{V} = 0.5$ to 0 is given by the Q at $\overline{V} = 0.5$. With this interpretation for all the flight plans the heat input for decelerating from $\overline{V} = 0.5$ to 0 is generally an order of magnitude less than the

total heat input for decelerating from any supercircular speed. A precise determination of the total heat input at the low speeds is not essential to an accurate estimate of the total heat input in decelerating from supercircular speeds. This implies that neglecting the low-speed anomalies previously discussed in regard to the point functions has little effect on the accuracy of calculating the total heat input for the deceleration from supercircular speeds, and therefore these anomalies have been neglected in the present calculations. For most flight paths the total heat input to the windward side of the vehicle is about 15 percent of the total heat input, for a vehicle with an $(L/D)_{max}$ of 1.0.

The second family of deceleration flight paths considered is shown in figure 13. Each point in the figure represents a complete deceleration flight path having the $\overline{V}_i$ given by the abscissa and $G_i = 10$ g's. The values for $\overline{V}_i = 2.0$ for all the flight plans and for the complete curve for constant G are the same for figures 12 and 13. In the supercircular speed range the flight paths generally rank in the same order as for the preceding family of curves. The equations for the constant α path are of questionable accuracy for the very low L/D's ($L/D < 0.03$) that result for $\overline{V}_i$ close to unity, and hence results are not shown at $\overline{V}$ less than 1.2.

The relation of the ablated weight to the total heat input is given by equation (26). An ablation system based on the extrapolation of the data of references 14 and 15 to the conditions at supercircular speeds and a system utilizing the boiling of lithium (ref. 16) both indicate the possibility of an effective heat-absorbing capacity of about 10,000 Btu per pound of ablated weight. Using this value for C in equation (26) for $\overline{V}_i = 2.0$ and $G_i = 10$ g's gives values of the ablated weight as a fraction of the vehicle gross weight of 0.033 and 0.085 for the flight paths of constant G and constant α, respectively. Halving the value of C would double the ablated weight. From the consideration of the ablated weight it is concluded that entries at $\overline{V} = 2.0$ and greater are feasible.

The distribution of heat between the windward side and the leading edge of the vehicle depends on the G load, as illustrated in figure 14 for a family of constant α flight paths with $\overline{V}_i = 2.0$ and for a vehicle with an $(L/D)_{max}$ of 1.0. As the initial G load decreases, the vehicle angle of attack and initial flight altitude must increase to satisfy equations (4a) and (5). Because of the assumption of constant C_R and C_D/C_R the other flight plans cannot be considered over this wide a range of G or α. The curves show that the heat input to both

the leading-edge region and the windward side of the vehicle increases with decreasing G load. Reducing the initial G_i from 10 to 4.25 g's about doubles the total heat input. The value G_i = 4.25 g's is the minimum at which the constant α path can be initiated. Also the proportion of the heat input to the windward side of the vehicle increases from about 19 percent at G_i = 10 g's to 47 percent at G_i = 4.25 g's. The increased angle of attack accounts for the increased proportion of heat to the windward side of the vehicle.

While the heat input for the constant α, G_i = 4.25 g path is 2.2 times that for the constant α, G_i = 10 g path, it is 4.9 times larger than that for the constant G = 10 g path. This indicates the importance of both the G level and the type of deceleration flight path to the vehicle heat input.

Figure 14 also shows the Reynolds numbers at $\overline{V}_i$ = 2.0. Decreasing the G load decreases the free-stream Reynolds number almost directly, as would be expected from equation (18) (for constant C_R). Increasing angle of attack, however, increases the ratio of local to free-stream Reynolds number (see appendix D), so that decreasing G_i has essentially no effect on the local Reynolds number.

Control of Landing Location

One of the practical requirements that may be placed on an entry vehicle is that it have the capability of landing at a predesignated location. The problem of achieving a low total heat input on a flight path that will also yield control of the landing location can be studied to a first-order approximation with the present solutions.

To land at a predesignated location requires control of motion both down and cross range with respect to the Earth's surface. By column 14 of table I the down range for the constant α case is indefinitely large. For this case the analysis implies that at $\overline{V}$ = 1.0 the vehicle glides up out of the atmosphere into an orbit of indefinite duration. (The details of this maneuver are not defined by the equation. If the vehicle exits from the atmosphere at a small angle as indicated by fig. 6, a small rocket may be required to "circularize" the orbit, and then a second small rocket may be required to initiate reentry.) Cross range movement may be obtained by waiting for the Earth to rotate through the plane of the orbit If, for example, the vehicle had glided into a polar circular orbit, all of Earth's surface passes through the plane of the vehicle in 1/2 revolution of Earth or in 12 hours. This time corresponds to about 8 revolutions of the vehicle about Earth. A down-range capability of 8

revolutions thus yields a control of cross range. With the aerodynamic cross-range capability such that half the distance between the traces on the Earth's surface of two successive orbits can be traversed during the deceleration from the circular orbit, the vehicle can potentially land at any predesignated location.

The present discussion deals with the down range and total heat input for some possible flight plans that include control of landing location by control of the flight through $\bar{V} = 1.0$. The flight plans considered are illustrated in figure 15 in terms of the G history against $\bar{V}$. The flight paths are composites of the constant G and constant α flight paths, and all begin at $\bar{V} = 2.0$ with an initial deceleration of G = 10 g's. Figure 15(a) shows the constant α case modified by a constant G segment through $\bar{V} = 1.0$. The magnitude of the deceleration during this constant G segment is designated G_{min}, because it is the minimum deceleration that occurs during the deceleration. Then G_{min} can be considered an independent variable. For $G_{min} = 0$ the general path reduces to the constant α case and for $G_{min} = 10$ g's to the constant G case.

The variation of Q and range with G_{min} is presented in figure 16. The minimum Q and range occur for $G_{min} = 10$, and the values are 390 Btu per pound of gross weight and 0.032 of the Earth circumference, respectively. The maximum Q and range occur at $G_{min} = 0$. At $G_{min} = 0$ the value of Q is a little more than twice the minimum, and the range is indefinitely large. These data show that increased range results in an increase in total heat input and that the maximum total heat input is finite and occurs for an indefinitely large range.

Figure 15(b) illustrates a family of flight paths, all of which, according to the present analysis, have indefinitely large range. The deceleration begins at $\bar{V} = 2.0$ along a constant G path. At a specified velocity designated $\bar{V}_\alpha$ the flight path is changed to a constant α path, which yields an indefinitely large range. With $\bar{V}_\alpha$ considered an independent variable, for $\bar{V}_\alpha = 2.0$ this case reduces to the constant α case previously considered. Figure 17 presents the total heat input plotted against $\bar{V}_\alpha$. Decreasing $\bar{V}_\alpha$ reduces the total heat input. At $\bar{V}_\alpha = 1.3$ the total heat input is 32 percent more than the value for a constant G of 10 g's, compared with 120 percent more for $\bar{V}_\alpha = 2.0$, which is the constant α case.

To obtain control of the range the flight paths of figure 15(b), like those of figure 15(a), can also be modified by a constant G segment through $\bar{V} = 1$ as shown in figure 15(c). From the discussion of the

flight paths of figure 15(a), it can be concluded that the heat inputs for the flight paths of figure 15(c) will fall between the two curves of figure 17.

Several comments about the limitations of the present range control calculations may be made. The composite flight paths considered in this section have mathematical discontinuities in flight-path angle at the junctions of the various types of flight paths, so that some transition maneuver is required. The details of the transitions, however, are not expected to have a significant effect on the total heat input to the vehicle.

The details of the flight path through $\bar{V} = 1.0$ for the constant α flight plan and the determination of a minimum permissible value of $\bar{V}_\alpha$ both require a more detailed study than can be made with the present assumptions.

Generalizing the Results with Respect to Vehicle Gross Weight and Vehicle Density

The numerical results for the heat input have been calculated for a specific vehicle with a gross weight of 10,000 pounds and a vehicle density of 20 pounds per cubic foot. With the assumption of a laminar boundary layer for all vehicles, these results can be applied to vehicles of different gross weight and average density by the following reasoning. Consider the results of columns 17 and 18 with the substitutions given at the bottom of the table. In the present application the product $(C_D/C_R)C_R$ is approximately $C_{D,o}$. For configurations like that of figure 3, the drag coefficient at $\alpha = 0$, $C_{D,o}$, depends only on the vehicle proportions, that is, on the thickness ratio d/c and sweep angle Λ, if the contribution of friction is neglected. The contribution of friction is small for the low L/D configuration considered in this report. The Q/W for a configuration with $(L/D)_{max} = 1$ but with any given weight and fuselage density may hence be estimated from the curves of this report by the relation:

$$\frac{Q}{W} = \left(\frac{Q}{W}\right)_{curves} \times \left(\frac{10{,}000}{W}\right)^{1/3}\left(\frac{20}{\rho}\right)^{1/6}$$

CONCLUSIONS

An approximate analysis of flight paths for the descent from circular and supercircular speeds has yielded closed-form solutions for the

following flight-path characteristics: altitude, lift coefficient, G load, path angle, free-stream and local Reynolds numbers, heating rate, heat input per square foot, total heat input to the vehicle, range, and time of flight. The heating analysis considers separately the heating of the leading-edge region and the windward side of the vehicle. The six deceleration flight paths considered are constant values of altitude, angle of attack, G load, heating rate, and free-stream Reynolds number, and a case of modulated roll. Limitations on altitude, G load, lift coefficient, and Reynolds number have been considered. The following conclusions may be drawn:

1. Of the flight paths considered, all except the constant-heating-rate path stayed within the following physical limitations: Altitude greater than 0, net acceleration G equal to or less than 10 g's, and lift coefficient less than 0.9 for flight- to circular-velocity ratios equal to or less than 2.0 and a vehicle maximum lift-drag ratio of 1.0. Entry velocity ratios up to 2.8 are aerodynamically possible.

2. Changing the type of flight path or the G level of the flight path has little effect on the value of the local Reynolds number, although the value of the free-stream Reynolds number may vary a large amount. For the present examples the value of the local Reynolds number is about 0.7×10^6, a value for which one can be hopeful of achieving a laminar boundary layer.

3. The flight path with the minimum total heat input is the one with the highest allowable G load.

4. With a laminar boundary layer and a maximum deceleration of 10 g's, entry velocities of twice circular and higher appear aerodynamically and thermodynamically feasible for a vehicle with a maximum lift-drag ratio of 1.0. About 85 percent of the total heat input to the vehicle is to the leading-edge region. The ablated weight is estimated to be about 5 percent of the vehicle gross weight to decelerate from twice circular to zero velocity along a constant 10 G path. A constant-angle-of-attack path with an initial G load of 4.25 g's has a heat input 4.9 times higher than that of the constant 10 G path.

5. For an initial velocity of twice circular, incorporating landing point control into a constant 10 G path by controlling the flight path in the vicinity of circular velocity increases the heat input about 32 percent.

6. For a delta wing vehicle for which the useful volume is the volume in the wing, the heat input per square foot varies directly with the one-half power of the average fuselage density and inversely with the one-half power of the G load and resultant force coefficient. For vehicles of this type, with the same sweep back, the total heat input

varies inversely with the one-half power of the G load, the one-third power of the gross weight, and the one-sixth power of the vehicle average density and drag coefficient.

Lewis Research Center
National Aeronautics and Space Administration
Cleveland, Ohio, August 7, 1961

APPENDIX A

SYMBOLS

E-1001

A	reference area for aerodynamic coefficients, plan area of vehicle (see fig. 3), sq ft
A_f	projected frontal area of vehicle (see fig. 3), sq ft
b	span of vehicle (see fig. 3), ft
C	effective heat-absorbing capacity of ablation heat protection system, Btu/lb
C_D	aerodynamic drag coefficient, $\frac{D}{\frac{1}{2}\rho V^2 A}$
$C_{D,o}$	aerodynamic drag coefficient at zero lift
C_f	friction coefficient, dimensionless
C_L	component of aerodynamic lift coefficient in vertical direction, $\frac{L}{\frac{1}{2}\rho V^2 A}$
$C_{L,a}$	total aerodynamic lift coefficient
C_P	pressure coefficient, $2(p_e - p)/\rho V^2$
C_p	specific heat at constant pressure, Btu/(slug)($^\circ$R)
C_R	aerodynamic resultant-force coefficient
C_ρ	$\frac{2W}{C_R A g r \frac{C_L}{C_R}}$
C_φ	$\frac{C_D g A}{2\beta W}$
c	root chord of vehicle, ft
c_A	leading-edge axial force coefficient, leading-edge axial force$/\frac{1}{2}\rho V^2 A_f$

c_D leading-edge drag coefficient, leading-edge drag$/\frac{1}{2}\rho V^2 A_f$

c_L leading-edge lift coefficient, leading-edge lift$/\frac{1}{2}\rho V^2 A_f$

c_N leading-edge normal force coefficient, leading-edge normal force$/\frac{1}{2}\rho V^2 A_f$

c' general wing chord, ft

D aerodynamic drag, lb

d thickness of vehicle (see fig. 3), ft

F see column 19 of table I

f linear distance along streamline from leading-edge stagnation point to end of leading-edge region (beginning of windward side) (see fig. 3), ft

G net acceleration, g's

g acceleration due to gravity, essentially the planet surface value, ft/sec^2

H see column 19 of table I

h altitude, ft

h_{se} total enthalpy at edge of boundary layer, Btu/lb

h_w wall enthalpy, Btu/lb

$\bar{h}$ heat-transfer coefficient, Btu/(sq ft)(sec)($^\circ$R)

J mechanical equivalent of heat, 778 ft-lb/Btu

j see eq. (7a)

k see columns 11, 17, 18, and 19 of table I

L component of aerodynamic lift in vertical direction

L_a total aerodynamic lift, lb force

L/D	lift-drag ratio
$(L/D)_{max}$	$(L_a/D)_{max}$
l	distance along leading edge of wing (see fig. 3), ft
M	Mach number, dimensionless
m	entry vehicle gross mass, slugs
n	exponent defining variation of altitude density with $\overline{V}$ for general flight path of table I
p	static pressure, lb force/sq ft
Pr	Prandtl number, dimensionless
Q	total heat input, $Q_l + Q_w$, Btu
Q_l	total heat input to leading edge, Btu
Q_w	total heat input to windward side, Btu
q	heat input per square foot, Btu/sq ft
$\overline{q}$	dimensionless function $\overline{Q}$ of ref. 4, proportional to total heat input per unit area for laminar flow
$\overline{\dot{q}}$	dimensionless function $\overline{q}$ of ref. 4, proportional to heating rate for laminar flow
$\dot{q}$	heating rate, Btu/(sq ft)(sec)
$\dot{q}_{l,\lambda=0}$	$\dot{q}_l$ at $\lambda=0$, maximum heating rate on swept leading edge (see fig. 3 for λ), Btu/(sq ft)(sec)
R	range, ft
R_N	leading-edge radius, ft
$\mathfrak{R}$	gas constant, 1716 ft-lb/(slug)(^oR)
Re	free-stream Reynolds number, dimensionless
Re_l	Reynolds number at outer edge of boundary layer, dimensionless

r	radius of planet, ft
St	Stanton number, dimensionless
T	total temperature, ^{o}R
t	static temperature, ^{o}R
V	flight velocity, ft/sec
V_c	component of velocity normal to leading edge (see fig. 3)
V_N	component of velocity normal to any surface (see fig. 3)
$\overline{V}$	ratio of flight to circular velocity, $V/\sqrt{gr}$, dimensionless
$\overline{V}_\alpha$	dimensionless velocity at which change from constant G to constant α type of flight path occurs
W	entry vehicle gross weight, Earth lb
W/A	wing loading, Earth lb/sq ft
W_p	ablated weight, Earth lb
x	distance from leading edge in stream direction, ft
x,ξ,η	coordinate systems on vehicle (see fig. 3)
α	angle of attack with respect to free stream
α_c	cross-flow angle of attack (see fig. 3)
β	exponent describing exponential variation of density with altitude in equation $\frac{\rho}{\rho_{SL}} = e^{-\beta h}$, ft ($\beta^{-1} = 2.35\times10^4$ ft for Earth)
γ	ratio of specific heats, dimensionless
δ	angle of surface with respect to free-stream direction
ϵ	emissivity, dimensionless
θ	roll angle (see fig. 1) (zero for lift in vertical plane directed upward)
κ	conductivity, Btu/(ft)(sec)(^{o}R)

Λ	geometric leading-edge sweep angle (see fig. 3)
Λ_c	effective sweep angle (see fig. 3)
λ	leading-edge radius coordinate angle (see fig. 3)
μ	viscosity, slugs/(ft)(sec) or (lb force)(sec)/sq ft
ν	exponent defining variation of laminar heating rate with wing sweepback angle
ρ	atmospheric density, slugs/cu ft
ρ_f	average entry vehicle density, Earth lb/cu ft
ρ'_f	average entry vehicle density, slugs/cu ft
σ	Stefan-Boltzmann constant, 0.48×10^{-12} Btu/(sq ft)(sec)($^\circ R^4$)
τ	time, sec
φ	flight-path angle with respect to local horizontal (see fig. 1)
ω	leading-edge surface angle (see fig. 3)

Subscripts:[1]

aw	adiabatic wall
e	at edge of boundary layer
i	beginning of deceleration flight path
l	leading edge
max	maximum
min	minimum
n	general subscript for summation in appendix B
SL	sea level
s	stagnation point

[1]Flight quantities of M, p, $\mathfrak{R}$, Re, t, t/T, V, γ, μ, and ρ with no subscript or superscript are free-stream values.

w	windward side of vehicle
$\bar{w}$	wall
v	vertical component of flight velocity
1,2	stations along deceleration flight path

Superscript:[1]

*	reference condition in "reference temperature" or "reference enthalpy" method of calculating heat transfer

[1]Flight quantities of M, p, $\mathcal{R}$, Re, t, t/T, V, γ, μ, and ρ with no subscript or superscript are free-stream values.

APPENDIX B

VEHICLE AERODYNAMICS

The vehicle aerodynamics are estimated by assuming hypersonic flow and using the approximation to the leading edge of the vehicle shown in figure 3.

The pressure coefficient on windward surfaces is in general

$$C_p = (\gamma + 1)\sin^2\delta = (\gamma + 1)\left(\frac{V_N}{V}\right)^2 \tag{B1}$$

and for a surface on the leading edge

$$C_p = (\gamma + 1)\left(\frac{V_c}{V}\right)^2 |\cos(\omega - \alpha_c)|\cos(\omega - \alpha_c) \tag{B2}$$

In equation (B2) if C_p is positive, the surface is windward, if negative, the surface is leeward. The pressure coefficient on leeward surfaces is assumed to be zero (rather than the value given by eq. (B2)). From figure 3

$$\left(\frac{V_c}{V}\right)^2 = \sin^2\alpha + \cos^2\alpha\,\cos^2\Lambda = 1 - \cos^2\alpha\,\sin^2\Lambda \tag{B3}$$

and

$$\alpha_c = \arctan\frac{\tan\alpha}{\cos\Lambda} \tag{B4}$$

Equation (B2) hence becomes

$$C_p = (\gamma+1)(1-\cos^2\alpha\,\sin^2\Lambda)\left|\cos\left(\omega - \arctan\frac{\tan\alpha}{\cos\Lambda}\right)\right|\cos\left(\omega - \arctan\frac{\tan\alpha}{\cos\Lambda}\right) \tag{B5}$$

For a leading edge composed of multiple flat surfaces of equal width, the axial force coefficient of the leading edge using the projected frontal area of the vehicle as a reference area is

$$c_A = \frac{\sum_1^n C_{P,n} \cos \omega_n}{\sum_1^n \cos \omega_n} \tag{B6}$$

Similarly the normal force coefficient for the nose is

$$c_N = \frac{\sum_1^n C_{P,n} \sin \omega_n}{\cos \Lambda \sum_1^n \cos \omega_n} \tag{B7}$$

The contribution of the leading edge to the drag and lift, from the results of equations (B6) and (B7), is

$$c_D = c_A \cos \alpha + c_N \sin \alpha \tag{B8}$$

$$c_L = c_N \cos \alpha - c_A \sin \alpha \tag{B9}$$

The total lift and drag coefficients of the vehicle based on the reference area of the vehicle (see fig. 3) are then

$$C_{L,a} = (\gamma + 1)\sin^2\alpha \cos \alpha + c_L \frac{A_f}{A} \tag{B10}$$

$$C_D = (\gamma + 1)\sin^3\alpha + c_D \frac{A_f}{A} \tag{B11}$$

where the first terms on the right side of the equations are the contribution of the reference area A to lift and drag coefficients, and the second terms are the contribution of the leading edge.

If one considers a family of vehicles having the general plan form shown in figure 3, that is, having the same sweepback angle but various values of c/d, or what is equivalent, various values of $(L/D)_{max}$, then the following relation may be derived for low angles of attack:

$$C_D \sim C_{D,o} = c_{D,o} \frac{A_f}{A}$$

where $c_{D,o}$ is a constant for a given sweepback angle. From equation (E1)

$$A = \frac{1}{2} bc$$

and

$$A_f = bd$$

E-1001

so that

$$C_D \frac{c}{d} = 2c_{D,o} = \text{Constant} \qquad (B12)$$

APPENDIX C

WINDWARD-SIDE HEATING ANALYSIS

A simple analytic expression for the laminar heat transfer to the windward side of the vehicle at high velocities is developed herein.

Off the stagnation point for moderate angles of attack the heat transfer to the windward side is analyzed using an approximation to the "reference temperature" (ref. 9). The relations required are:

$$\dot{q} = \bar{h}(t_{aw} - t_{\overline{w}}) \tag{C1}$$

$$St = \frac{\bar{h}}{\rho^* V_e C_p} \tag{C2}$$

$$St = \frac{C_f}{2} (Pr^*)^{-2/3} \tag{C3}$$

$$C_f = 0.664\sqrt{\frac{\mu^*}{\rho^* V_e x}} \tag{C4}$$

$$t_{aw} = t + \sqrt{Pr^*}\,\frac{V^2}{2C_p J} \approx \sqrt{Pr^*}\,\frac{V^2}{2C_p J} \tag{C5}$$

$$Pr^* = \frac{\mu^* C_p^*}{\kappa^*} \tag{C6}$$

$$t^* = t_e + 0.5(t_{\overline{w}} - t_e) + 0.22(t_{aw} - t_e) \tag{C7}$$

Assuming $t_{\overline{w}} \ll t_{aw}$ and combining equations (C1) to (C5) yield

$$\dot{q} = \frac{0.166}{J Pr^{*0.167}}\sqrt{\frac{\rho^* V_e \mu^*}{x}}\, V^2 \tag{C8}$$

The three terms in the numerator of the square root term of equation (C8) may be evaluated as follows, as an approximation of Southerland's

viscosity equation for high temperatures (ref. 17, eq. (A3)):

$$\mu^* = 2.27\times10^{-8}\,\frac{t^{*3/2}}{t^* + 198} \approx 2.27\times10^{-8}\,t^{*1/2} \tag{C9}$$

The reference density is given by

$$\rho^* = \rho\,\frac{p_e}{p}\,\frac{t}{t^*} \tag{C10}$$

At moderate angles of attack, by Newtonian aerodynamics,

$$V_e = V\cos\alpha \tag{C11}$$

The terms t^* and p_e/p in equations (C9) and (C10) must now be evaluated. In equation (C7) for low and moderate angles of attack, t_e and $(t_w - t_e)$ are small compared with $(t_{aw} - t_e)$ and t_{aw}, so that equation (C7), combined with equation (C5), becomes

$$t^* \approx 0.22\,t_{aw} = \frac{0.11\sqrt{Pr^*}\,V^2}{C_p J} \tag{C7a}$$

From hypersonic aerodynamics

$$C_{p,e} = \left(\frac{p_e}{p} - 1\right)\frac{1}{\frac{\gamma}{2}M^2} = (\gamma + 1)\sin^2\alpha \tag{C13}$$

where at supercircular speed ($M > 25$) and for moderate angles of attack $p_e/p \gg 1.0$. At the low angles of attack where the assumption produces maximum error, the heat input to the windward side of the vehicle is generally small compared with the heat input to the leading edge (see fig. 14). The error in estimating the total heat input to the vehicle can thus still be small at small angles of attack. Then, since

$$M^2 = \frac{V^2}{\gamma \mathfrak{R} t}$$

equation (C13) becomes

$$\frac{p_e}{p} = 1 + \frac{\gamma + 1}{2}\frac{V^2}{\mathfrak{R}t}\sin^2\alpha \approx \frac{\gamma + 1}{2}\frac{\gamma^2}{\mathfrak{R}t}\sin^2\alpha \tag{C14}$$

E-1001

Making the appropriate substitution in equation (C8) gives

$$\dot{q} = \frac{0.166}{J^{0.75} Pr^{*0.292}} \sqrt{\frac{2.27 \times 10^{-8}}{R \sqrt{\frac{0.11}{C_p}}}} \sqrt{\frac{\gamma + 1}{2} \frac{\rho V^2 \cos \alpha \sin^2 \alpha}{x}} \bar{V}^2 \, gr \qquad (C15)$$

The following values are assumed to be constants:

$$Pr^* = 0.71$$

$$\gamma = 1.2$$

$$R = 1716 \text{ ft-lb/(slug)}(^\circ R)$$

$$C_p = \frac{\gamma R}{J(\gamma - 1)} = 13.2 \text{ Btu/(slug)}(^\circ R)$$

$$J = 778 \text{ ft-lb/Btu}$$

From the hypersonic aerodynamics of the configuration, equation (B11), and equation (6)

$$\frac{L}{A \cos \theta} = \frac{L_a}{A} = \frac{\gamma + 1}{2k_c^2} \rho V^2 \sin^2 \alpha \cos \alpha \qquad (C16)$$

where

$$k_c = \left(1 + \frac{A_f c_L}{A(\gamma + 1) \sin^2 \alpha \cos \alpha} \right)^{-1/2} \qquad (C17)$$

so that equation (C15) becomes, with the assigned constants,

$$\dot{q}_w = 1.5 \times 10^{-8} k_c gr \sqrt{\frac{|L|}{Ax |\cos \theta|}} \bar{V}^2 \qquad (C18)$$

The absolute value signs are used to indicate that the heating is real and positive irrespective of the sign of L and $\cos \theta$. By use of the value of $\frac{V}{g} \frac{d\varphi}{d\tau}$ given in column 6 of table I, one may solve for L in equation (4b) and substitute in equation (C18) to arrive at the results given in column 10 of table I. For example, for the constant Re case

with $\theta = 0$

$$\dot{q}_w = 1.50\times10^{-8} k_c g^{3/2} r \sqrt{\frac{m}{Ax}} \sqrt{1 - \overline{V}^2 - k_{Re}}\, \overline{V}^2 = 10.2\, k_c \sqrt{\frac{W}{Ax}} \sqrt{1 - \overline{V}^2 - k_{Re}}\, \overline{V}^2 \tag{C19}$$

The term k_c^2 is the ratio of the lift produced by the vehicle windward side to the sum of the windward-side and leading-edge lift. Approximately, for angles of attack from 0° to 15°

$$k_c = \left[1 + \frac{A_f}{A} \frac{dc_L}{d(\sin\alpha)} \frac{1}{(\gamma + 1)\sin\alpha}\right]^{-1/2}$$

where $dc_L/d(\sin\alpha)$ is approximately constant and depends on the sweep angle. For the present configuration with $\Lambda = 60^\circ$ and $dc_L/d(\sin\alpha) = 0.88$, $A_f/A = 0.569$, $\alpha = 5.3^\circ$, and $k_c = 0.535$.

The term k_c, in general, varies over the flight path. For supercircular entry velocities a conservative estimate of the heat input is obtained by evaluating k_c at the maximum velocity. This is done in the present calculations. The value of k_c approaches unity and constancy for small values of A_f/A or high values of $(L/D)_{max}$.

APPENDIX D

METHOD USED FOR CALCULATING RATIO OF LOCAL TO FREE-STREAM REYNOLDS NUMBER

The procedure for calculating the local Reynolds number at supersonic speeds for cones and wedges with unswept edges is presented in reference 18. A relation for calculating the local Reynolds number at hypersonic speeds for the case of a flat plate at angle of attack with a swept blunt leading edge is developed herein. The nomenclature is illustrated in figures 3 and 18.

At a station sufficiently far downstream from the leading edge, where the surface static pressure for a blunt body is approximately that for a nonblunt body, the ratio of local to free-stream Reynolds number per foot or for the same length may be written

$$\frac{Re_l}{Re} \equiv \frac{\rho_e}{\rho} \frac{V_e}{V} \frac{\mu}{\mu_e} \tag{D1}$$

In equation (D1) the velocity ratio is taken as the Newtonian value,

$$\frac{V_e}{V} = \cos \alpha \tag{D2}$$

The viscosity approximation is the same as that used in equation (C9),

$$\mu_e = 2.27 \times 10^{-8} \, t_e^{1/2} \tag{D3}$$

where for this case

$$t_e = t_s \left(\frac{\rho_e}{\rho_s} \right)^{\gamma - 1} \tag{D4}$$

where

$$t_s = t + \frac{V^2 \cos^2 \Lambda_c}{2JC_p} \approx \frac{V^2 \cos^2 \Lambda_c}{2JC_p} \tag{D5}$$

Hence equation (D3) becomes

$$\mu_e = 2.27\times10^{-8}\,\frac{V\cos\Lambda_c}{\sqrt{2JC_p}}\left(\frac{\rho_e}{\rho_s}\right)^{\frac{\gamma-1}{2}} \tag{D6}$$

The term ρ_e/ρ in equation (D1) may be written

$$\frac{\rho_e}{\rho} = \frac{\rho_s}{\rho}\,\frac{\rho_e}{\rho_s} \tag{D7}$$

and equation (D1) then becomes

$$\frac{Re_l}{Re} = \frac{\mu\cos\alpha\sqrt{2JC_p}\,\frac{\rho_s}{\rho}}{2.27\times10^{-8}\,\bar{V}\sqrt{gr}\cos\Lambda_c}\left(\frac{\rho_e}{\rho_s}\right)^{\frac{3-\gamma}{2}} \tag{D8}$$

The ratio ρ_e/ρ_s may be written by use of the perfect gas law as

$$\frac{\rho_e}{\rho_s} = \left(\frac{p_e}{p_s}\right)^{1/\gamma} = \left(\frac{p_e}{p}\right)^{1/\gamma}\left(\frac{p_s}{p}\right)^{-1/\gamma} \tag{D9}$$

Hypersonic aerodynamics gives (see also eq. (C14))

$$\frac{p_e}{p} = 1 + \frac{\gamma+1}{2}\,\frac{V^2}{Rt}\sin^2\alpha \tag{D10}$$

and

$$\frac{p_s}{p} = 1 + \frac{\gamma+1}{2}\,\frac{V^2}{Rt}\cos^2\Lambda_c \approx \frac{\gamma+1}{2}\,\frac{V^2}{Rt}\cos^2\Lambda_c \tag{D11}$$

where the approximation is valid for sweep angles less than about 87°. From figure 3 (see also eq. (B3))

$$\cos^2\Lambda_c = (1 - \sin^2\Lambda\cos^2\alpha) \tag{D12}$$

The density ratio across the shock at the cross-flow stagnation point is

$$\frac{\rho_s}{\rho} = \frac{\gamma+1}{\gamma-1} \tag{D13}$$

With the appropriate substitution, equation (D8) gives finally

$$\frac{Re_l}{Re} = \frac{\mu \cos \alpha \sqrt{2JC_p\left(\frac{\gamma + 1}{\gamma - 1}\right)}}{2.27\times10^{-8}\, \bar{V}\sqrt{gr}\,(1 - \sin^2\Lambda \cos^2\alpha)^{1/2}}\left[\frac{\frac{2Rt}{(\gamma + 1)\bar{V}^2 gr} + \sin^2\alpha}{1 - \sin^2\Lambda \cos^2\alpha}\right]^{\frac{3-\gamma}{2\gamma}} \qquad (D14)$$

The following values were assumed in the present calculations:

$$\gamma = 1.2$$

$$R = 1716 \text{ ft-lb/(slug)}(^{\circ}R)$$

$$C_p = \frac{\gamma R}{J(\gamma - 1)} = 13.2 \text{ Btu/(slug)}(^{\circ}R)$$

$$t = 500^{\circ} R$$

$$\mu = 0.37\times10^{-6} \text{ (lb force)(sec)/sq ft}$$

$$J = 778 \text{ ft-lb/Btu}$$

The term $\bar{V}$ is the independent variable, and α is determined by the lift coefficient (column 7 of table I) and the vehicle aerodynamics.

This calculation takes no detailed account of the boundary-layer history on the leading edge of the vehicle.

Typical curves of the ratio of local to free-stream Reynolds number are shown in figure 18 as a function of angle of attack for several values of $\bar{V}$. Both $\bar{V}$ and angle of attack have a strong effect on the Reynolds number ratio.

APPENDIX E

INTEGRATION OF HEAT INPUT OVER VEHICLE

The vehicle geometry over which the integration of the local heat per square foot q is carried out is shown in figure 3 together with the symbols and coordinate systems used. The constant Re case is used as an example.

E-1001

Vehicle Geometry

The following approximate relations can be derived from the vehicle geometry:

$$
\left.
\begin{gathered}
A = \frac{1}{2} bc = \frac{c^2}{\tan \Lambda} = \frac{W}{W/A} = \frac{m}{m/A} \\
A_f = bd = \frac{2}{\rho_f}\left(\frac{W \frac{W}{A}}{\tan \Lambda}\right)^{1/2} = \frac{2}{\rho_f'}\left(\frac{m \frac{m}{A}}{\tan \Lambda}\right)^{1/2} \\
\frac{W}{A} = \rho_f d \\
\frac{A_f}{A} = \frac{2d}{c} = \frac{2(W/A)^{3/2}}{\rho_f (W \tan \Lambda)^{1/2}} \\
R_N = \frac{d}{2} \\
b = 2l \cos \Lambda \\
c = \left(\frac{W \tan \Lambda}{W/A}\right)^{1/2} \\
\frac{W}{R_N A} = 2\rho_f \qquad \text{or} \qquad \frac{m}{R_N A} = 2\rho_f'
\end{gathered}
\right\} \tag{E1}
$$

Integration Over Leading-Edge Region

The integration over the vehicle is divided into two parts, that over leading-edge regions, and that over the windward side of the vehicle. To illustrate the integration over the leading-edge regions, q_l may be taken from column 15 of table I (hence the subscript 15 on k) or the integration of equation (37) and written as

$$q_l = k_{15}\left[1 - \sin^2\Lambda \cos^2\alpha\right]^{\nu/2} \cos \lambda \tag{E2}$$

where for constant Re

$$k_{15} = 12.1\times10^3\sqrt{\frac{W}{R_N A}}\,\frac{1}{\frac{C_D}{C_R}C_R}\,\frac{\left[\frac{\bar{V}_1^{2.5} - \bar{V}_2^{2.5}}{2.5}\right]}{\sqrt{\left\{\frac{G}{C_R\bar{V}}\right\}}}$$

The general form of the integration desired is (see fig. 3)

$$Q_l = 2\int_0^l \int_{-(\pi/2-\alpha_c)}^{\pi/2} q_l R_N \, d\lambda \, dl \tag{E3}$$

Carrying out the interior integration and using equations (E1) and (E2) yield

$$Q_l = k_{15} d \int_0^l \left[1 - \sin^2\Lambda \cos^2\alpha\right]^{\nu/2} (1 + \cos \alpha_c) dl \tag{E4}$$

where from figure 3

$$\alpha_c = \arctan \frac{\tan \alpha}{\cos \Lambda} \tag{E5}$$

Equation (E4) may be written

$$Q_l = 2k_{15} d \int_0^l k_l \cos^{\nu}\Lambda \, dl \tag{E6}$$

where

$$k_l = \frac{\left\{1 - \sin^2\Lambda \cos^2\alpha\right\}^{\nu/2}\left\{1 + \cos \text{ arc } \tan\left(\frac{\tan \alpha}{\cos \Lambda}\right)\right\}}{2 \cos^{\nu}\Lambda} \tag{E7}$$

For $\alpha = 0$, $k_l = 1.0$; for $\alpha = 12^\circ$, $\nu = 1.5$, and $\Lambda = 60^\circ$, $k_l = 1.05$; thus, for the integrations over the flight paths for which the angle of attack is small, k_l is assumed to be unity. For the constant α case, which is used at higher α, k_l is a constant and may be evaluated. With k_l a constant and by use of equation (E1), equation (E6) can be written

$$Q_l = k_{15}k_l d \cos^{(\nu-1)}\Lambda \int_0^{b/2} db \tag{E8}$$

so that finally integration gives

$$Q_l = \frac{1}{2} k_{15}k_l bd \cos^{(\nu-1)}\Lambda = \frac{1}{2} k_{15}k_l A_f \cos^{(\nu-1)}\Lambda \tag{E9}$$

Writing this result in terms of the gross weight and wing loading, by using equation (E1), yields

$$\frac{Q_l}{W} = \frac{k_{15}k_l \cos^{(\nu-1)}\Lambda}{\rho_f}\left(\frac{W/A}{W \tan \Lambda}\right)^{1/2} \tag{E10}$$

or

$$\frac{Q_l}{m} = \frac{k_{15}k_l \cos^{(\nu-1)}\Lambda}{\rho'_f}\left(\frac{m/A}{m \tan \Lambda}\right)^{1/2}$$

and substituting for k_{15} (eq. (E2)) and for $W/R_N A$ from equation (E1) results in

$$\frac{Q_l}{12.1\times10^3 W k_l \cos^{(\nu-1)}\Lambda} = \sqrt{2}\left(\frac{W/A}{\rho_f W \tan \Lambda}\right)^{1/2} \frac{\left[\frac{\overline{V}_1^{2.5} - \overline{V}_2^{2.5}}{2.5}\right]}{\frac{C_D}{C_R} C_R \sqrt{\left\{\frac{G}{C_R \overline{V}}\right\}}} \tag{E11}$$

or

$$\frac{Q_l}{21.9\times10^{-9} mgr^{3/2} k_l \cos^{(\nu-1)}\lambda} = \sqrt{2}\left(\frac{m/A}{\rho_f' m \tan\Lambda}\right)^{1/2} \frac{\left[\frac{\bar{V}_1^{2.5} - \bar{V}_2^{2.5}}{2.5}\right]}{\frac{C_D}{C_R} C_R\sqrt{\left\{\frac{G}{C_R\bar{V}}\right\}}}$$

Comparing equations (E2) and (E11) yields

$$\frac{Q_l}{W} = \frac{q_l}{\sqrt{\frac{W}{R_N A}}\,(1 - \sin^2\Lambda\cos^2\alpha)^{\nu/2}\cos\lambda} \frac{\sqrt{2}k_l \cos^{(\nu-1)}\Lambda}{\left(\frac{\rho_f W \tan\Lambda}{W/A}\right)^{1/2}} \qquad \text{(E12)}$$

Equation (E12) results from an integration over the vehicle and hence is true for all flight paths. It is listed in column 17 of table I and a similar relation is given in table II.

Integration Over Windward Side of Airplane

For this case q_w may be taken from column 16 of table I (hence the subscript 16 on k) or the integration of equation (38) and may be written as

$$q_w = \frac{k_{16}}{\sqrt{x}} \qquad \text{(E13)}$$

where, for example, for the constant Re case for $\bar{V} > 1$,

$$k_{16} = 8.2\times10^3\, k_c \sqrt{\frac{W}{A}} \frac{\left[\frac{(\bar{V}^2 - 1 + k_{Re})^{3/2}}{3}\right]_{\bar{V}_2}^{\bar{V}_1}}{\frac{C_D}{C_R} C_R\left\{\frac{G}{C_R\bar{V}}\right\}}$$

The integration desired is then (see fig. 3)

$$Q_w = 2k_{16}\int_0^{b/2}\int_{f+\eta\tan\Lambda}^{f+c} \frac{d\xi\, d\eta}{\sqrt{\xi - \eta\tan\Lambda}} \qquad \text{(E14)}$$

The integration results in

$$Q_w = \frac{8}{3} k_{16}\left[\frac{(f + c)^{3/2}}{\tan \Lambda} - \frac{f^{3/2}}{\tan \Lambda} - \frac{3f^{1/2} b}{4}\right] \tag{E15}$$

Equation (E15) may be written

$$Q_w = \frac{8}{3} k_{16} k_w \frac{c^{3/2}}{\tan \Lambda} \tag{E16}$$

where, using equation (E1),

$$k_w = \left(1 + \frac{f}{c}\right)^{3/2} - \left(\frac{f}{c}\right)^{3/2} - \frac{3}{2}\left(\frac{f}{c}\right)^{1/2} \tag{E17}$$

In terms of gross weight and wing loading and by use of relations from equation (E1),

$$\frac{Q_w}{W} = \frac{8}{3} k_{16} k_w \frac{1}{\left(\frac{W}{A}\right)^{3/4} (W \tan \Lambda)^{1/4}} \tag{E18}$$

Substituting for k_{16} (eq. (E13)) gives

$$\frac{Q_w}{8.2 \times 10^3 W} = \frac{8}{3} k_w k_c \frac{1}{\frac{C_D}{C_R} C_R \left\{\frac{G}{C_R \bar{V}}\right\}} \frac{\left[\frac{(\bar{V}^2 - 1 + k_{Re})^{3/2}}{3}\right]_{\bar{V}_2}^{\bar{V}_1}}{\left(\frac{W}{A} W \tan \Lambda\right)^{1/4}} \tag{E19}$$

Comparing equations (E13) and (E19) gives

$$\frac{Q_w}{W} = \frac{q_w}{\sqrt{\frac{W}{Ax}}} \frac{8}{3} \frac{k_w}{\left(\frac{W}{A} W \tan \Lambda\right)^{1/4}} \tag{E20}$$

Equation (E20) holds for all flight paths and is given in column 18 of table I. A similar result is given in table II.

From section AA of figure 3 the ratio f/c may be written approximately for small angles of attack as

$$\frac{f}{c} = \frac{\pi}{4}\frac{R_N}{c}\left[1 + \frac{1}{\cos\Lambda} - \frac{4}{\pi}\alpha_c\right] \tag{E21}$$

and by use of equation (E5)

$$\frac{f}{c} = \frac{\pi}{4}\frac{R_N}{c}\left[1 + \frac{1}{\cos\Lambda} - \frac{4}{\pi}\arctan\frac{\tan\alpha}{\cos\Lambda}\right] \tag{E22}$$

For the configuration used as an example in this report to generate numerical values, $R_N = 2.06$, $c = 14.5$, and $\Lambda = 60^\circ$. For $\alpha = 0^\circ$ and 5.3°, f/c is 0.34 and 0.31, respectively. The corresponding values of k_w (eq. (E17)) are 0.48 and 0.49, respectively. Note that k_w does not vary significantly for small changes in α, and hence it is assumed to be constant. A value of 0.49 was used for the calculations presented.

The most desirable form of some of the terms in equations (E11) and (E19) depends on what information is known. The following useful alternate forms may be derived if the parameter W/A is eliminated by use of one of the equations (E1):

$$\left(\frac{\rho_f W \tan\Lambda}{W/A}\right)^{1/2} = \left(\frac{c}{d}\tan\Lambda\right)^{1/3} W^{1/3}\rho^{1/6} \tag{E23}$$

$$\left(\frac{W}{A}W\tan\Lambda\right)^{1/4} = \frac{\tan^{1/3}\Lambda}{(c/d)^{1/6}} W^{1/3}\rho_f^{1/6} \tag{E24}$$

The term c/d depends on the vehicle sweep angle and maximum lift-drag ratio. For the present examples with $\Lambda = 60^\circ$, $c/d = 3.51$ and 21.7 for maximum lift-drag ratios of 1 and 2, respectively. Still another interesting form of the results of columns 17 and 18 may be written using the results of equations (E23), (E24), and (B13). For vehicle operation at low angles of attack where $C_R \sim C_D \sim C_{D,o}$, which is approximately the same assumption made to arrive at the results of columns 17 and 18,

$$\sqrt{C_D}\left(\frac{\rho_f W \tan\Lambda}{W/A}\right)^{1/2} = C_D^{1/6} W^{1/3}\rho_f^{1/6}(2c_D\tan\Lambda)^{1/3} \tag{E25}$$

$$\left(\frac{W}{A} W \tan \Lambda\right)^{1/4} = C_D^{1/6} W^{1/3} \rho_f^{1/6} \frac{\tan^{1/3}\Lambda}{(2c_D)^{1/6}} \tag{E26}$$

where c_D is constant for a given sweepback angle.

An example of the significance of this result is the following. For a family of vehicles having the same sweepback angle, gross weight, and fuselage density, the total heat input to the vehicle leading edge varies as

E-1001

$$Q_l \sim \frac{1}{C_D^{1/6}} \tag{E27}$$

(by the results of column 17 and eq. (E25) for k_l = Constant). On the other hand (by column 15) the heat input per square foot to the leading edge varies as

$$q_l \sim \frac{1}{C_D^{1/2}} \tag{E28}$$

Thus the change in the total heat input to the vehicle is much less sensitive to changes in C_D (or $(L/D)_{max}$) than is the heat input per square foot.

APPENDIX F

CASE OF CONSTANT ANGLE OF ATTACK

The determination of the term $\frac{V}{g}\frac{d\varphi}{d\tau}$ is more difficult for the case of constant angle of attack than for the other flight paths. However, the solution of this case permits a check on the accuracy of the results of the present analysis by comparison with the numerical integrations of references 4 and 13. The equations to be manipulated are repeated here

$$\frac{1}{g}\frac{dV}{d\tau} = -G\frac{C_D}{C_R} \tag{3}$$

$$G\frac{C_L}{C_R} = 1 - \bar{V}^2 + \frac{V}{g}\frac{d\varphi}{d\tau} \tag{4a}$$

$$G = \frac{C_R \rho \bar{V}^2 A g r}{2W} \tag{5}$$

$$\varphi = \frac{C_D g \bar{V} A}{2\beta W}\frac{d\rho}{d\bar{V}} \tag{19}$$

Using the mathematical identity

$$\frac{V}{g}\frac{d\varphi}{d\tau} = \frac{\bar{V}}{g}\frac{d\varphi}{d\bar{V}}\frac{dV}{d\tau} \tag{F1}$$

and equation (3) permits equation (4a) to be written

$$G = \frac{1 - \bar{V}^2}{\frac{C_L}{C_R}\left(1 + \frac{\bar{V}}{L/D}\frac{d\varphi}{dV}\right)} \tag{F2}$$

Solving equation (5) for ρ, by use of (F2) for G, yields

$$\rho = C_\rho\left(\frac{1}{\bar{V}^2} - 1\right)\left(1 + \frac{\bar{V}}{L/D}\frac{d\varphi}{dV}\right)^{-1} \tag{F3}$$

where

$$C_\rho \equiv \frac{2W}{C_R A g r \frac{C_L}{C_R}} \tag{F4}$$

Differentiating equation (19) gives

$$\frac{d\varphi}{d\bar{V}} = C_\varphi\left(\frac{d\rho}{d\bar{V}} + \bar{V}\frac{d^2\rho}{d\bar{V}^2}\right) \tag{F5}$$

where

$$C_\varphi \equiv \frac{C_D g A}{2\beta W} \tag{F6}$$

The term $d\varphi/d\bar{V}$ can be eliminated between equations (F3) and (F5) to yield a single differential equation for which a solution must be found. Herein, however, a solution to equations (F3) and (F5) was found by successive approximations. For a first approximation the flight-path angle is assumed to be a constant $\left(\frac{d\varphi}{d\bar{V}} = 0\right)$. Then from equation (F3)

$$\frac{d\rho}{d\bar{V}} = -\frac{2C_\rho}{\bar{V}^3} \tag{F7}$$

and

$$\frac{d^2\rho}{d\bar{V}^2} = \frac{6C_\rho}{\bar{V}^4} \tag{F8}$$

and equation (F5) becomes

$$\frac{d\varphi}{d\bar{V}} = \frac{4C_\varphi C_\rho}{\bar{V}^3} = \frac{4}{\beta r \bar{V}^3 \frac{L}{D}} \tag{F9}$$

The value for $d\varphi/d\bar{V}$ given by equation (F9) may now be introduced into equation (F3) to obtain a second approximation. Thus,

$$\rho = C_\rho\left(\frac{1}{\bar{V}^2} - 1\right)\left(1 + \frac{k}{\bar{V}^2}\right)^{-1} \tag{F10}$$

where

$$k \equiv \frac{4}{\beta r (L/D)^2} \tag{F11}$$

Repeating the steps of equations (F7) to (F9) results in

$$\frac{d\rho}{d\bar{V}} = C_\rho \left\{ \frac{2k}{\bar{V}^3}\left(\frac{1}{\bar{V}^2} - 1\right)\left(1 + \frac{k}{\bar{V}^2}\right)^{-2} - \frac{2}{\bar{V}^3}\left(1 + \frac{k}{\bar{V}^2}\right)^{-1} \right\} \tag{F12}$$

$$\frac{d^2\rho}{d\bar{V}^2} = C_\rho \left\{ \frac{8k^2}{\bar{V}^6}\left(\frac{1}{\bar{V}^2} - 1\right)\left(1 + \frac{k}{\bar{V}^2}\right)^{-3} - \frac{6k}{\bar{V}^4}\left(\frac{1}{\bar{V}^2} - 1\right)\left(1 + \frac{k}{\bar{V}^2}\right)^{-2} + \frac{6}{\bar{V}^4}\left(1 + \frac{k}{\bar{V}^2}\right)^{-1} \right\} \tag{F13}$$

$$\frac{d\varphi}{d\bar{V}} = \frac{4}{\beta r \bar{V}^3 \frac{L}{D}\left(1 + \frac{k}{\bar{V}^2}\right)} \left[1 + \frac{(1 - \bar{V}^2)k}{\bar{V}^2 + k}\left(\frac{2k}{\bar{V}^2 + k} - 1\right) \right] \tag{F14}$$

Higher order approximations may be obtained. If this degree of approximation is accepted, equation (F2) for G becomes

$$G = \frac{1 - \bar{V}^2}{F \frac{C_L}{C_R}} \tag{F15}$$

where

$$F = 1 + \frac{k}{\bar{V}^2 + k} \left[1 + \frac{(1 - \bar{V}^2)k}{\bar{V}^2 + k}\left(\frac{2k}{\bar{V}^2 + k} - 1\right) \right] \tag{F16}$$

With G known, ρ can be determined from equation (5), and this is the result given in table I.

From equations (19) and (F12)

$$\varphi = -\frac{2H}{\beta r \bar{V}^2 \frac{L}{D}} \tag{F17}$$

where

$$H = \frac{1}{1 + \frac{k}{\bar{V}^2}} \left[1 - \frac{k(1 - \bar{V}^2)}{\bar{V}^2 + k} \right] \tag{F18}$$

From equation (F1), by use of equations (3) and (F14),

$$\frac{V}{g}\frac{d\varphi}{d\tau} = -\frac{F-1}{F}(1-\overline{V}^2) \qquad \text{(F19)}$$

which is the result given in column 6 of table I.

APPENDIX G

COMPARISON WITH OTHER ANALYSES

The results of reference 4 are essentially for a three-dimensional stagnation point, or $j = 1$ in equation (7a). The result of column 10 of table I for constant angle of attack for a three-dimensional stagnation point can be written in the modified form

$$\dot{q} = \sqrt{2}\ 14.9\sqrt{g}\ \frac{\sqrt{\frac{m}{C_D R_N A}}}{\sqrt{L/D}}\ \frac{\sqrt{1 - \bar{V}^2}}{\sqrt{F}}\ \bar{V}^2 \tag{G1}$$

From equation (36) of reference 4 for Earth, and in the nomenclature of this report,

$$\bar{\dot{q}} = \frac{\dot{q}}{590\sqrt{\frac{m}{C_D R_N A}}} \tag{G2}$$

Substituting equation (G1) in (G2) gives

$$\bar{\dot{q}} = 0.202\ \frac{\sqrt{1 - \bar{V}^2}\ \bar{V}^2}{\sqrt{F\ \frac{L}{D}}} \tag{G3}$$

The equation from column 15 of table I for a three-dimensional nose is, in modified form,

$$q = \sqrt{2}\ 12.05\times10^3\sqrt{g}\ \sqrt{F\ \frac{L}{D}}\sqrt{\frac{m}{C_D R_N A}}\left[\frac{\arcsin \bar{V} - \bar{V}\sqrt{1 - \bar{V}^2}}{2}\right]_{\bar{V}_2}^{\bar{V}_1} \tag{G4}$$

From equation (39a) of reference 4, and in the nomenclature of this report,

$$\bar{q} = \frac{q}{15{,}900\sqrt{\frac{m}{C_D R_N A}}} \tag{G5}$$

Evaluating (G4) for $\bar{V}_1 = 0.99$ and $\bar{V}_2 = 0$, the values used in reference 4, and substituting in equation (G5) yield

$$\bar{q} = 3.91\sqrt{F\,\frac{L}{D}} \tag{G6}$$

As a point of interest, the total heat input per square foot q or $\bar{q}$ is quite sensitive to the initial velocity for this case. For example, evaluating equation (G4) from $\bar{V}_1 = 1.0$ to $\bar{V}_2 = 0$ gives for equation (G6)

$$q = 4.76\sqrt{F\,\frac{L}{D}} \tag{G7}$$

which is an increase of 22 percent over the case for $\bar{V}_1 = 0.99$. In the present calculation the term F is evaluated at the highest value of $\bar{V}$. If the flight path is divided into several parts, F is evaluated at the highest value of $\bar{V}$ in each part.

Reference 4 also presents the horizontal component of the G load, G_H. For small flight-path angles, an assumption already made in the present analysis,

$$G_H \approx G\,\frac{C_D}{C_R} \tag{G8}$$

With the result given for G in column 4 of table I for the constant α case,

$$G_H = \frac{1 - \bar{V}^2}{F\,\frac{L}{D}} \tag{G9}$$

Part of the difference in heating rate between the present analysis and reference 4 is due to the use of a slightly different value of the constant in equation (7a).

REFERENCES

1. Himmel, S. C., Dugan, J. F., Jr., Luidens, R. W., and Weber, R. J.: A Study of Manned Nuclear-Rocket Missions to Mars. Paper 61-49, Inst. Aerospace Sci., Inc., 1961.

2. Luidens, Roger W.: Approximate Analysis of Atmospheric Entry Corridors and Angles. NASA TN D-590, 1961.

3. Chapman, Dean R.: An Analysis of the Corridor and Guidance Requirements for Supercircular Entry into Planetary Atmospheres. NASA TR R-55, 1960.

4. Chapman, Dean R.: An Approximate Analytical Method for Studying Entry into Planetary Atmospheres. NASA TR R-11, 1959. (Supersedes NACA TN 4276.)

5. Eggers, Alfred J., Jr., Allen, H. Julian, and Neice, Stanford E.: A Comparative Analysis of the Performance of Long-Range Hypervelocity Vehicles. NACA TN 4046, 1957. (Supersedes NACA RM A54L10.)

6. Loh, W. H. T.: Dynamics and Thermodynamics of Re-Entry. Paper presented at 4th U. S. Symposium on Ballistic Missiles and Space Tech., Univ. Calif., Aug. 24-27, 1959.

7. Marshall, Francis J.: Optimum Re-Entry into the Earth's Atmosphere by Use of a Variable Control Force. TR 59-515, WADC, Oct. 1959.

8. Hankey, Wilber L., Jr., Neumann, Richard D., and Flinn, Evard H.: Design Procedures for Computing Aerodynamic Heating at Hypersonic Speeds. TR 59-610, WADC, June 1960.

9. Wisniewski, Richard J.: Methods of Predicting Laminar Heat Rates on Hypersonic Vehicles. NASA TN D-201, 1959.

10. Lees, Lester: Space Technology. Lecture 6A, Eng. Extension, Univ. Calif., 1958.

11. Goodwin, Glen, Creager, Marcus O., and Winkler, Ernest L.: Investigation of Local Heat-Transfer and Pressure Drag Characteristics of a Yawed Circular Cylinder at Supersonic Speeds. NACA RM A55H31, 1956.

12. Feller, William V.: Investigation of Equilibrium Temperatures and Average Laminar Heat-Transfer Coefficients for the Front Half of Swept Circular Cylinders at a Mach Number of 6.9. NACA RM L55F08a, 1955.

13. Becker, John V., and Korycinski, Peter F.: The Surface Coolant Requirements of Hypersonic Gliders. NASA MEMO 1-29-59L, 1959.

14. Georgiev, Steven, Hidalgo, Henry, and Adams, Mac C.: On Ablating Heat Shields for Satellite Recovery. Res. Rep. 65, Avco-Everett Res. Lab., Avco Corp., July 1959.

15. Steg, Leo: Materials for Re-Entry Heat Protection of Satellites. Paper 836-59, Am. Rocket Soc., Inc., 1959.

16. Esgar, Jack B., Hickel, Robert O., and Stepka, Francis S.: Preliminary Survey of Possible Cooling Methods for Hypersonic Aircraft. NACA RM E57L19, 1958.

17. Ames Research Staff: Equations, Tables, and Charts for Compressible Flow. NACA Rep. 1135, 1953. (Supersedes NACA TN 1428.)

18 Moeckel, W. E.: Some Effects of Bluntness on Boundary-Layer Transition and Heat Transfer at Supersonic Speeds. NACA Rep. 1312, 1957. (Supersedes NACA TN 3653.)

TABLE I. - FLIGHT-

[G, C_R, C_D/C_R, $C_{L,a}$

1	2	3	4	5	6	7	8
Point functions							
Any planet							
Flight path	Constant of flight path	Altitude density, ρ, slugs/cu ft	G load, g's	Flight-path angle, θ, radians	$\frac{V}{g}\frac{dg}{dt}$	Lift coefficient, C_L	Free-stream Reynolds number, $\mu Re/l$
Modulated angle of attack; $\theta \approx 0$							
Constant altitude ρ = Constant or $\theta = 0$	$\left(\frac{g}{C_R V^2}\right) = \frac{2\mu g r^2}{W}$	$\frac{\rho V}{\mu}\frac{1}{gr}\left(\frac{g}{C_R V^2}\right)$	$\left(\frac{g}{C_R V^2}\right) V^2 C_R$	0	0	$\frac{1 - V^2}{\left(\frac{g}{C_R V^2}\right) V^2}$	$\rho V\sqrt{gr}$
[a]Constant α	(C_L), (C_D), (C_R)	$\frac{\rho V}{(C_L)_\alpha}\frac{1}{gr}\left(\frac{1 - V^2}{V^2 \rho}\right)$	$\frac{1 - V^2}{(C_L/C_R)_\alpha V}$	$-\frac{2}{gr}\frac{1}{(L/D)}\frac{H}{V^2}$	$-\frac{\gamma - 1}{\gamma}(1 - V^2)$	[b]$\left(\frac{C_L}{C_R}\right) = \frac{1 - V^2}{V^2}$	$\rho V\sqrt{gr}$
Constant σ	$(\sigma) = \frac{C_R \rho A g r V^2}{W}$	$\frac{\rho V}{C_R A}\frac{1}{gr}\frac{(\sigma)}{V^2}$	Constant	$-\frac{2}{gr}\frac{C_D}{C_R}\frac{(\sigma)}{V^2}$	$-\frac{K_\sigma}{V^2}$	[b]$\frac{C_L}{C_R} = \frac{1 - V^2 - \frac{K_\sigma}{V^2}}{(\sigma)}$	$\rho V\sqrt{gr}$
Constant q_1	$\left(\frac{qr^2}{C_R}\right) = \frac{2\mu g r^2 V^2}{W}$	$\frac{\rho V}{\mu}\frac{1}{gr}\frac{\left(\frac{qr^2}{C_R}\right)}{V^4}$	$\frac{\left(\frac{qr^2}{C_R}\right)}{V^4} C_R$	$-\frac{4}{gr} C_D \frac{\left(\frac{qr^2}{C_R}\right)}{V^4}$	$-\frac{K_1}{V^4 C}$	$\frac{\left(1 - V^2 - \frac{K_1}{V^4 C}\right) V^4}{\left(\frac{qr^2}{C_R}\right)}$	$\rho V\sqrt{gr}$
Constant free-stream Reynolds number	$\left(\frac{q}{C_R V^2}\right) = \frac{2\mu g r^2}{W}$	$\frac{\rho V}{\mu}\frac{1}{gr}\left(\frac{q}{C_R V^2}\right)\frac{1}{V}$	$\left(\frac{q}{C_R V^2}\right) V C_R$	$-\frac{C_D}{gr}\left(\frac{q}{C_R V^2}\right)\frac{1}{V}$	$-K_{Re}$	$\frac{1 - V^2 - K_{Re}}{\left(\frac{q}{C_R V^2}\right) V}$	Constant
General case	$\left(\frac{q}{C_R V^n}\right) = \frac{2\mu g r^{2-n}}{W}$	$\frac{\rho V}{\mu}\frac{1}{gr}\left(\frac{q}{C_R V^n}\right) V^{n-2}$	$\left(\frac{q}{C_R V^n}\right) V^n C_R$	$\frac{C_D(n - 2)}{gr}\left(\frac{q}{C_R V^n}\right) V^{n-2}$	$-K_n V^{n-2}$	$\frac{1 - V^2 - K_n V^{n-2}}{\left(\frac{q}{C_R V^n}\right) V^n}$	$\rho V\sqrt{gr}$
Modulated roll			Modulated roll				
Modulated roll $\cos\theta = \frac{1 - V^2 - \frac{K_R}{V^2}}{\left\lvert 1 - V_1^2 - \frac{K_R}{V_1^2}\right\rvert_1}$	(G), $(C_{L,a})$, (C_D), (C_R)	$\frac{\rho V(G)}{C_R A g r}\frac{1}{V^2}$	$\frac{\left\lvert 1 - V^2 - \frac{K_R}{V^2}\right\rvert_1}{\left(\frac{C_{L,a}}{C_R}\right)}$	$-\frac{2}{gr}\frac{C_D(G)}{C_R V^2}$	$-\frac{K_R}{V^2}$	$(C_{L,a})\cos\theta$	$\rho V\sqrt{gr}$
Auxiliary relations or definitions							
		$\frac{W}{A} = \frac{W^{1/3}\rho^{2/3}\tan^{1/3}\Lambda}{(c/d)^{2/3}}$					

[a]Where two equations are entered at one location the applicable equation is the one that yields real numbers

[b]This is an exception to the general column heading.

[c]Two-dimensional leading edge.

PATH CHARACTERISTICS

are always positive.]

9	10	11	12	13	14
Point functions			Integrated functions		
Any planet	Earth only		Any planet		
Boundary-layer edge Reynolds number, Re_1	Heating rate to leading-edge^c region for $\alpha = 0^o$ to 30^o, $\dot{q}_1/14.9(1 - \sin^2 A \cos^2\alpha)^{1/2} \cos\lambda$, Btu/(sq ft)(sec)	Heating rate to windward side for $\alpha = 0^o$ to 30^o, $\dot{q}_w/10.2\ K_c$ Btu/(sq ft)(sec)	Additional assumptions made for integrated functions	Time of flight, t, sec	Range, R, ft
Modulated angle of attack; $\theta = 0$					
$Re\left(\frac{Re_1}{Re}\right)$	$\sqrt{\frac{\rho}{\rho_{SL}}}\sqrt{\frac{1}{C_R\overline{rr}}}\ \overline{V}^6$	$\sqrt{\frac{\rho}{\rho_{SL}}}\sqrt{\lvert 1 - \overline{V}^4 \rvert}\ \overline{V}^6$	C_R, C_D/C_R, κ_1, κ_w, κ_c are constant	$\frac{1}{C_D/C_R}C_R\sqrt{\frac{\beta}{g}}\left\lvert\frac{1}{C_R\overline{rr}}\right\rvert\left(\frac{1}{\overline{V}_2} - \frac{1}{\overline{V}_1}\right)$	$\frac{1}{C_D/C_R}r\left\lvert\frac{g}{C_R\overline{rr}}\right\rvert\ln\frac{\overline{V}_1}{\overline{V}_2}$
$Re\left(\frac{Re_1}{Re}\right)$	$\sqrt{\frac{\rho}{\rho_{SL}}}\sqrt{\frac{1 - \overline{V}^4}{C_L\overline{rr}}}\ \overline{V}^6$	$\sqrt{\frac{\rho}{\rho_{SL}}}\sqrt{\frac{\lvert 1 - \overline{V}^4 \rvert}{\gamma}}\ \overline{V}^6$	γ = Constant	$\frac{1}{2}\gamma\left(\frac{\beta}{g}\right)\sqrt{\frac{\beta}{g}}\ln\left[\frac{1 + \overline{V}_1}{1 - \overline{V}_1}\cdot\frac{1 + \overline{V}_2}{1 - \overline{V}_2}\right]$ $-\frac{1}{2}\gamma\left(\frac{\beta}{g}\right)\sqrt{\frac{\beta}{g}}\ln\left[\frac{\overline{V}_1 - 1}{\overline{V}_1 + 1}\cdot\frac{\overline{V}_2 + 1}{\overline{V}_2 - 1}\right]$	$\gamma\left(\frac{\beta}{g}\right)\frac{r}{g}\ln\left[\frac{1 - \overline{V}_1^2}{1 - \overline{V}_2^2}\right]$ $-\gamma\left(\frac{\beta}{g}\right)\frac{r}{g}\ln\left[\frac{\overline{V}_1^2 - 1}{\overline{V}_2^2 - 1}\right]$
$Re\left(\frac{Re_1}{Re}\right)$	$\sqrt{\frac{\rho}{\rho_{SL}}}\sqrt{\frac{1}{C_R\overline{rr}}}\sqrt{\lvert Q \rvert}\ \overline{V}^6$	$\sqrt{\frac{\rho}{\rho_{SL}}}\sqrt{1 - \overline{V}^4 - \frac{\kappa_c}{\lvert Q \rvert}}\ \overline{V}^6$	C_R, C_D/C_R, κ_1, κ_w, κ_c are constant	$\frac{1}{C_D/C_R}\sqrt{\frac{\beta}{g}}\frac{(\overline{V}_1 - \overline{V}_2)}{\lvert Q \rvert}$	$\frac{1}{C_D/C_R}\frac{r}{g}\frac{\overline{V}_1^2 - \overline{V}_2^2}{\lvert Q \rvert}$
$Re\left(\frac{Re_1}{Re}\right)$	Approx constant	$\sqrt{\frac{\rho}{\rho_{SL}}}\sqrt{1 - \overline{V}^4 - \frac{\kappa_c}{\sqrt{Q}}}\ \overline{V}^6$	C_R, C_D/C_R, κ_1, κ_w, κ_c are constant	$\frac{1}{5}\frac{1}{C_D/C_R}C_R\sqrt{\frac{\beta}{g}}\left\lvert\frac{1}{C_R\overline{rr}}\right\rvert\left(\overline{V}_1^5 - \overline{V}_2^5\right)$	$\frac{1}{C_D/C_R}C_R\frac{r}{g}\left\lvert\frac{\overline{V}_1^4 - \overline{V}_2^4}{C_R\overline{rr}}\right\rvert$
$Re\left(\frac{Re_1}{Re}\right)$	$\sqrt{\frac{\rho}{\rho_{SL}}}\sqrt{\frac{1}{C_R\overline{rr}}}\ \overline{V}^{6+n/2}$	$\sqrt{\frac{\rho}{\rho_{SL}}}\sqrt{1 - \overline{V}^4 - \kappa_{Re}}\ \overline{V}^6$	C_R, C_D/C_R, κ_1, κ_w, κ_c are constant	$\frac{1}{C_D/C_R}C_R\sqrt{\frac{\beta}{g}}\left\lvert\frac{1}{C_R\overline{rr}}\right\rvert\ln\frac{\overline{V}_1}{\overline{V}_2}$	$\frac{1}{C_D/C_R}C_R\left\lvert\frac{r}{C_R\overline{rr}}\right\rvert(\overline{V}_1 - \overline{V}_2)$
$Re\left(\frac{Re_1}{Re}\right)$	$\sqrt{\frac{\rho}{\rho_{SL}}}\sqrt{\frac{1}{C_R\overline{rr}}}\ \overline{V}^{6+(n/2)}$	$\sqrt{\frac{\rho}{\rho_{SL}}}\sqrt{1 - \overline{V}^4 - \kappa_n\overline{V}^{6n-2}}\ \overline{V}^6$	C_R, C_D/C_R, κ_1, κ_w, κ_c are constant	$\frac{1}{C_D/C_R}C_R\sqrt{\frac{\beta}{g}}\left\lvert\frac{1}{C_R\overline{rr}}\right\rvert\frac{1}{1 - n}\left[\overline{V}_1^{1-n} - \overline{V}_2^{1-n}\right]$ $(n \neq 1)$	$\frac{1}{C_D/C_R}C_R\left\lvert\frac{r}{C_R\overline{rr}}\right\rvert(2 - n)\left[\overline{V}_1^{2-n} - \overline{V}_2^{2-n}\right]$ $n \neq 2$
Modulated roll					
$Re\left(\frac{Re_1}{Re}\right)$	$\sqrt{\frac{\rho}{\rho_{SL}}}\sqrt{\frac{1}{C_R\overline{rr}}}\sqrt{\lvert Q \rvert}\ \overline{V}^6$	$\sqrt{\frac{\rho}{\rho_{SL}}}\sqrt{\lvert Q \rvert\left(\frac{C_{L_\alpha}\alpha}{C_R}\right)}\ \overline{V}^6$	None	$\frac{1}{C_D/C_R}\sqrt{\frac{\beta}{g}}\frac{(\overline{V}_1 - \overline{V}_2)}{\lvert Q \rvert}$	$\frac{1}{C_D/C_R}\frac{r}{g}\frac{\overline{V}_1^2 - \overline{V}_2^2}{\lvert Q \rvert}$
Auxiliary relations or definitions					
	$\frac{\rho}{\rho_{SL}} = e^{\beta r}$	$\frac{w}{A} = \frac{w^{1/3}\rho^{2/3}\tan^{1/3}\Lambda}{(c/d)^{2/3}}$ $\kappa_c = \left[1 + \frac{A_f C_{L_\alpha}}{A(\gamma + 1)\sin^2\alpha\cos\alpha}\right]^{-1/2}$			

TABLE I. - Concluded.

[G, C_R, C_D/C_R, $C_{L,a}$

1	15	16
	Functions integrated over the flight path	
	Earth only	
Flight path	Heat input per square foot to leading-edge[c] region for $\alpha \approx 0^\circ$ to 30°, $q_1/12.1\times10^3(1 - \sin^2 \Lambda \cos^2\alpha)^{V/2} \cos \lambda$, Btu/sq ft	Heat input per square foot to windward side for $\alpha \approx 0^\circ$ to 30°, $q_W/R\ 2\times10^{-3}\ k_c$, Btu/sq ft
	Modulated angle of attack; $\theta = 0$	
Constant altitude ρ = Contant or $\gamma = 0$	$\sqrt{\frac{W}{R_N A}}\frac{1}{\frac{C_D}{C_R}C_R}\frac{1}{\sqrt{\left\{\frac{G}{C_R \nabla^2}\right\}}}\left[\frac{\nabla_1^2 - \nabla_2^2}{2}\right]$	$\sqrt{\frac{W}{\lambda x}}\frac{1}{\frac{C_D}{C_R}C_R\left\{\frac{G}{C_R\nabla^2}\right\}}\left[\frac{\nabla}{2}\sqrt{1-\nabla^2}+\frac{1}{2}\arcsin\nabla\right]_{\nabla_2}^{\nabla_1}$ $\sqrt{\frac{W}{\lambda x}}\frac{1}{\frac{C_D}{C_R}C_R\left\{\frac{G}{C_R\nabla^2}\right\}}\left[\frac{\nabla}{2}\sqrt{\nabla^2-1}-\frac{1}{2}\ln\left(\nabla+\sqrt{\nabla^2-1}\right)\right]_{\nabla_2}^{\nabla_1}$
[d]Constant α	$\sqrt{\frac{W}{C_D R_N A}}\sqrt{P\left\|\frac{L}{D}\right\|}\left[-\frac{\nabla}{2}\sqrt{1-\nabla^2}+\frac{1}{2}\arcsin\nabla\right]_{\nabla_2}^{\nabla_1}$ $\sqrt{\frac{W}{C_D R_N A}}\sqrt{P\left\|\frac{L}{D}\right\|}\left[\frac{\nabla}{2}\sqrt{\nabla^2-1}+\frac{1}{2}\ln\left(\nabla+\sqrt{\nabla^2-1}\right)\right]_{\nabla_2}^{\nabla_1}$	$\sqrt{\frac{W}{\lambda x}}\left\|\left(\frac{L}{D}\right)\right\|\left[-\frac{\nabla}{2}\sqrt{1-\nabla^2}+\frac{1}{2}\arcsin\nabla\right]_{\nabla_2}^{\nabla_1}$ $\sqrt{\frac{W}{\lambda x}}\left\|\left(\frac{L}{D}\right)\right\|\left[\frac{\nabla}{2}\sqrt{\nabla^2-1}+\frac{1}{2}\ln\left(\nabla+\sqrt{\nabla^2-1}\right)\right]_{\nabla_2}^{\nabla_1}$
Constant G	$\sqrt{\frac{W}{R_N A}}\frac{1}{\frac{C_D}{C_R}C_R^{1/2}}\frac{1}{\sqrt{(G)}}\left[\frac{\nabla_1^3 - \nabla_2^3}{3}\right]$	$\sqrt{\frac{W}{\lambda x}}\frac{1}{(G)\frac{C_D}{C_R}}\left[\frac{1-2\nabla^2}{8}\sqrt{-k_0+\nabla^2-\nabla^4}-\frac{4k_0-1}{16}\sin^{-1}\left(\frac{1-2\nabla^2}{\sqrt{1-4k_0}}\right)\right]_{\nabla_2}^{\nabla_1}$ $\sqrt{\frac{W}{\lambda x}}\frac{1}{(G)\frac{C_D}{C_R}}\left[\frac{2\nabla^2-1}{8}\sqrt{k_0-\nabla^2+\nabla^4}+\frac{4k_0-1}{16}\ln\left(\sqrt{k_0-\nabla^2+\nabla^4}+\nabla^2-\frac{1}{2}\right)\right]_{\nabla_2}^{\nabla_1}$
Constant q_1	$\sqrt{\frac{W}{R_N A}}\frac{1}{\frac{C_D}{C_R}C_R}\frac{1}{\sqrt{\left\{\frac{Q\nabla^4}{C_R}\right\}}}\left[\frac{\nabla_1^5 - \nabla_2^5}{5}\right]$	
Constant free-stream Reynolds number	$\sqrt{\frac{W}{R_N A}}\frac{1}{\frac{C_D}{C_R}C_R}\frac{1}{\sqrt{\left\{\frac{G}{C_R\nabla}\right\}}}\left[\frac{\nabla_1^{2.5} - \nabla_2^{2.5}}{2.5}\right]$	$\sqrt{\frac{W}{\lambda x}}\frac{1}{\frac{C_D}{C_R}C_R\left\{\frac{G}{C_R\nabla}\right\}}\left[-\frac{\left(1-\nabla^2-k_{Re}\right)^{3/2}}{3}\right]_{\nabla_2}^{\nabla_1}$ $\sqrt{\frac{W}{\lambda x}}\frac{1}{\frac{C_D}{C_R}C_R\left\{\frac{G}{C_R\nabla}\right\}}\left[\frac{\left(\nabla^2-1+k_{Re}\right)^{3/2}}{3}\right]_{\nabla_2}^{\nabla_1}$
General case	$\sqrt{\frac{W}{R_N A}}\frac{1}{\frac{C_D}{C_R}C_R}\frac{1}{\sqrt{\left\{\frac{G}{C_R\nabla^n}\right\}}}\left[\frac{\nabla_1^{3-(n/2)} - \nabla_2^{3-(n/2)}}{3-\frac{n}{2}}\right]$, $n\neq6$	
	Modulated roll	
Modulated roll $\cos\theta = \frac{1-\nabla^2-\frac{k_M}{\nabla^2}}{\left\|1-\nabla^2-\frac{k_M}{\nabla^2}\right\|}$	$\sqrt{\frac{W}{R_N A}}\frac{1}{\frac{C_D}{C_R}C_R^{1/2}}\frac{1}{\sqrt{(G)}}\left[\frac{\nabla_1^3 - \nabla_2^3}{3}\right]$	$\sqrt{\frac{W}{\lambda x}}\left(\left\{\frac{C_{L,a}}{C_D}\right\}\frac{1}{(G)\frac{C_D}{C_R}}\right)^{1/2}\left[\frac{\nabla_1^3 - \nabla_2^3}{3}\right]$
	Auxiliary relations or definitions	
	$\frac{W}{R_N A} = 2\rho_f$	$\frac{W}{A} = \frac{W^{1/3}\rho_f^{2/3}\tan^{1/3}\Lambda}{(c/d)^{2/3}}$

[c]Two-dimensional leading edge.

[d]Where two equations are entered at one location, the applicable equation is the one that yields real numbers.

FLIGHT-PATH CHARACTERISTICS

are always positive.]

17	18	19
Functions integrated over flight path and over vehicle		
Earth only		
Heat input to leading-edge[c] region for $\alpha = 0^\circ$ to 30°, Q_l/W, Btu/lb of vehicle gross weight (e)	Heat input to windward side for $\alpha = 0^\circ$ to 30°, Q_w/W, Btu/lb of vehicle gross weight (f)	Definitions
Modulated angle of attack; $\theta = 0$		
$\frac{q_l}{\sqrt{\frac{V}{K_N R}}\left(1 - \sin^2\Lambda \cos^2\alpha\right)^{\nu/2} \cos\lambda} \frac{-\sqrt{2}k_l \cos^{\nu-1}\Lambda}{\left(\frac{\rho_f W \tan\Lambda}{W/A}\right)^{1/2}}$	$\frac{q_w}{\sqrt{\frac{V}{Lx}}} \frac{8}{3} \frac{K_w}{\left(\frac{W}{A} W \tan\Lambda\right)^{1/4}}$	
$\frac{q_l}{\sqrt{\frac{V}{K_N R}}\left(1 - \sin^2\Lambda \cos^2\alpha\right)^{\nu/2} \cos\lambda} \frac{-\sqrt{2}k_l \cos^{\nu-1}\Lambda}{\left(\frac{\rho_f W \tan\Lambda}{W/A}\right)^{1/2}}$	$\frac{q_w}{\sqrt{\frac{V}{Lx}}} \frac{8}{3} \frac{K_w}{\left(\frac{W}{A} W \tan\Lambda\right)^{1/4}}$	$K = \frac{4}{\beta r} \frac{1}{(L/D)^2}$ $F = 1 + \frac{k}{\bar{V}^2 + k}\left[1 + \frac{(1 - \bar{V}^2)k}{\bar{V}^2 + k}\left(\frac{2k}{\bar{V}^2 + k} - 1\right)\right]$ $H = -\frac{1}{1 + \frac{k}{\bar{V}^2}}\left[1 - \frac{(1 - \bar{V}^2)k}{\bar{V}^2 + k}\right]$
$\frac{q_l}{\sqrt{\frac{V}{K_N R}}\left(1 - \sin^2\Lambda \cos^2\alpha\right)^{\nu/2} \cos\lambda} \frac{-\sqrt{2}k_l \cos^{\nu-1}\Lambda}{\left(\frac{\rho_f W \tan\Lambda}{W/A}\right)^{1/2}}$	$\frac{q_w}{\sqrt{\frac{V}{Lx}}} \frac{8}{3} \frac{K_w}{\left(\frac{W}{A} W \tan\Lambda\right)^{1/4}}$	$K_Q = \frac{4}{\beta r} (G)^2 \left(\frac{C_D}{C_R}\right)^2$
		$K_{\dot{Q}} = \frac{36}{\beta r} \left\{\frac{gV^4}{C_R}\right\}^2 \left(\frac{C_D}{C_R}\right)^2 C_R^2$
$\frac{q_l}{\sqrt{\frac{V}{K_N R}}\left(1 - \sin^2\Lambda \cos^2\alpha\right)^{\nu/2} \cos\lambda} \frac{-\sqrt{2}k_l \cos^{\nu-1}\Lambda}{\left(\frac{\rho_f W \tan\Lambda}{W/A}\right)^{1/2}}$	$\frac{q_w}{\sqrt{\frac{V}{Lx}}} \frac{8}{3} \frac{K_w}{\left(\frac{W}{A} W \tan\Lambda\right)^{1/4}}$	$K_{Re} = \frac{1}{\beta r} \left\{\frac{g}{C_R \bar{V}^n}\right\}^2 \left(\frac{C_D}{C_R}\right)^2 C_R^2$
		$K_n = \frac{(n-2)^2}{\beta r} \left\{\frac{g}{C_R \bar{V}^n}\right\}^2 \left(\frac{C_D}{C_R}\right)^2 C_R^2$
Modulated roll		
$\frac{q_l}{\sqrt{\frac{V}{K_N R}}\left(1 - \sin^2\Lambda \cos^2\alpha\right)^{\nu/2} \cos\lambda} \frac{-\sqrt{2}k_l \cos^{\nu-1}\Lambda}{\left(\frac{\rho_f W \tan\Lambda}{W/A}\right)^{1/2}}$	$\frac{q_w}{\sqrt{\frac{V}{Lx}}} \frac{\pi}{3} \frac{K_w}{\left(\frac{W}{A} W \tan\Lambda\right)^{1/4}}$	$K_M = \frac{4}{\beta r} (g_l l)^2 \left(\frac{C_D}{C_R}\right)^2$
Auxiliary relations or definitions		
$k_l = \frac{\left\{1 - \sin^2\Lambda \cos^2\alpha\right\}^{\nu/2} \left\{1 + \cos\left[\arctan\left(\frac{\tan\alpha}{\cos\Lambda}\right)\right]\right\}}{2 \cos^\nu\Lambda}$ $\left(\frac{\rho W \tan\Lambda}{W/A}\right)^{1/2} = \left(\frac{\rho}{\beta} \tan\Lambda\right)^{1/3} W^{1/3} \rho_f^{1/6}$ (see also eq. (E25))	$K_w = \left(1 + \frac{r}{c}\right)^{3/2} - \left(\frac{r}{c}\right)^{3/2} - \frac{3}{2}\left(\frac{r}{c}\right)^{1/2}$ $\frac{r}{c} = \frac{\pi}{4} \frac{R_N}{c}\left[1 + \frac{1}{\cos\Lambda} - \frac{4}{\pi} \tan^{-1} \frac{\tan\alpha}{\cos\Lambda}\right]$ $\frac{W}{A} W \tan\Lambda^{1/4} = \frac{\tan^{1/3}\Lambda}{\left(\frac{r}{c}\right)^{1/6}} W^{1/3} \rho_f^{1/6}$ (see also eq. (E24))	

[c] q_l is given by column e.

[f] q_w is given by column f.

TABLE II. - FLIGHT-PATH CHARACTERISTICS APPLICABLE TO ANY PLANET WHICH HAS AN ATMOSPHERE WITH HEAT-TRANSFER CHARACTERISTICS SIMILAR TO EARTH'S

[See also table I.]

1 Flight path	10 Heating rate to leading-edge region for $\alpha = 0^\circ$ to 30°, $\dot{q}_1[21.9\times10^{-9} g^{3/2} r \times(1 - \sin^2\lambda \cos^2\alpha)^{\nu/2} \cos\lambda]^{-1}$, Btu/(sq ft)(sec)	11 Heating rate to windward side for $\alpha = 0^\circ$ to 30°, $q_w(15.0\times10^{-9} g^{3/2} r)^{-1}$, Btu/(sq ft)(sec)	15 Heat input per square foot to leading-edge region for $\alpha = 0^\circ$ to 30°, $q_1[21.9\times10^{-9} g r^{3/2} \times(1 - \sin^2\lambda \cos^2\alpha)^{\nu/2} \cos\lambda]^{-1}$, Btu/(sq ft)	16 Heat input per square foot to windward side for $\alpha = 0^\circ$ to 30°, $q_w(15.0\times10^{-9} g r^{3/2})^{-1}$, Btu/(sq ft)	17 Heat input to leading-edge region for $\alpha = 0^\circ$ to 30°, q_1/m, Btu/slug of vehicle gross mass	18 Heat input to windward side for $\alpha = 0^\circ$ to 30°, q_w/m, Btu/slug of vehicle gross mass
Constant free-stream Reynolds number	$\sqrt{\frac{\pi}{R_N A}}\sqrt{\frac{g}{C_R \bar{V}}}\,\bar{V}^{5/2}$	$\sqrt{\frac{\pi}{A x}}\sqrt{1 - \bar{V}^2 - K_{Re}}\,\bar{V}^2$	$\sqrt{\frac{\pi}{A R_N}}\,\frac{\left[\frac{\bar{V}_1^{2.5} - \bar{V}_2^{2.5}}{2.5}\right]}{\frac{C_D}{C_R} C_R \sqrt{\frac{g}{C_R \bar{V}}}}$	$\sqrt{\frac{\pi}{A x}}\,\frac{\left[\frac{\left(1 - \bar{V}^2 - K_{Re}\right)^{3/2}}{3}\right]_{\bar{V}_2}^{\bar{V}_1}}{\frac{C_D}{C_R} C_R \sqrt{\frac{g}{C_R \bar{V}}}}$	$\frac{q_1}{\sqrt{\frac{\pi}{A R_N}}\left(1 - \sin^2\lambda \cos^2\alpha\right)^{\nu/2} \cos\lambda}\,\frac{\sqrt{2}\, k_1 \cos^{\nu-1}\lambda}{\left(\frac{\rho_1 m \tan\lambda}{m/A}\right)^{1/2}}$	$\frac{q_w}{\sqrt{\frac{\pi}{A x}}}\,\frac{8}{3}\left(\frac{\pi}{A} m \tan\lambda\right)^{1/4}$

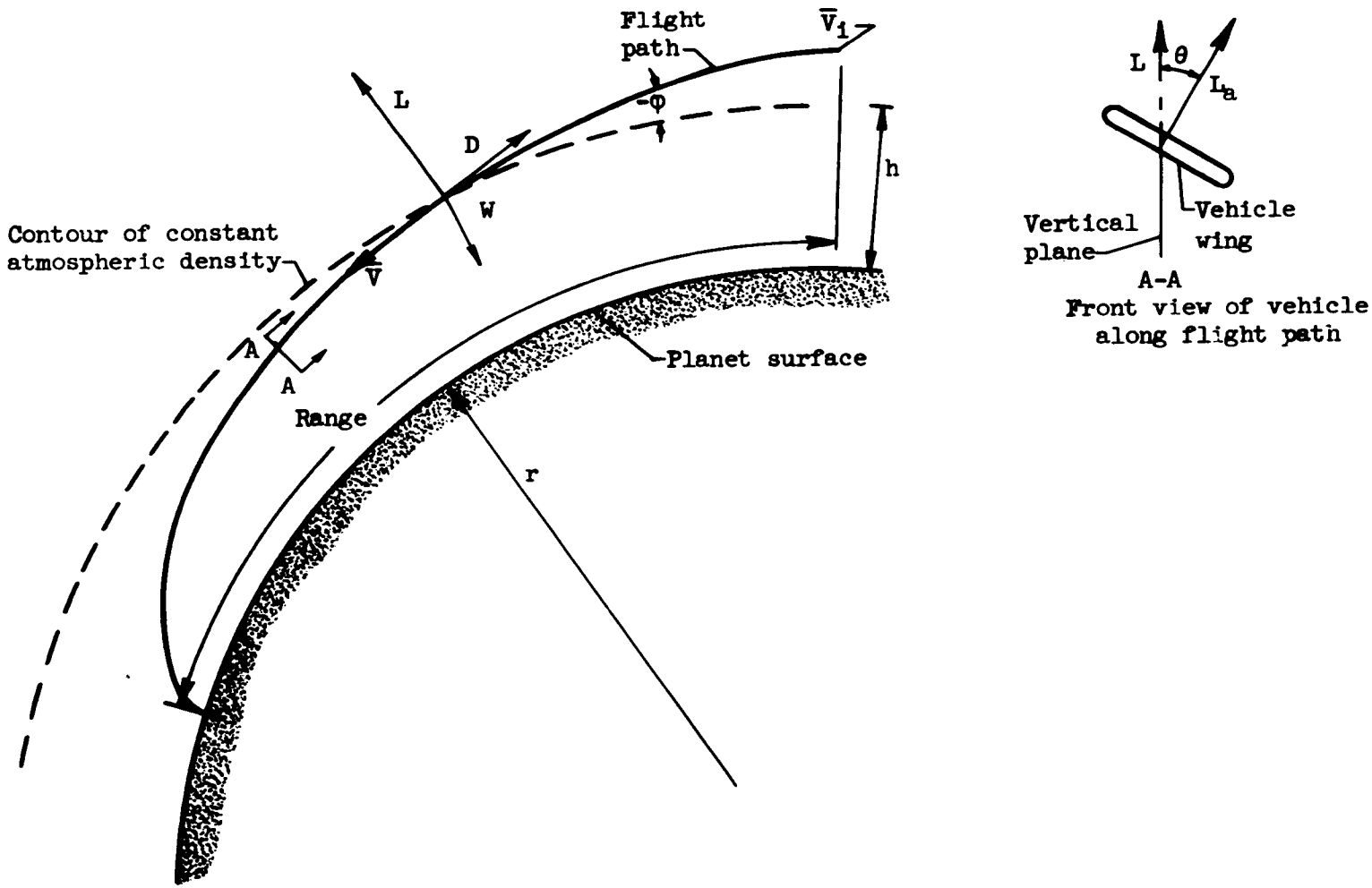

Figure 1. - Flight-path coordinate system and symbols.

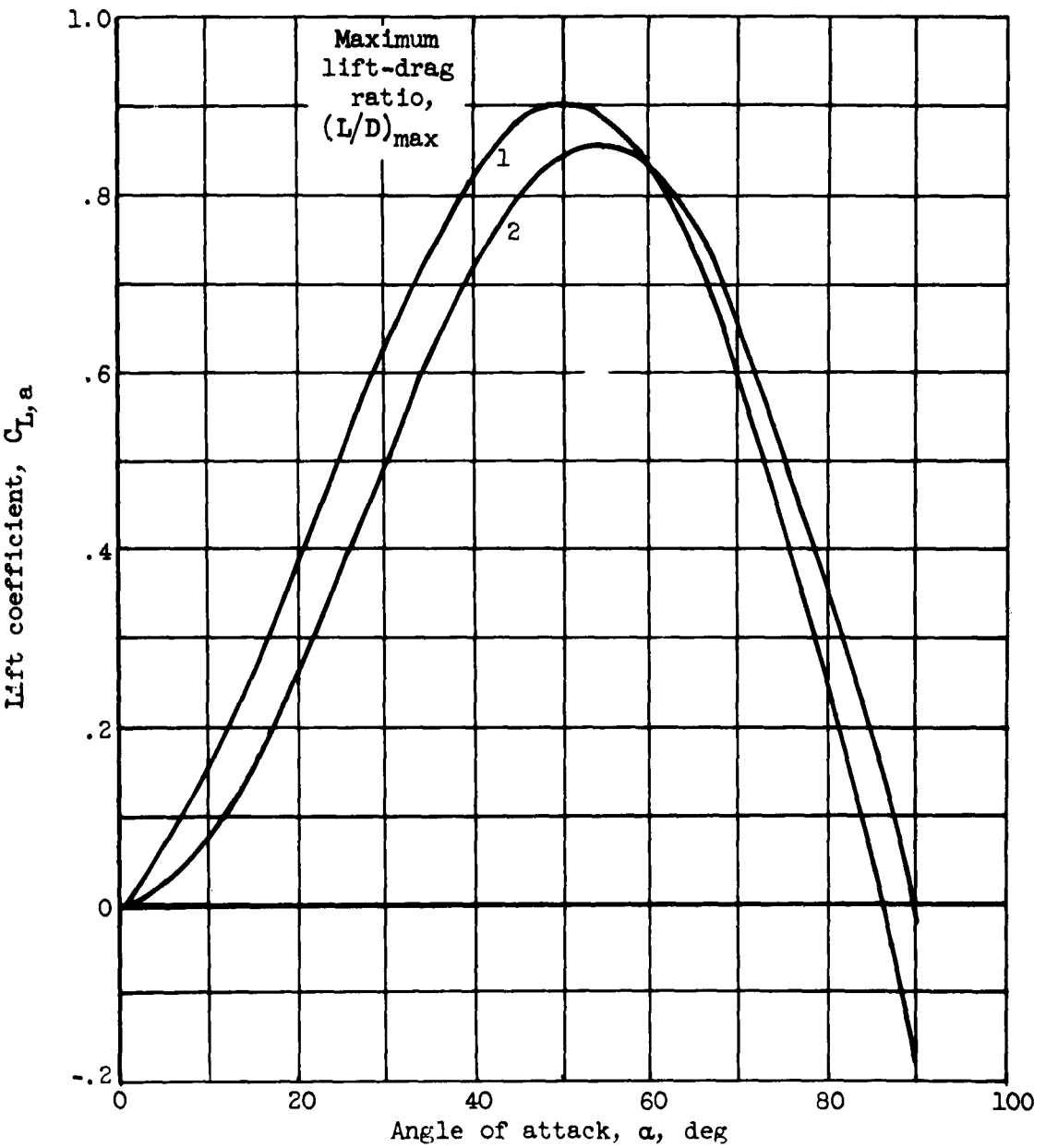

(a) Lift coefficient.

Figure 2. - Aerodynamic characteristics.

E-1001

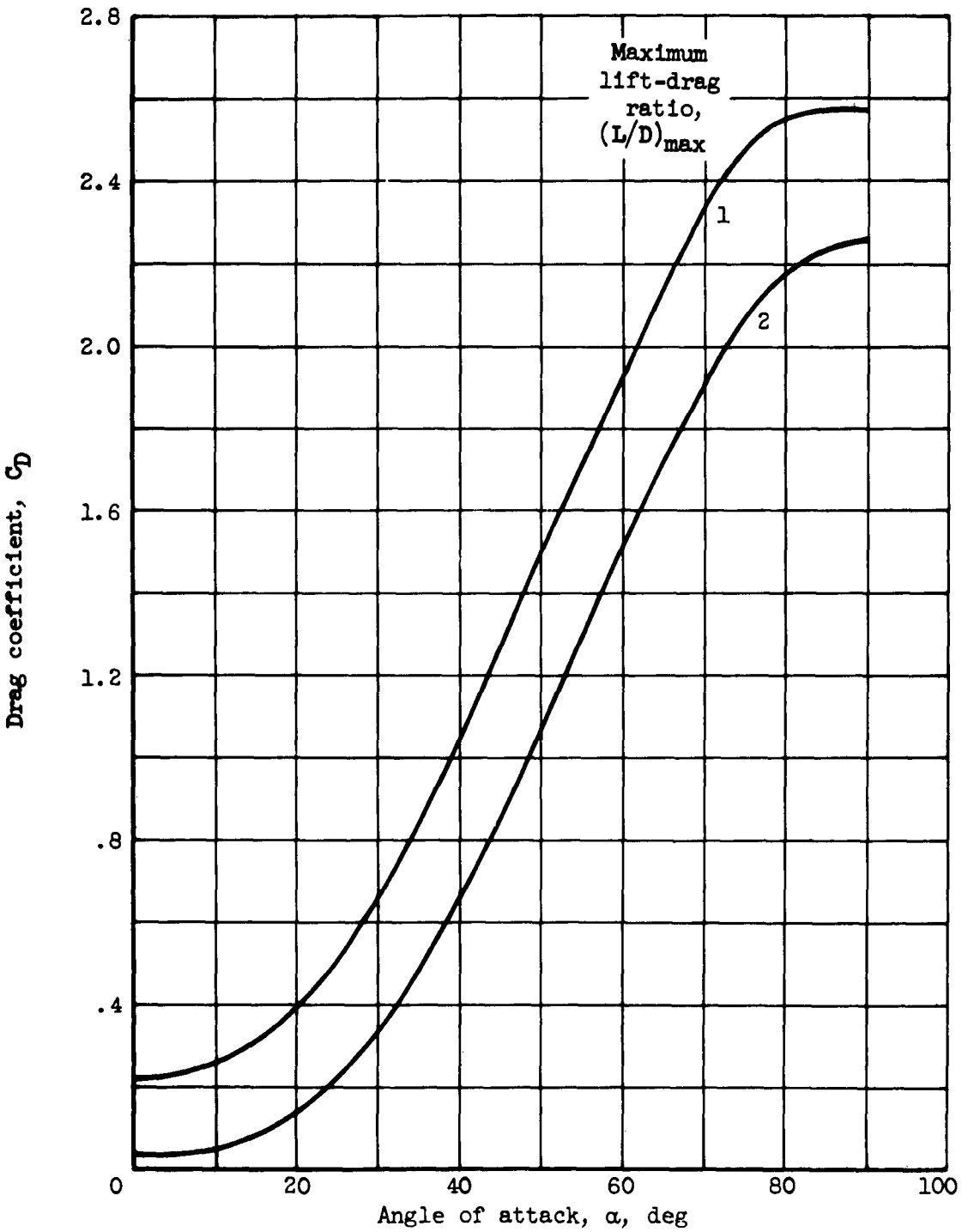

(b) Drag coefficient.

Figure 2. - Continued. Aerodynamic characteristics.

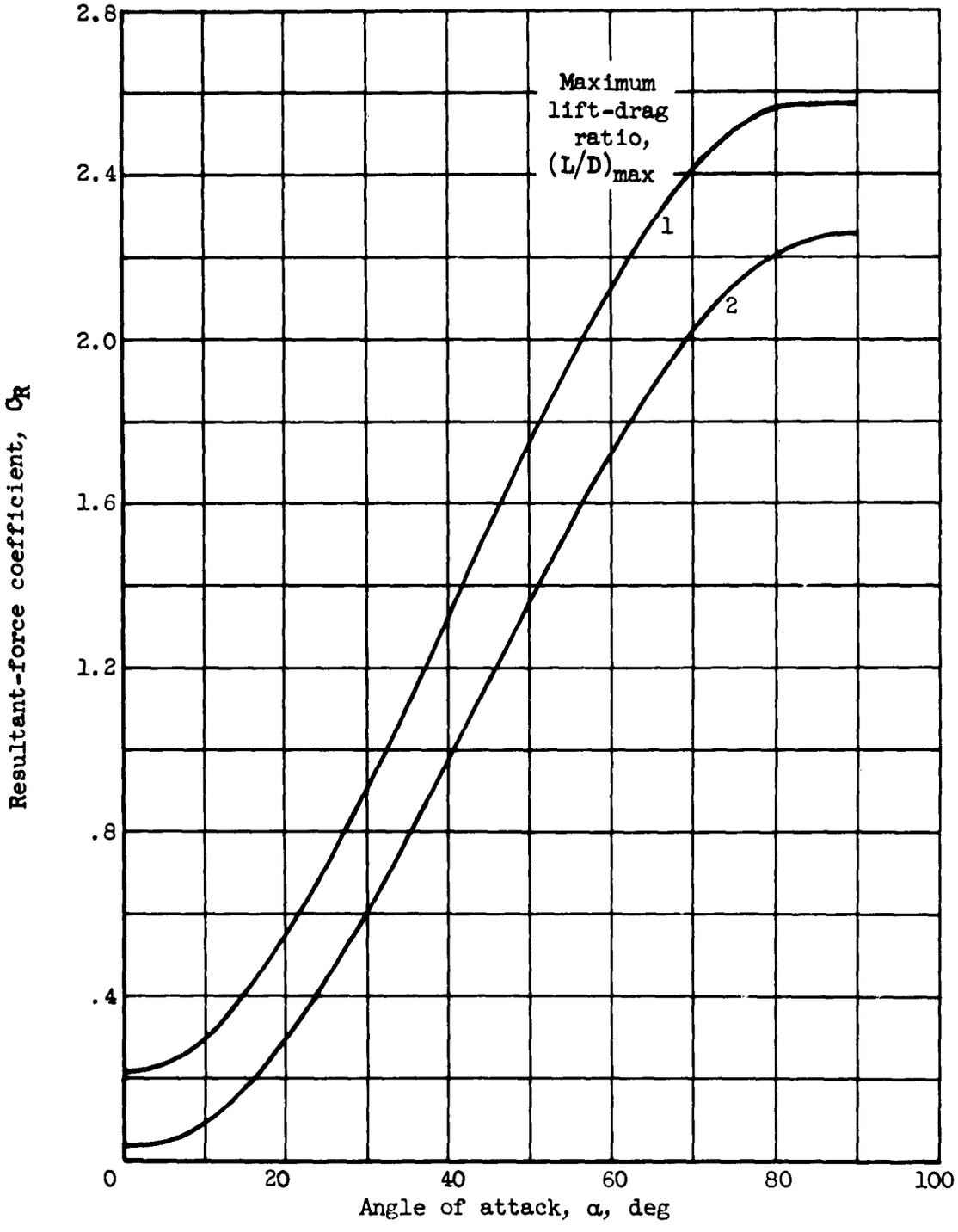

(c) Resultant-force coefficient.

Figure 2. - Continued. Aerodynamic characteristics.

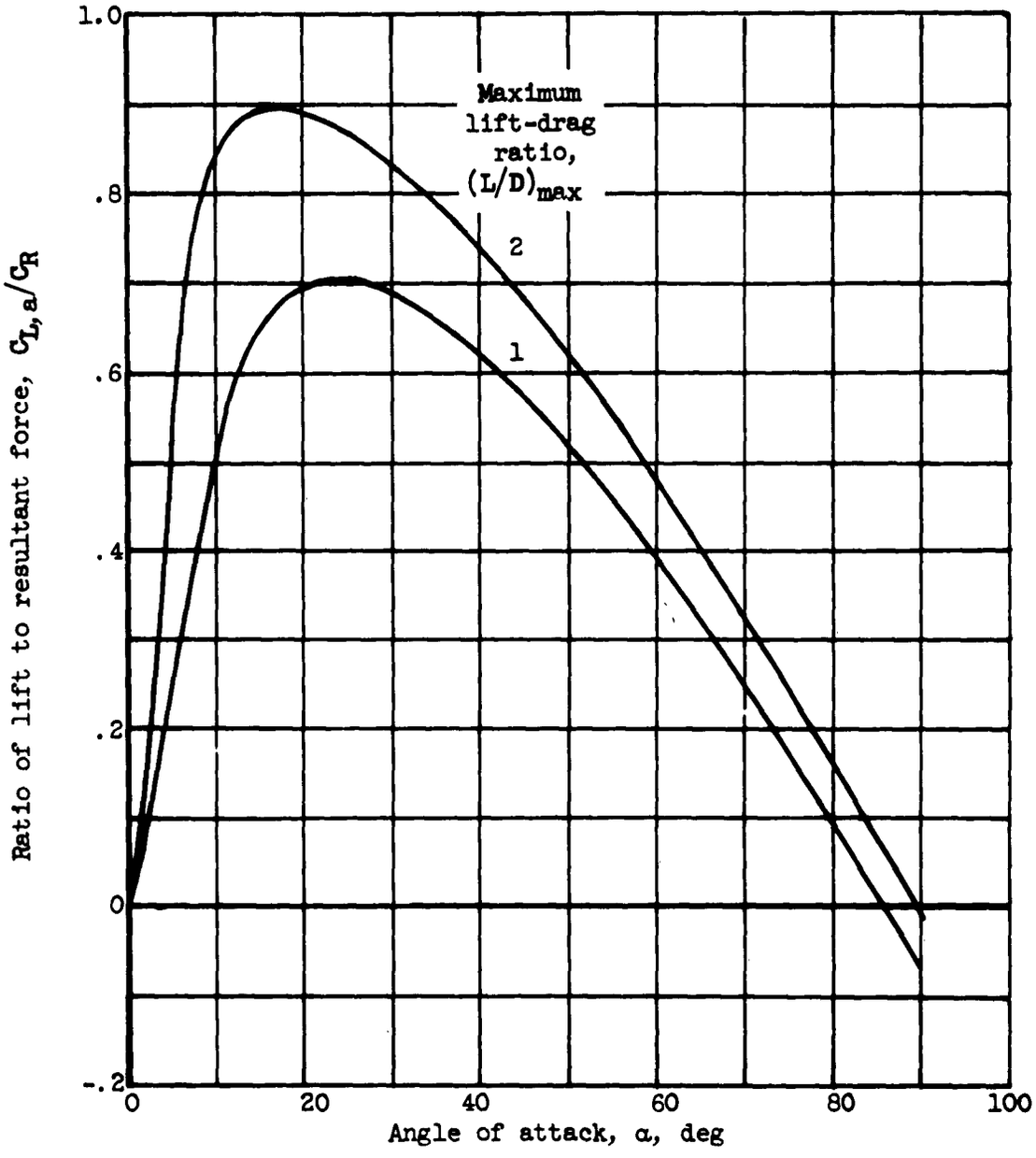

(d) Ratio of lift to resultant force.

Figure 2. - Continued. Aerodynamic characteristics.

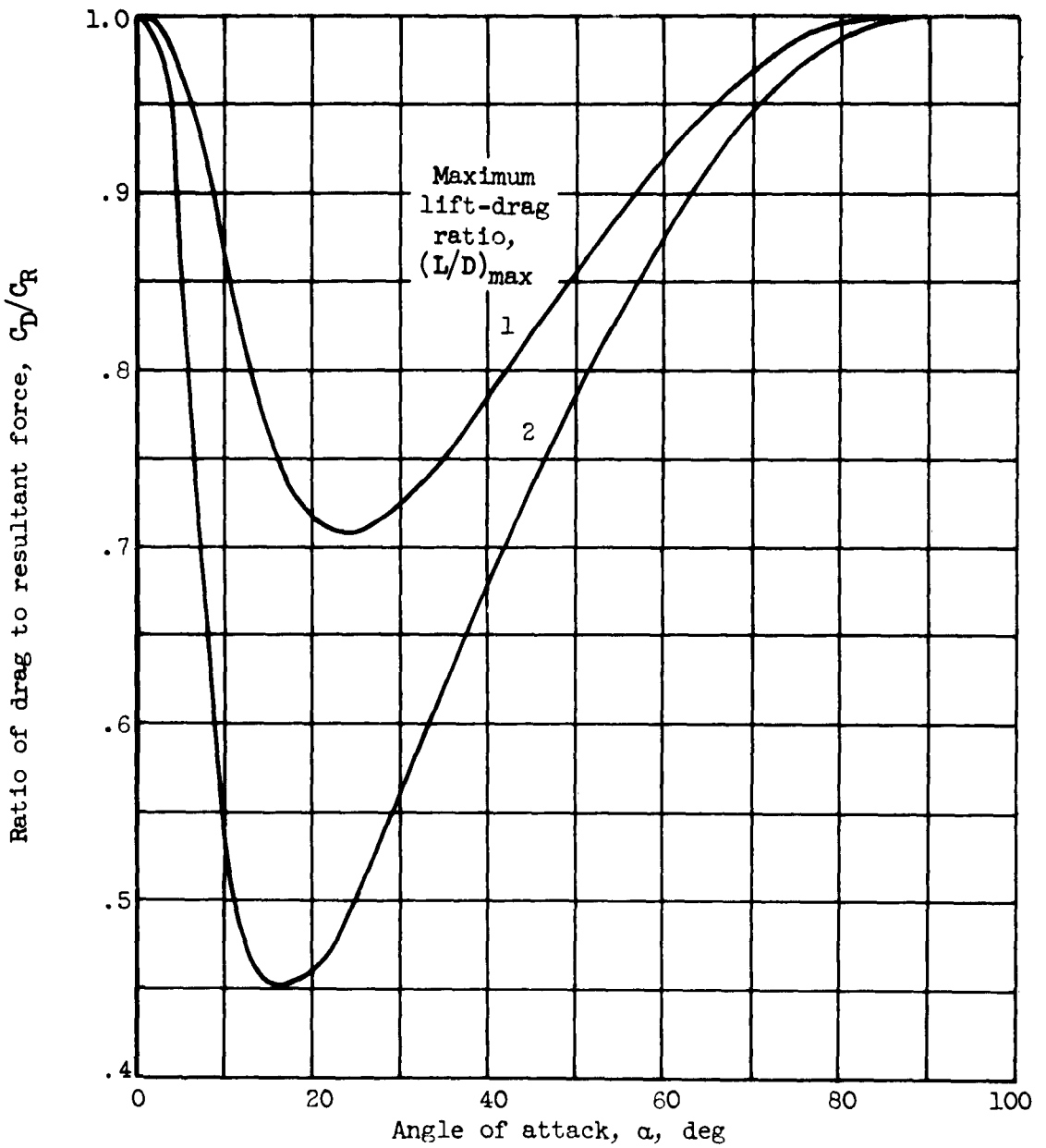

(e) Ratio of drag to resultant force.

Figure 2. - Continued. Aerodynamic characteristics.

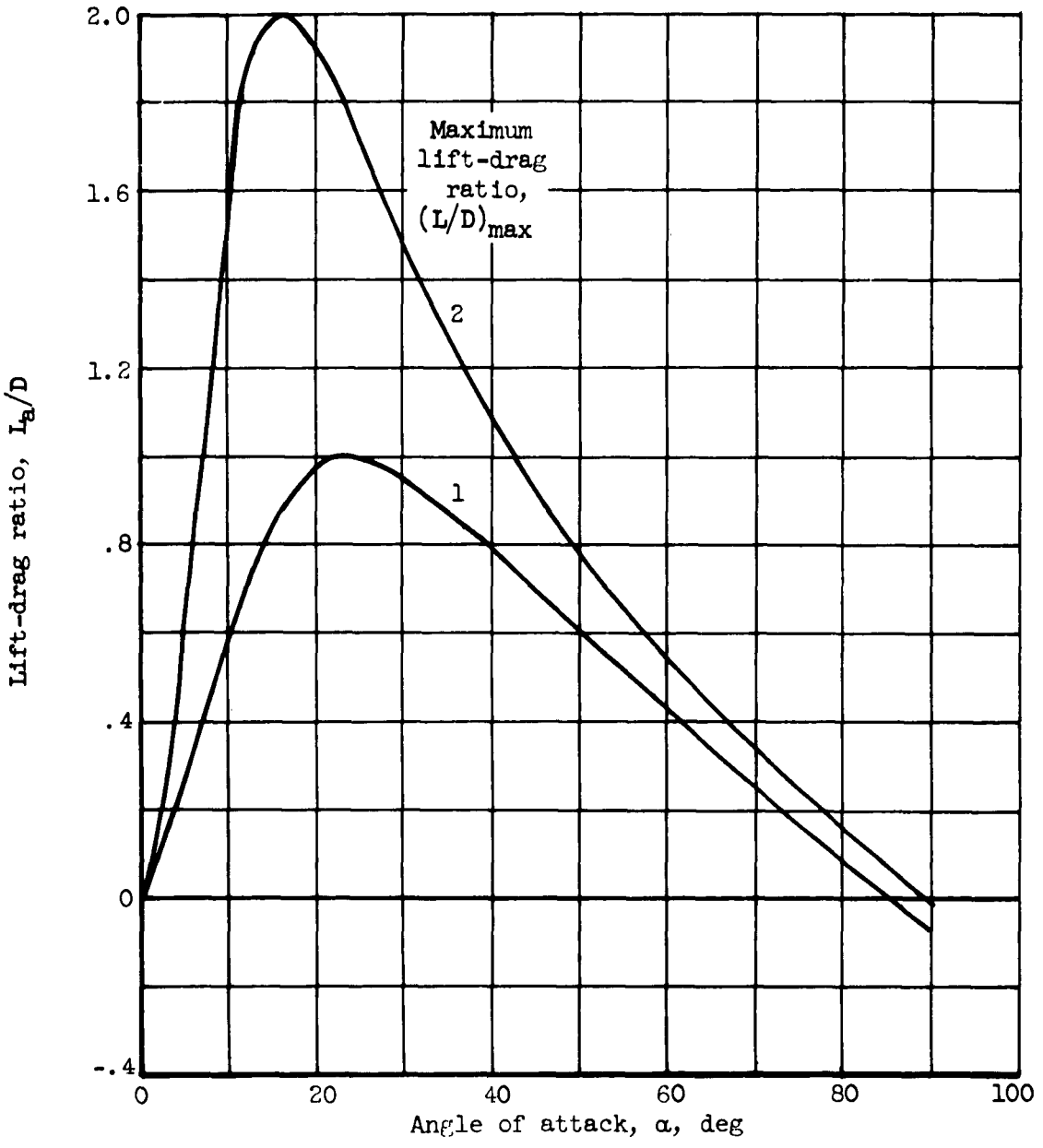

(f) Lift-drag ratio.

Figure 2. - Concluded. Aerodynamic characteristics.

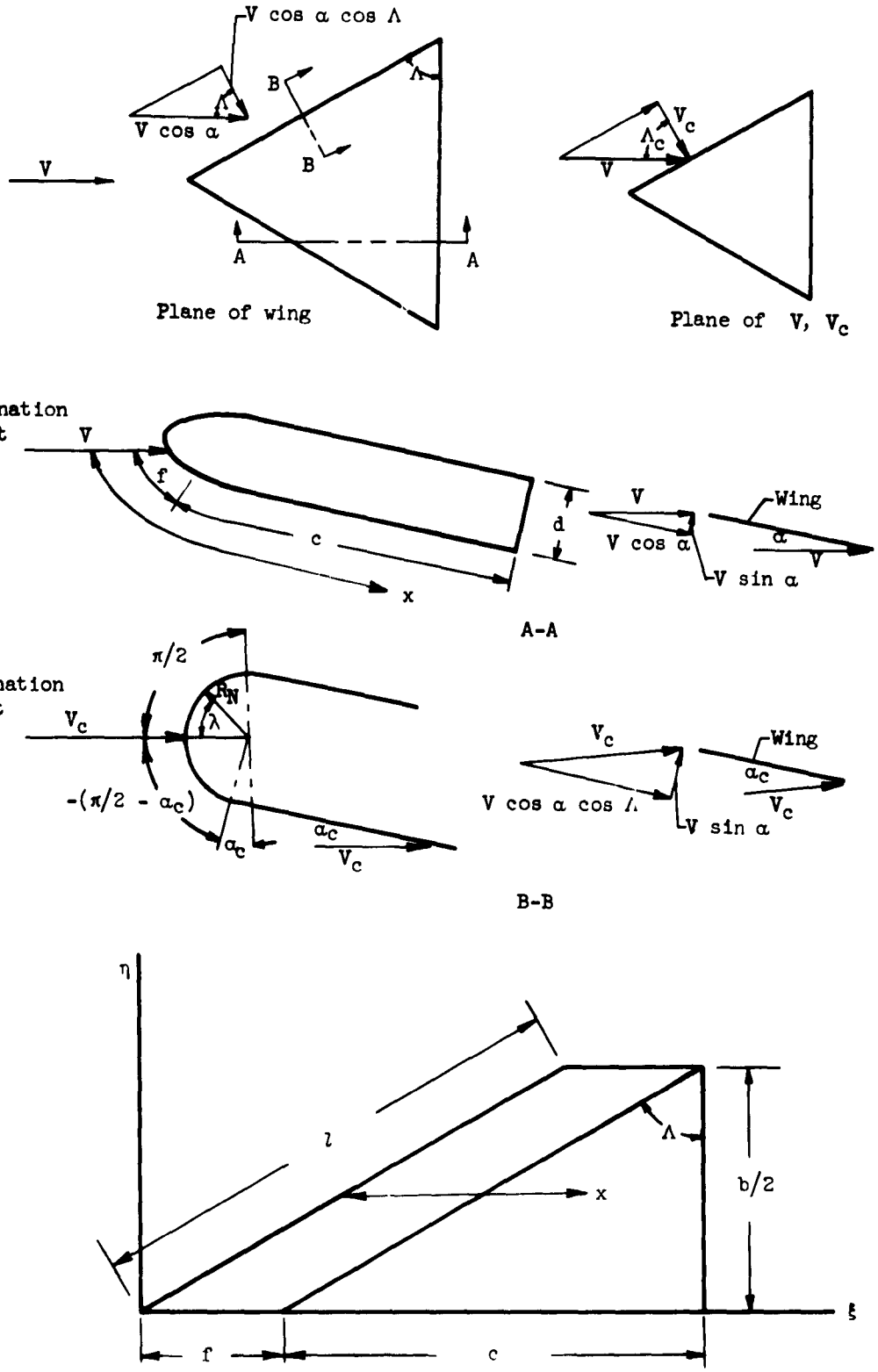

Figure 3. - Vehicle geometry, coordinate systems, and flow angles.

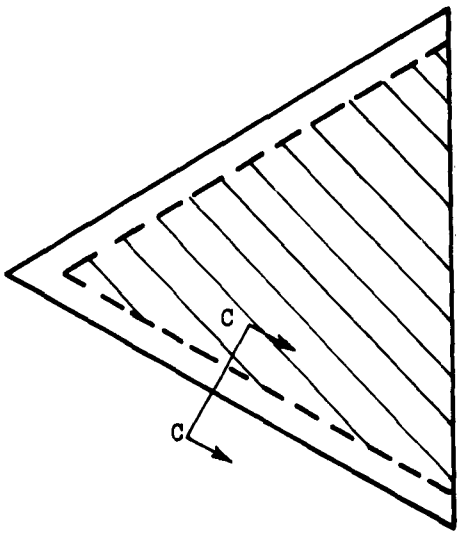

Reference area for aerodynamic coefficients and wing loading; also used for volume estimation

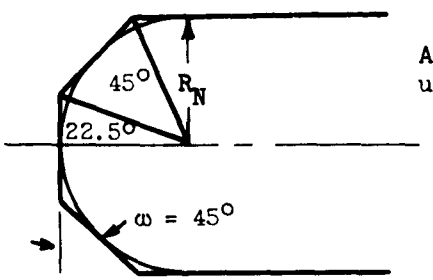

C-C

Approximation to leading edge used in aerodynamic calculations

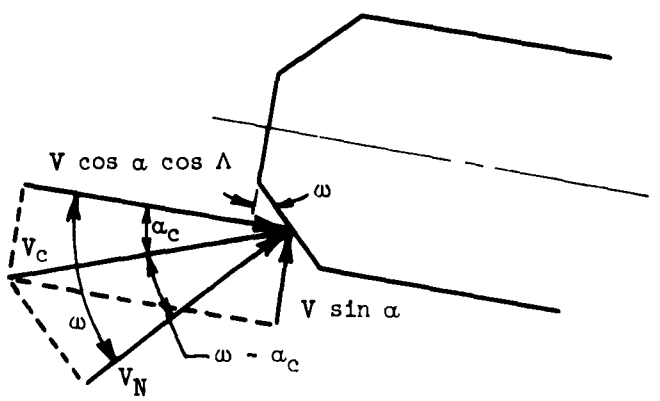

Figure 3. - Concluded. Vehicle geometry, coordinate systems, and flow angles.

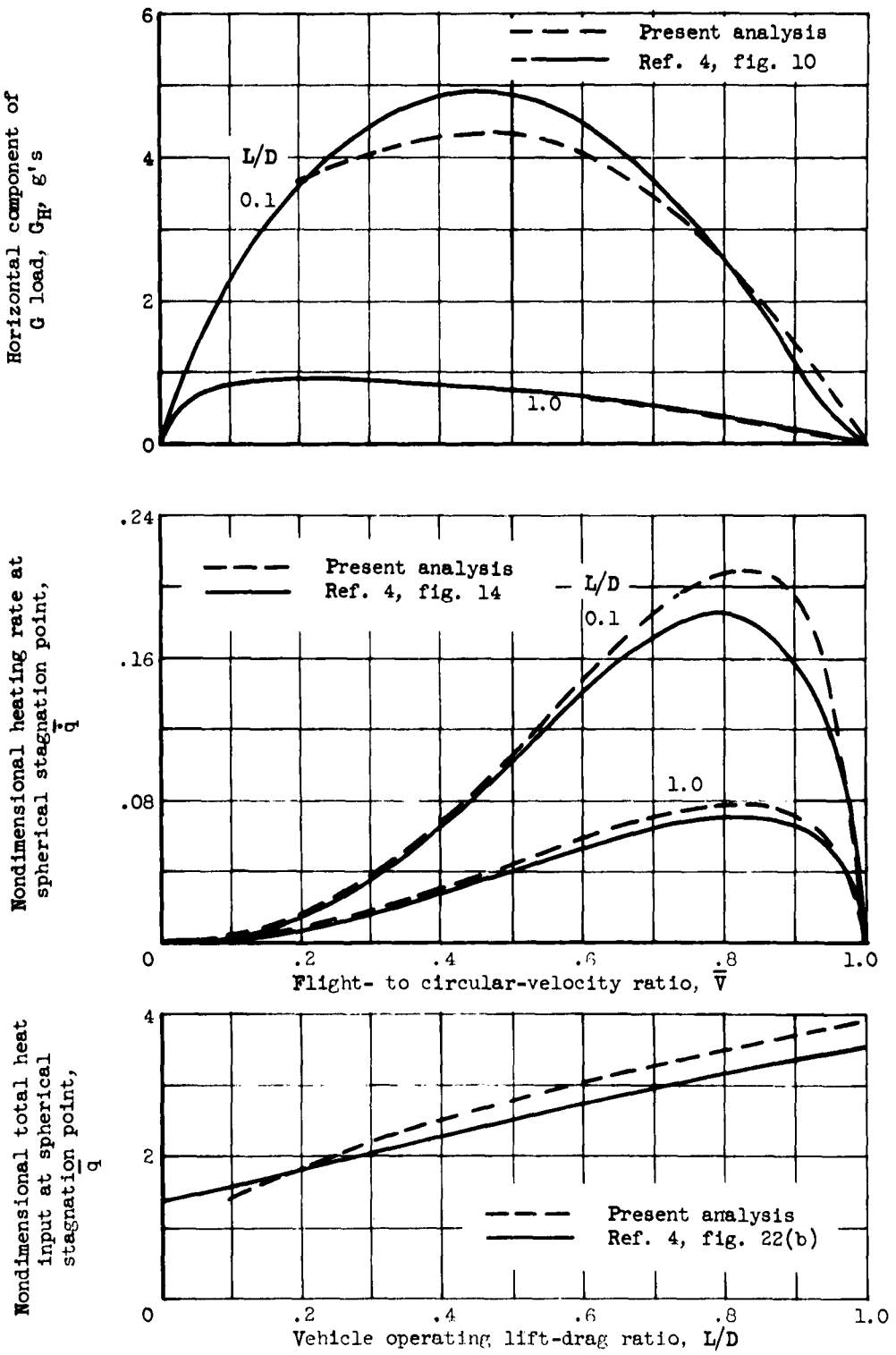

Figure 4. - Comparison of results of present analysis for stagnation-point heating with results of reference 4. Velocity ratio, 0.99 to 0; constant-angle-of-attack flight path.

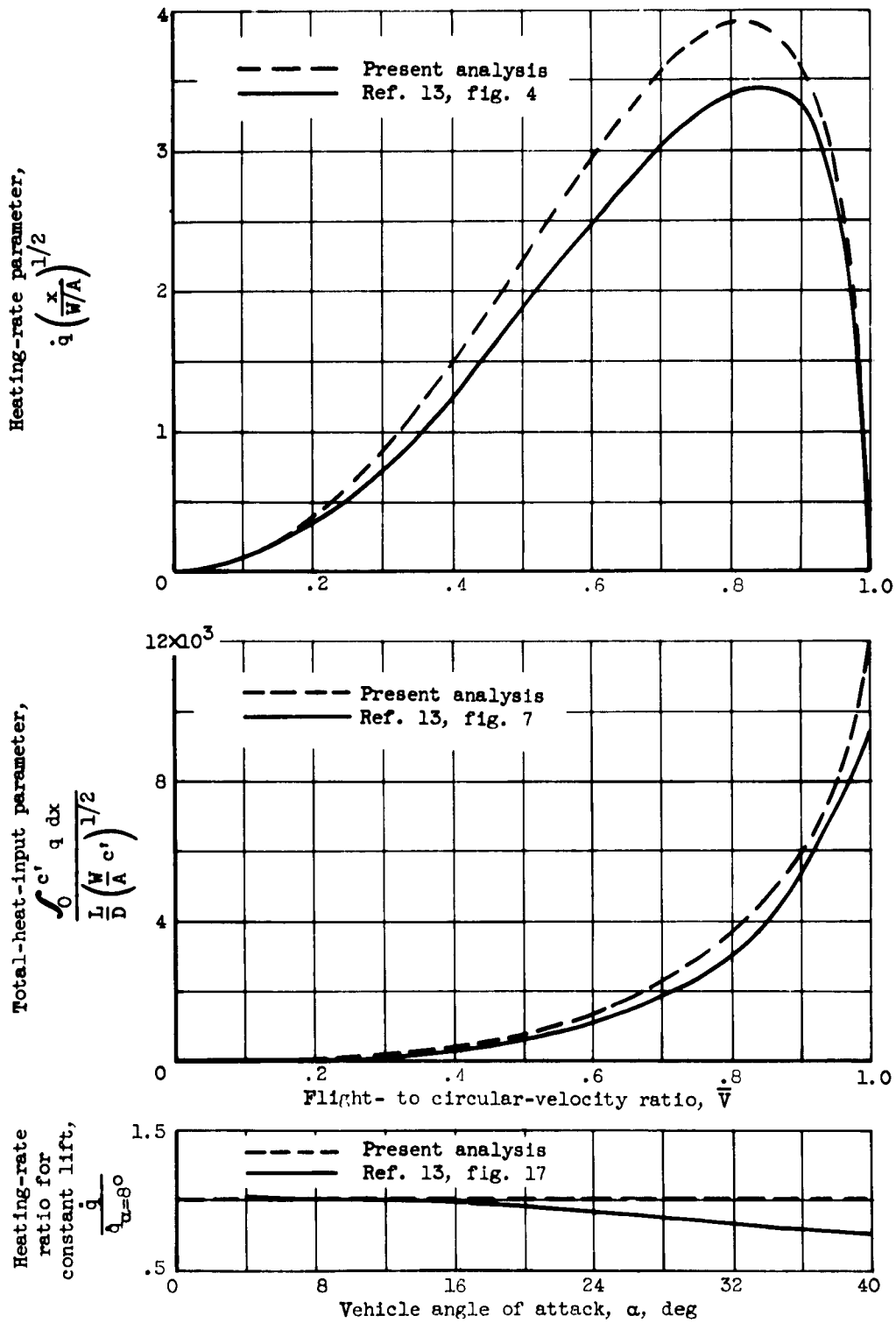

Figure 5. - Comparison of present analysis for windward-side heating with results of reference 13. Initial velocity ratio, 1.0; wall static temperature, 0° R; constant-angle-of-attack flight path.

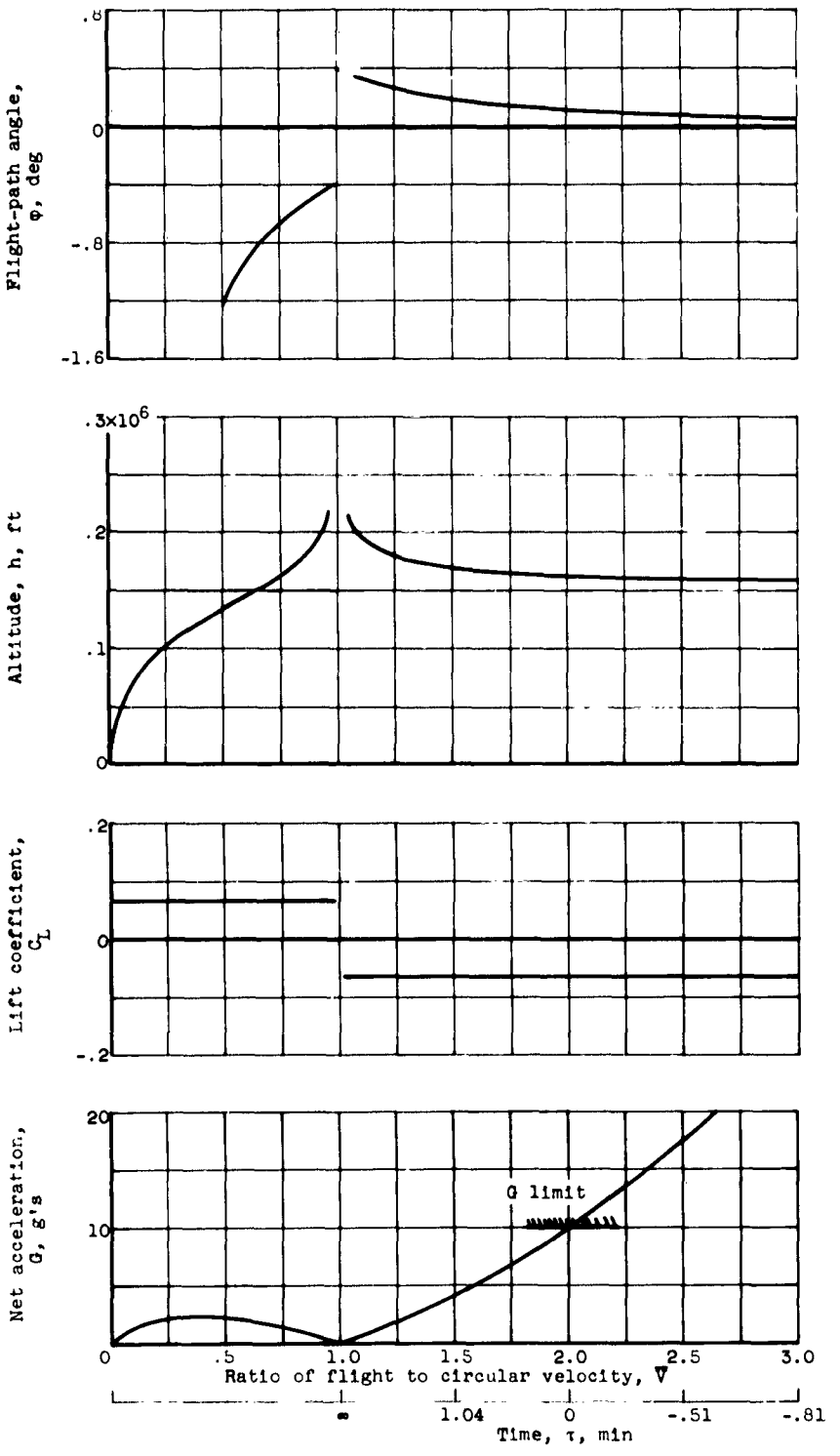

Figure 6. - Constant-angle-of-attack flight path for Earth atmosphere. Angle of attack, 5.3°; initial net acceleration, 10 g's; initial velocity ratio, 2.0; maximum lift-drag ratio, 1.0; entry vehicle gross weight, 10,000 pounds; average entry vehicle density, 20 pounds per cubic foot; geometric leading-edge sweep angle, 60°.

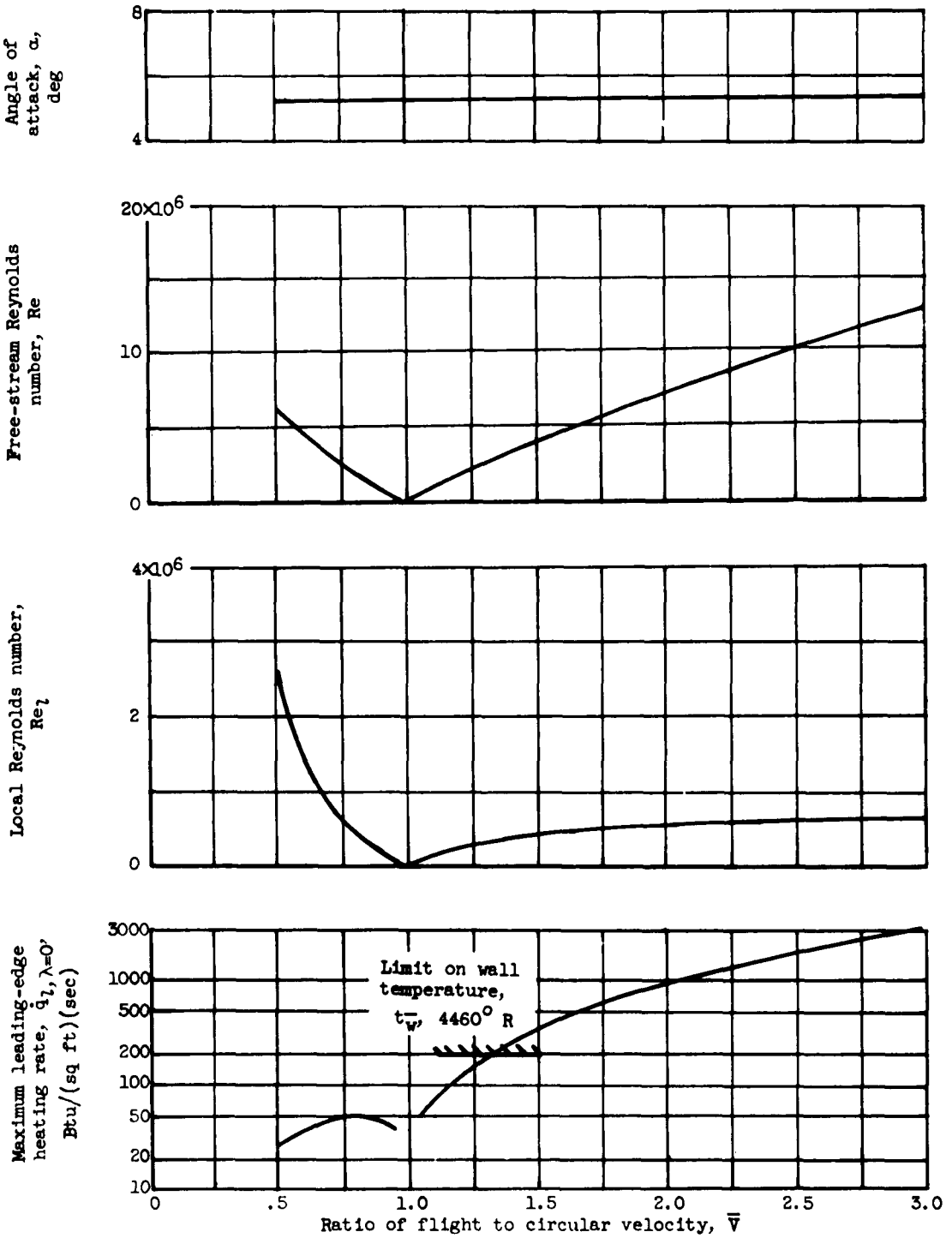

Figure 6. - Concluded. Constant-angle-of-attack flight path for Earth atmosphere. Angle of attack, 5.3°; initial net acceleration, 10 g's; initial velocity ratio, 2.0; maximum lift-drag ratio, 1.0; entry vehicle gross weight, 10,000 pounds; average entry vehicle density, 20 pounds per cubic foot; geometric leading-edge sweep angle, 60°.

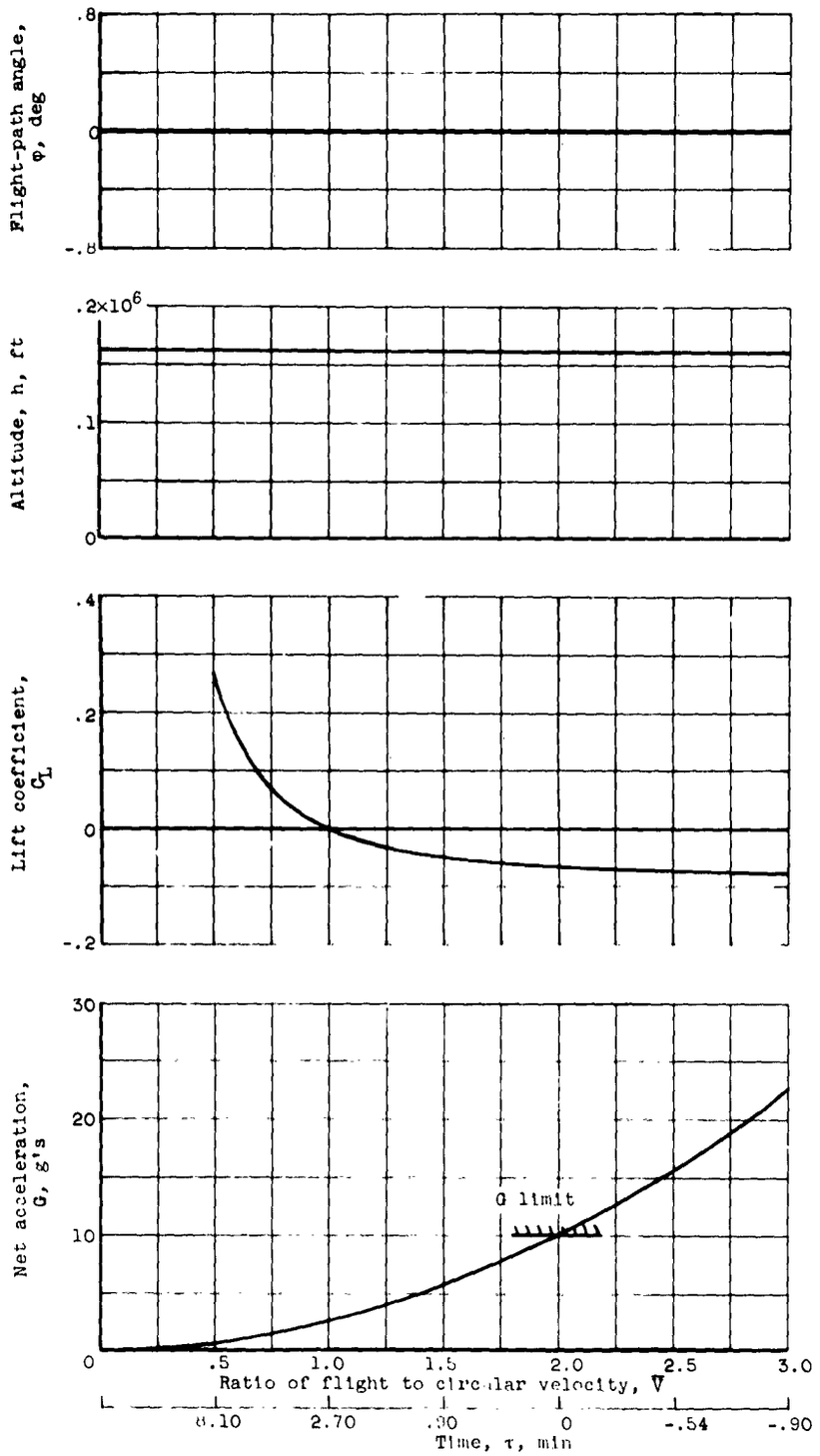

Figure 7. - Constant-altitude flight path for Earth atmosphere. Altitude, 162,000 feet; initial net acceleration, 10 g's; initial velocity ratio, 2.0; maximum lift-drag ratio, 1.0; entry vehicle gross weight, 10,000 pounds; average entry vehicle density, 20 pounds per cubic foot; geometric leading-edge sweep angle, 60°.

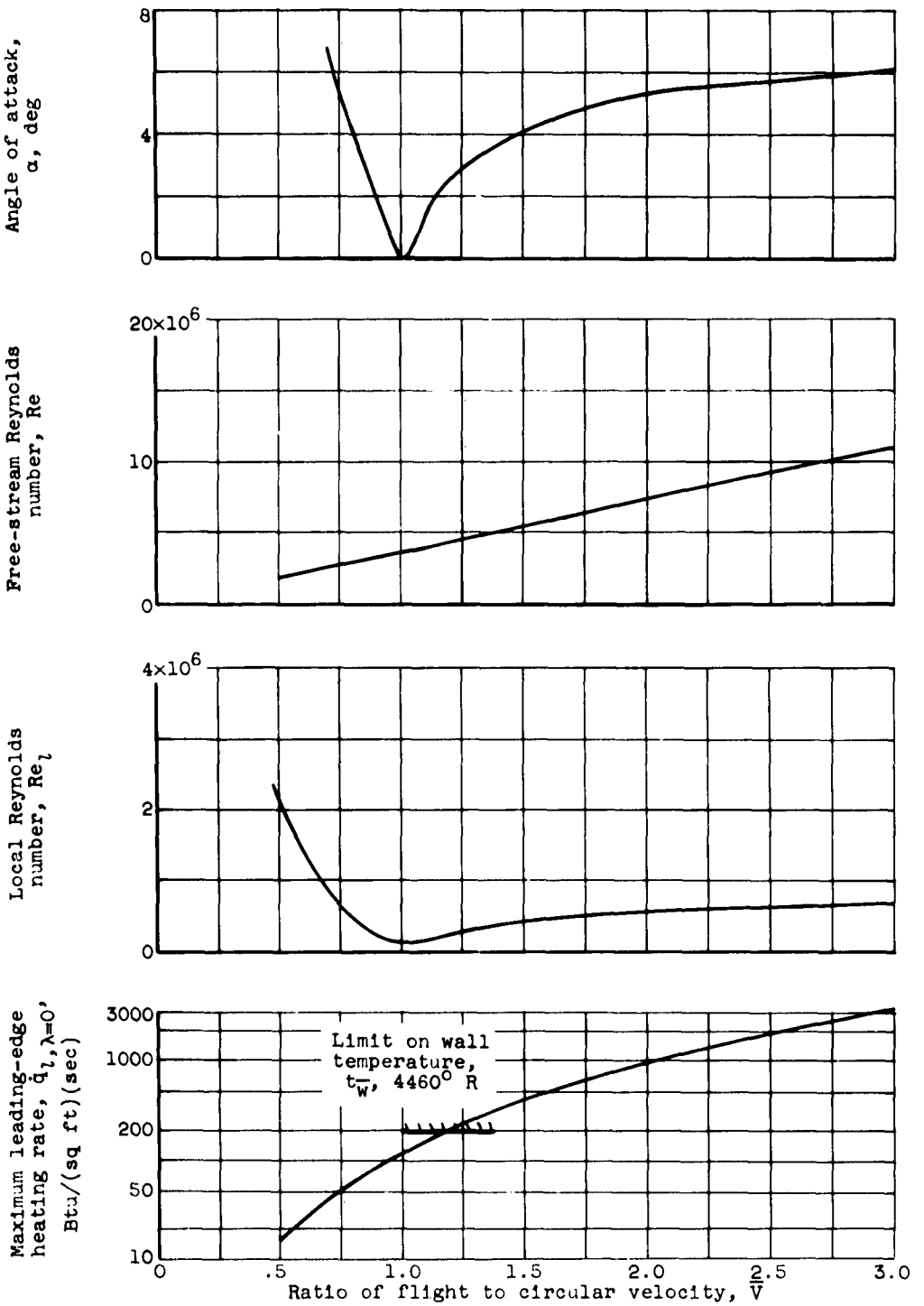

Figure 7. - Concluded. Constant-altitude flight path for Earth atmosphere. Altitude, 162,000 feet; initial net acceleration, 10 g's; initial velocity ratio, 2.0; maximum lift-drag ratio, 1.0; entry vehicle gross weight, 10,000 pounds; average entry vehicle density, 20 pounds per cubic foot; geometric leading-edge sweep angle, 60°.

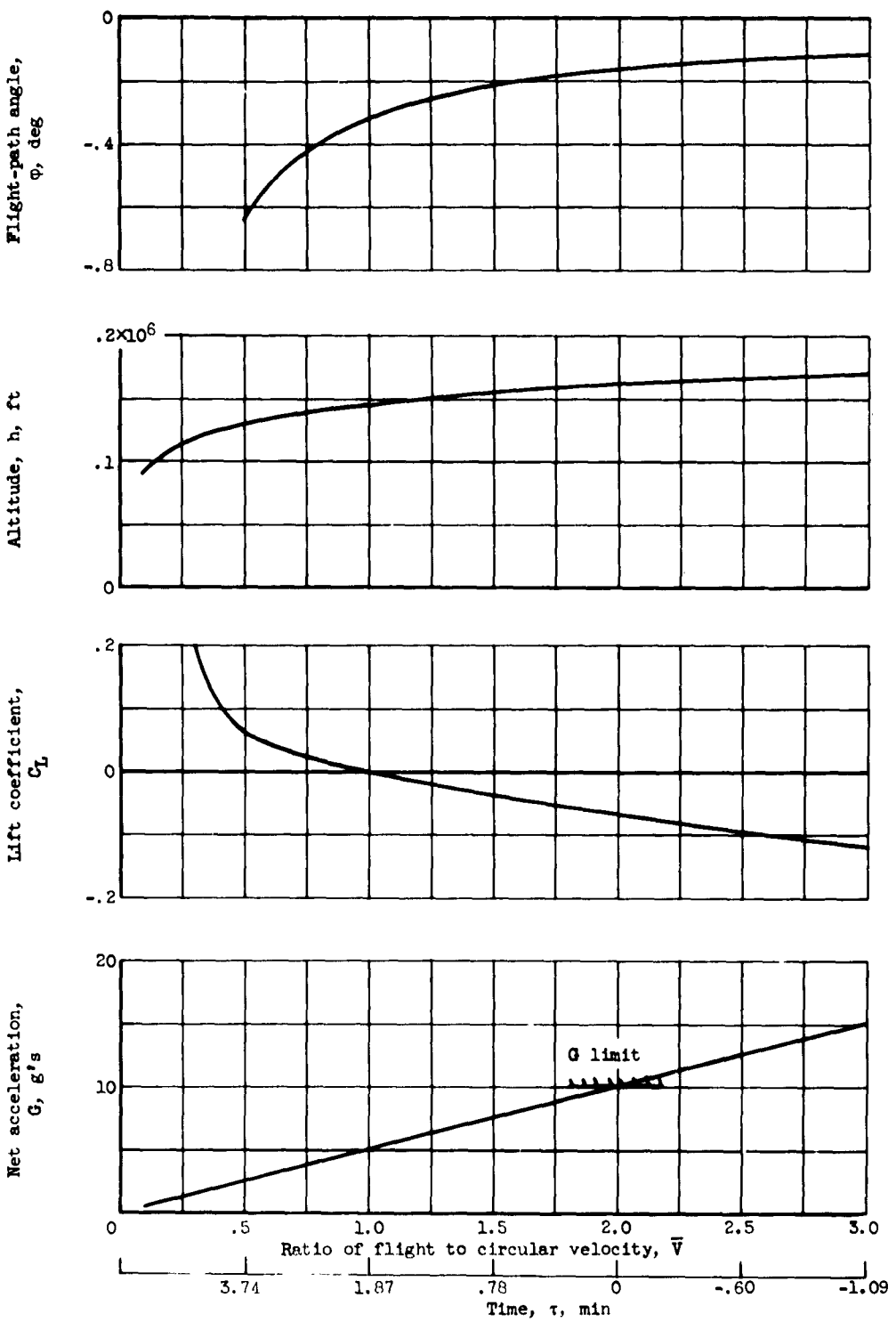

Figure 8. - Constant free-stream Reynolds number flight path for Earth atmosphere. Free-stream Reynolds number, 7.3×10^6; initial net acceleration, 10 g's; initial velocity ratio, 2.0; maximum lift-drag ratio, 1.0; entry vehicle gross weight, 10,000 pounds; average entry vehicle density, 20 pounds per cubic foot; geometric leading-edge sweep angle, 60°.

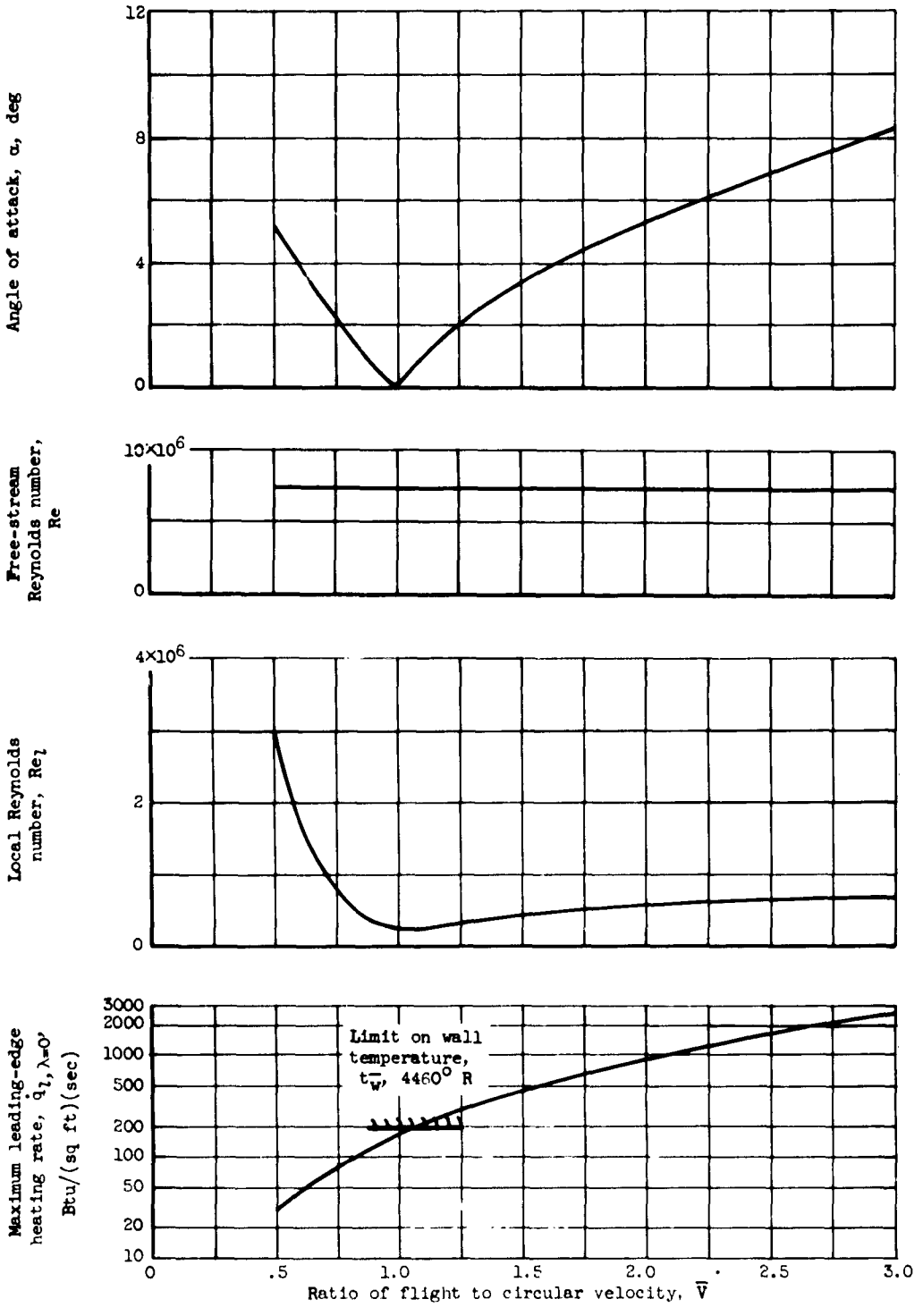

Figure 8. - Concluded. Constant free-stream Reynolds number flight path for Earth atmosphere. Free-stream Reynolds number, 7.3×10^6; initial net acceleration, 10 g's; initial velocity ratio, 2.0; maximum lift-drag ratio, 1.0; entry vehicle gross weight, 10,000 pounds; average entry vehicle density, 20 pounds per cubic foot; geometric leading-edge sweep angle, 60°.

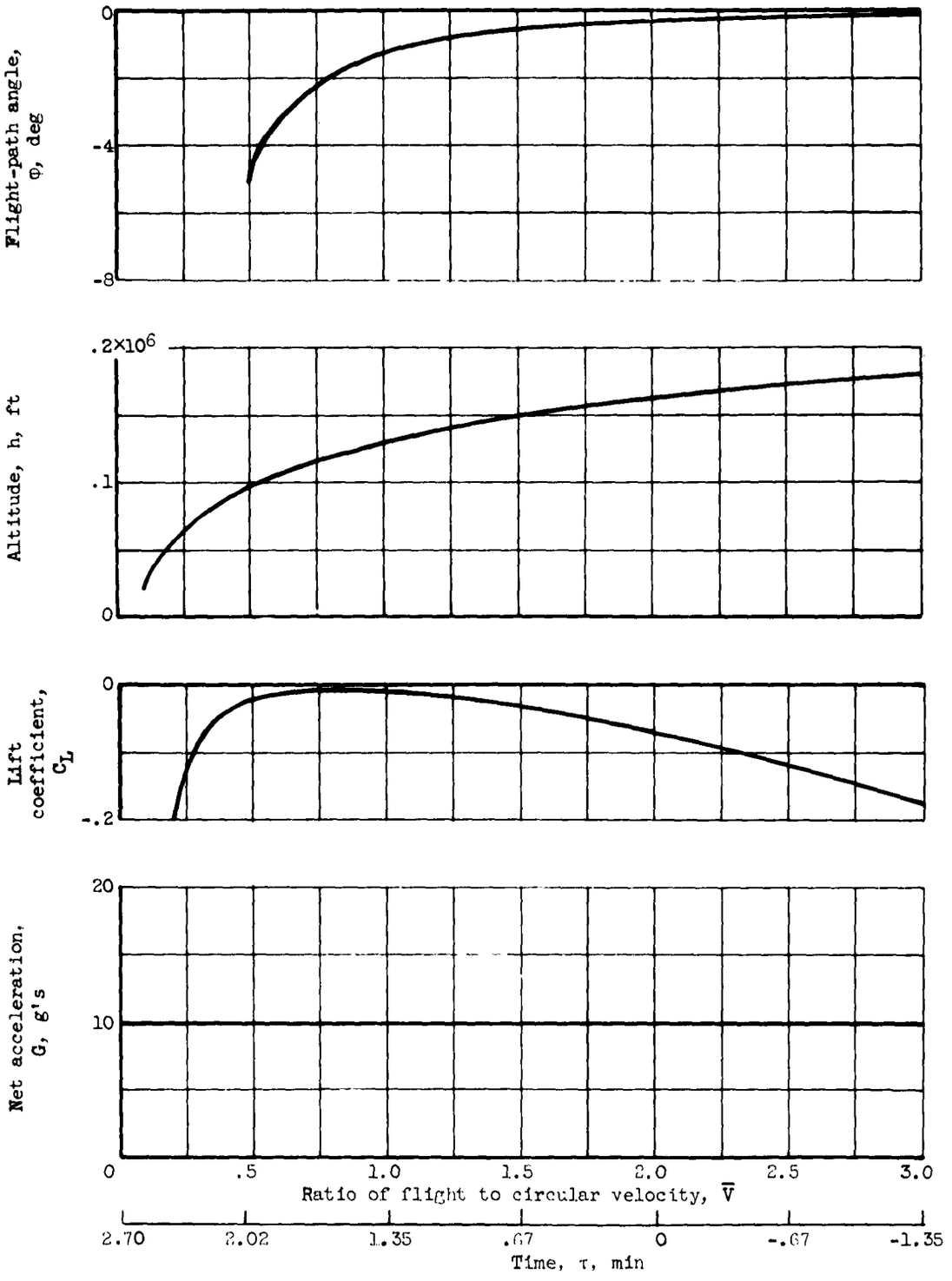

Figure 9. - Constant-net-acceleration flight path for Earth atmosphere. Net acceleration, 10 g's; initial velocity ratio, 2.0; maximum lift-drag ratio, 1.0; entry vehicle gross weight, 10,000 pounds; average entry vehicle density, 20 pounds per cubic foot; geometric leading-edge sweep angle, 60°.

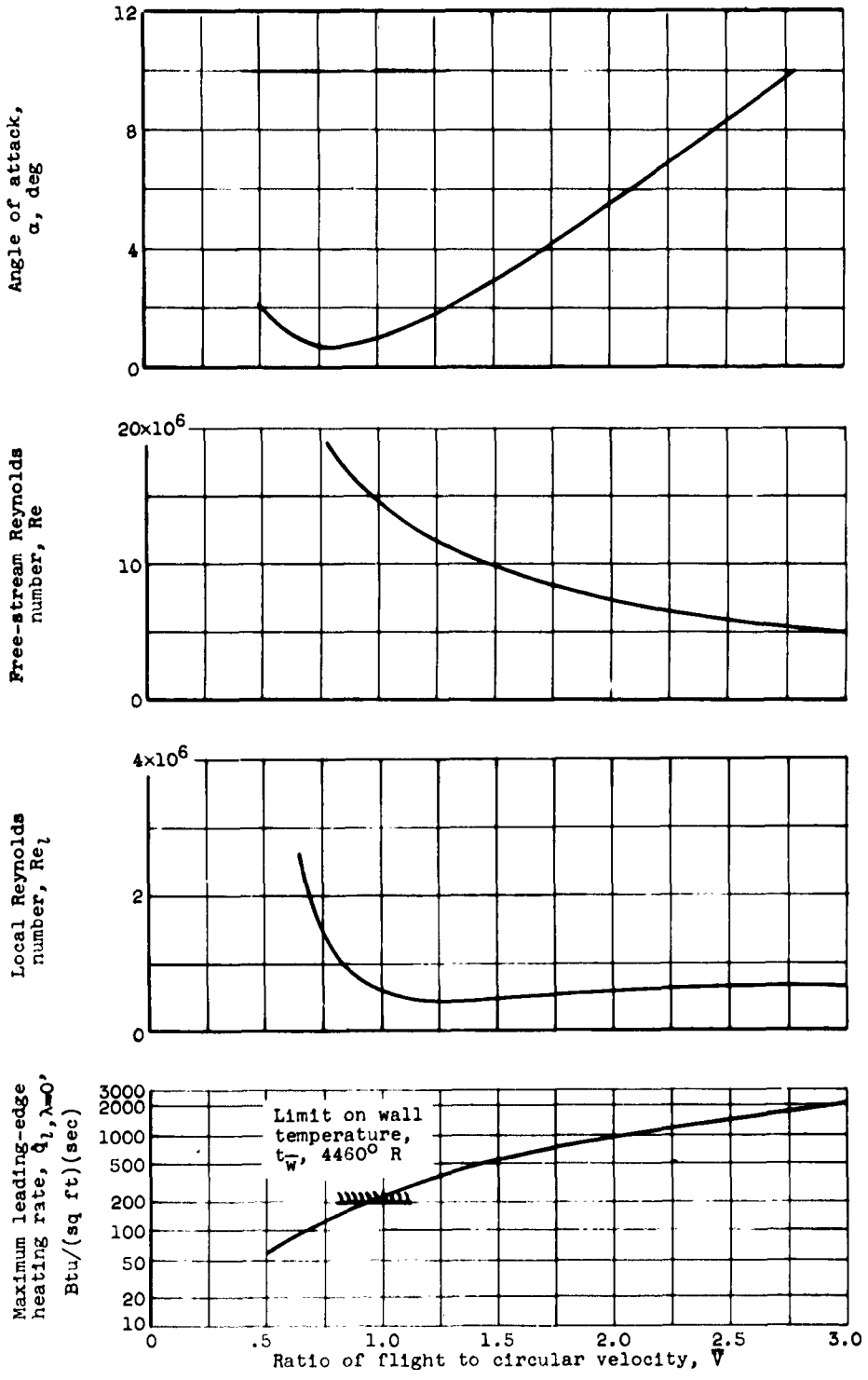

Figure 9. - Concluded. Constant-net-acceleration flight path for Earth atmosphere. Net acceleration, 10 g's; initial velocity ratio, 2.0; maximum lift-drag ratio, 1.0; entry vehicle gross weight, 10,000 pounds; average entry vehicle density, 20 pounds per cubic foot; geometric leading-edge sweep angle, 60°.

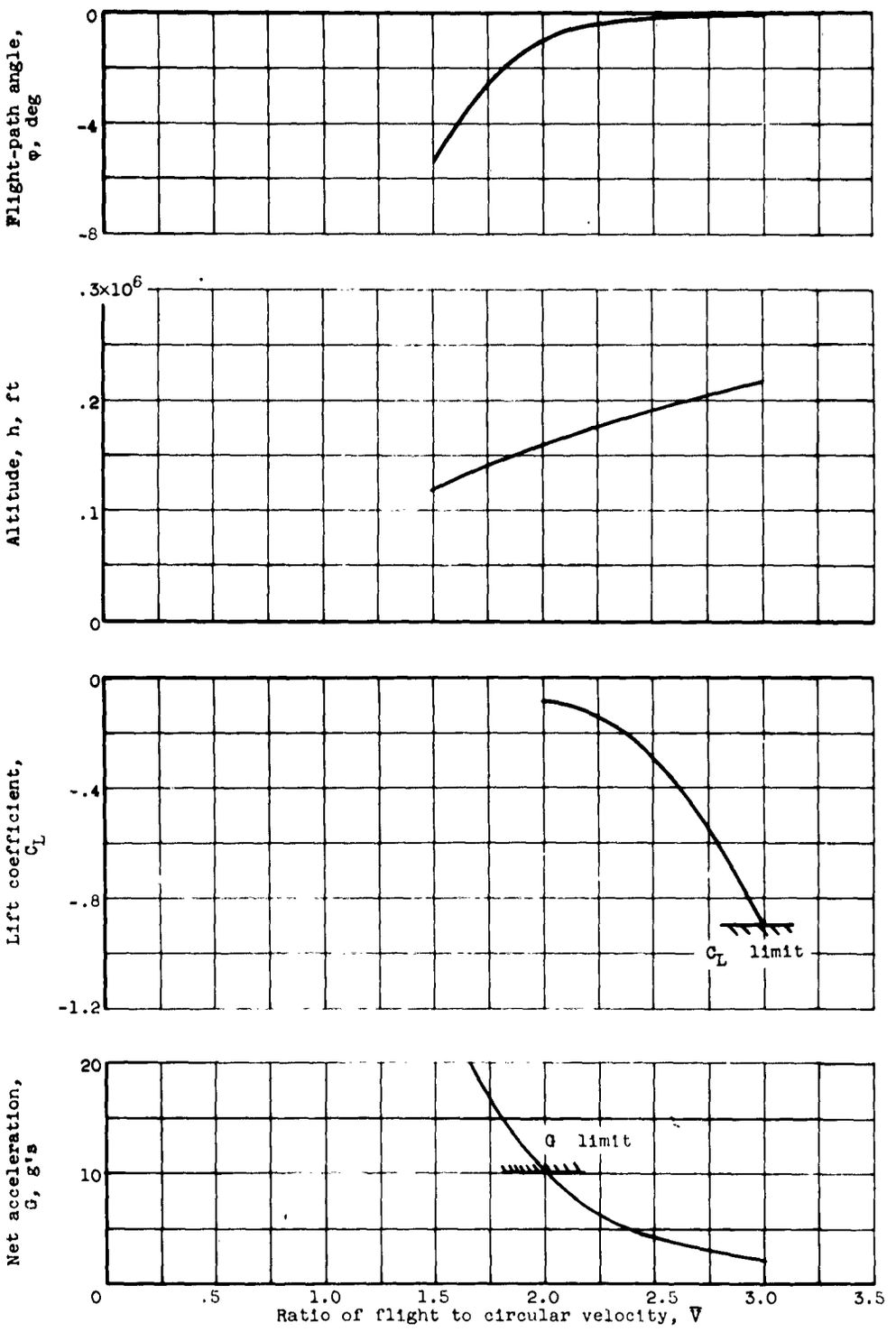

Figure 10. - Constant-heating-rate flight path for Earth atmosphere. Maximum leading-edge heating rate, 900 Btu per square foot per second; initial net acceleration, 10 g's; initial velocity ratio, 2.0; maximum lift-drag ratio, 1.0; entry vehicle gross weight, 10,000 pounds; average entry vehicle density, 20 pounds per cubic foot; geometric leading-edge sweep angle, 60°.

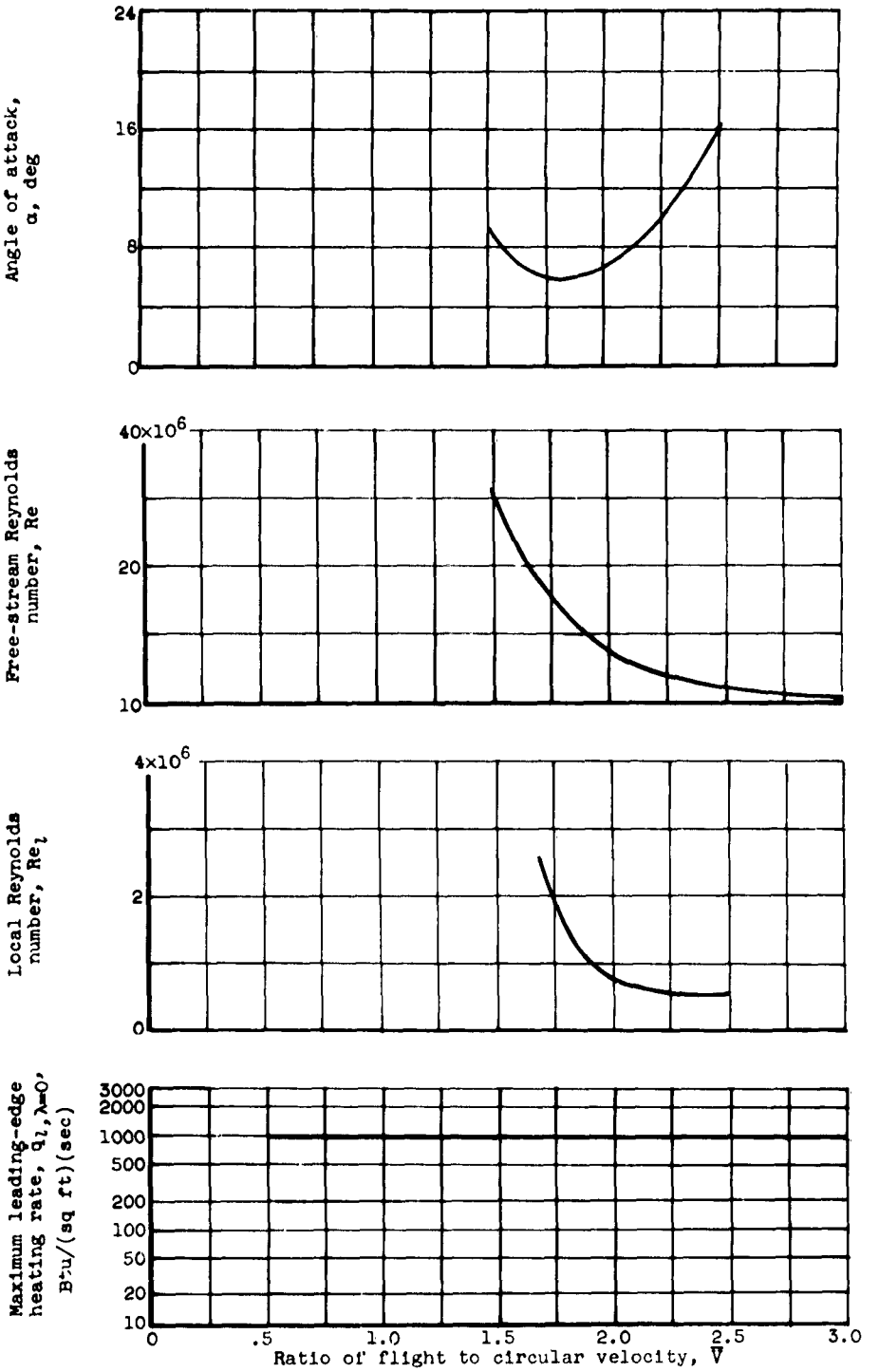

Figure 10. - Concluded. Constant-heating-rate flight path for Earth atmosphere. Maximum leading-edge heating rate, 900 Btu per square foot per second; initial net acceleration, 10 g's; initial velocity ratio, 2.0; maximum lift-drag ratio, 1.0; entry vehicle gross weight, 10,000 pounds; average entry vehicle density, 20 pounds per cubic foot; geometric leading-edge sweep angle, 60°.

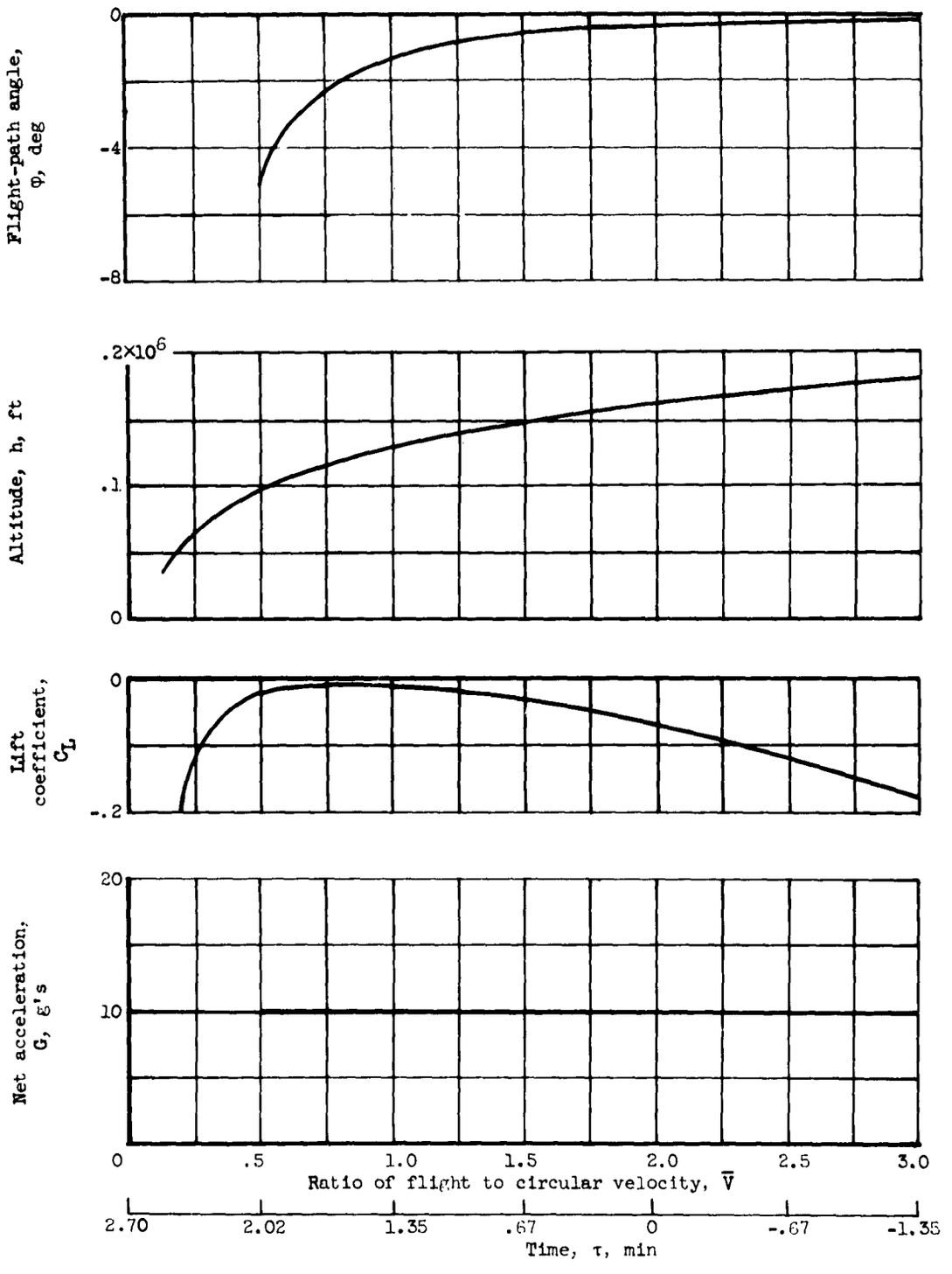

Figure 11. - Modulated roll flight path for Earth atmosphere. Initial roll angle, 0; initial net acceleration, 10 g's; initial velocity ratio, 2.0; maximum lift-drag ratio, 1.0; entry vehicle gross weight, 10,000 pounds; average entry vehicle density, 20 pounds per cubic foot; geometric leading-edge sweep angle, 60°.

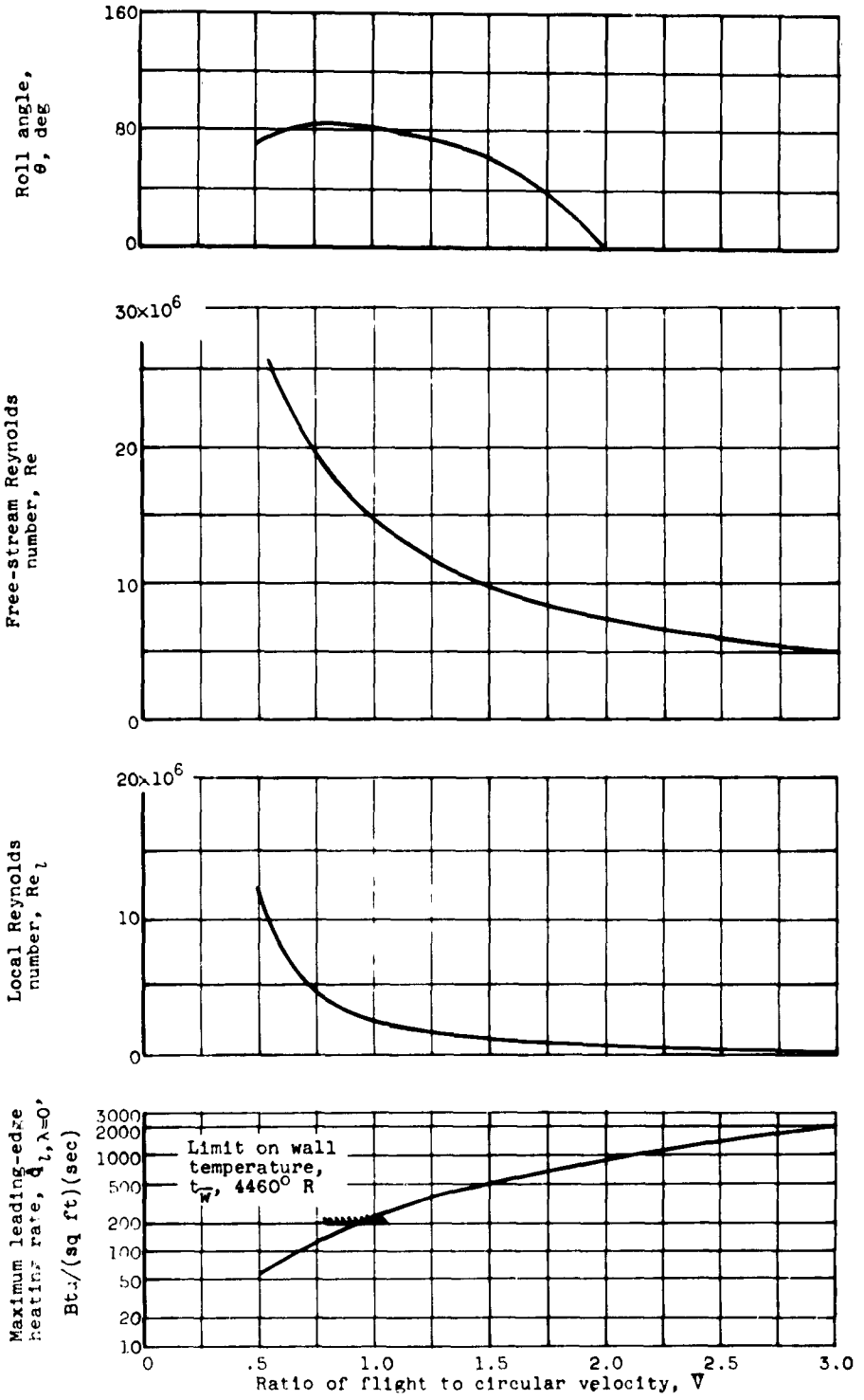

Figure 11. - Concluded. Modulated roll flight path for Earth atmosphere. Initial roll angle, 0; initial net acceleration, 10 g's; initial velocity ratio, 2.0; maximum lift-drag ratio, 1.0; entry vehicle gross weight, 10,000 pounds; average entry vehicle density, 20 pounds per cubic foot; geometric leading-edge sweep angle, 60°.

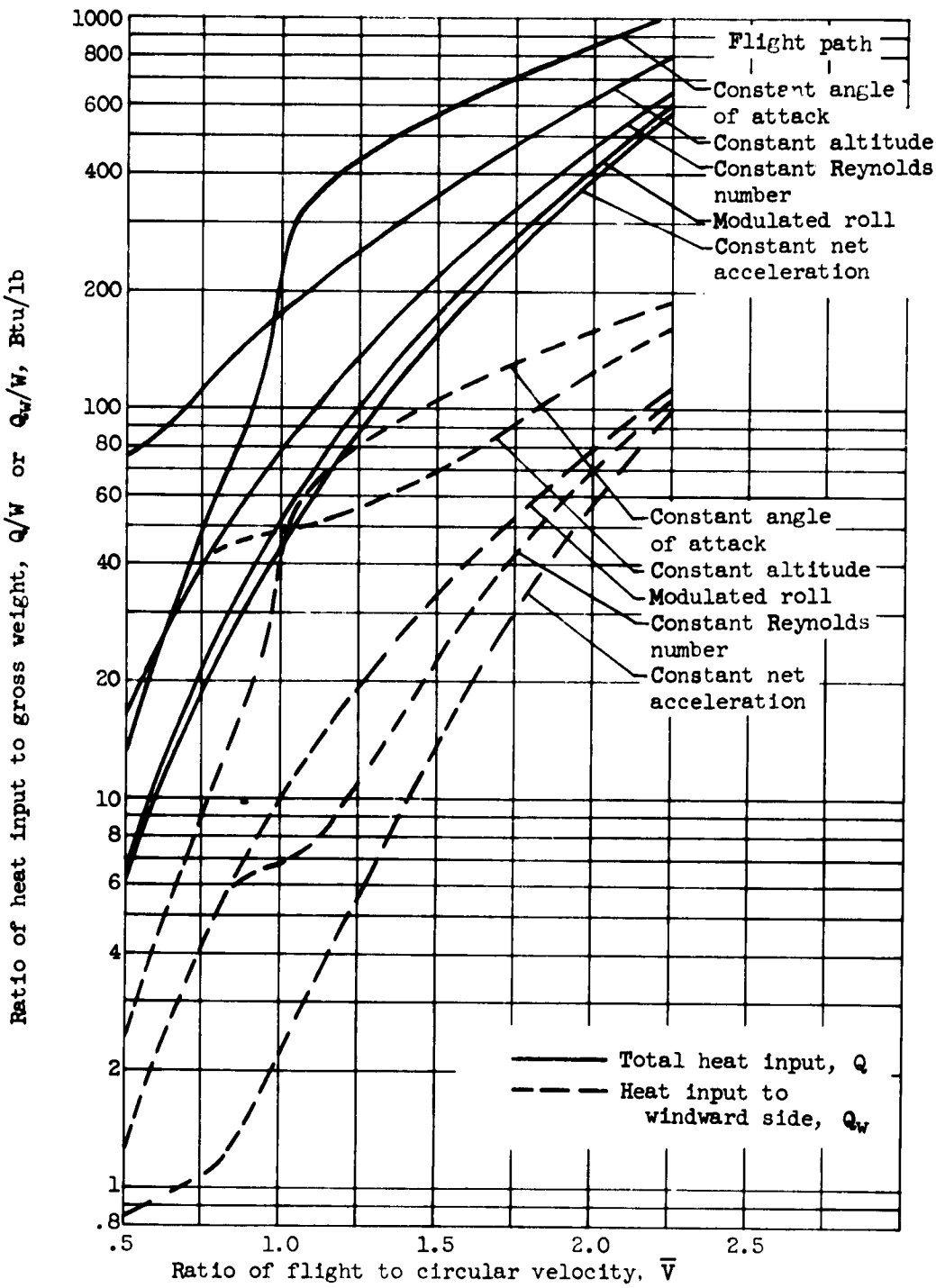

Figure 12. - Total heat input at Earth for flight paths with net acceleration of 10 g's at velocity ratio of 2.0. Maximum lift-drag ratio, 1.0; entry vehicle gross weight, 10,000 pounds; average entry vehicle density, 20 pounds per cubic foot; geometric leading-edge sweep angle, 60°.

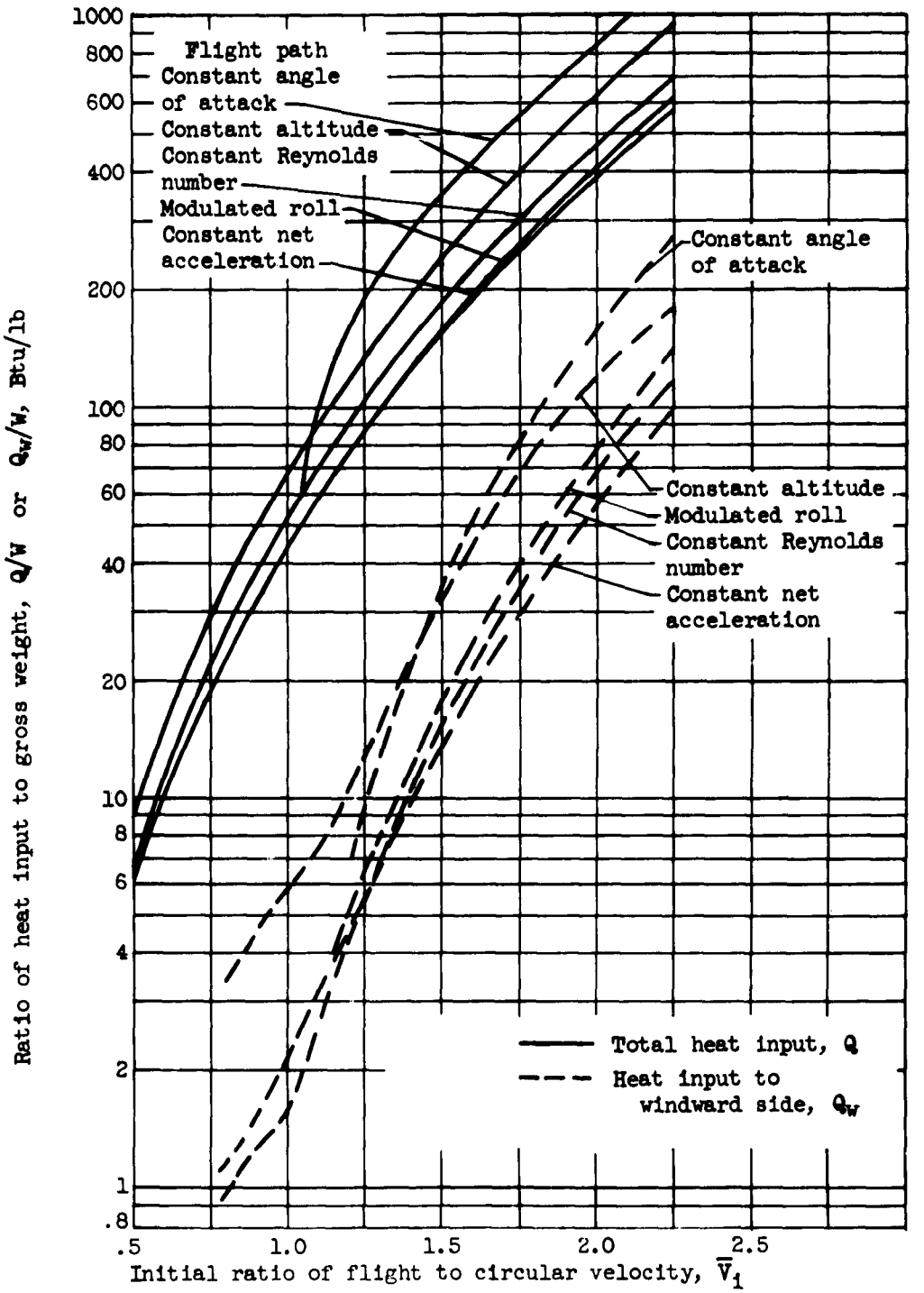

Figure 13. - Total heat input at Earth for flight path with initial net acceleration of 10 g's. Maximum lift-drag ratio, 1.0; entry vehicle gross weight, 10,000 pounds; average entry vehicle density, 20 pounds per cubic foot; geometric leading-edge sweep angle, 60°.

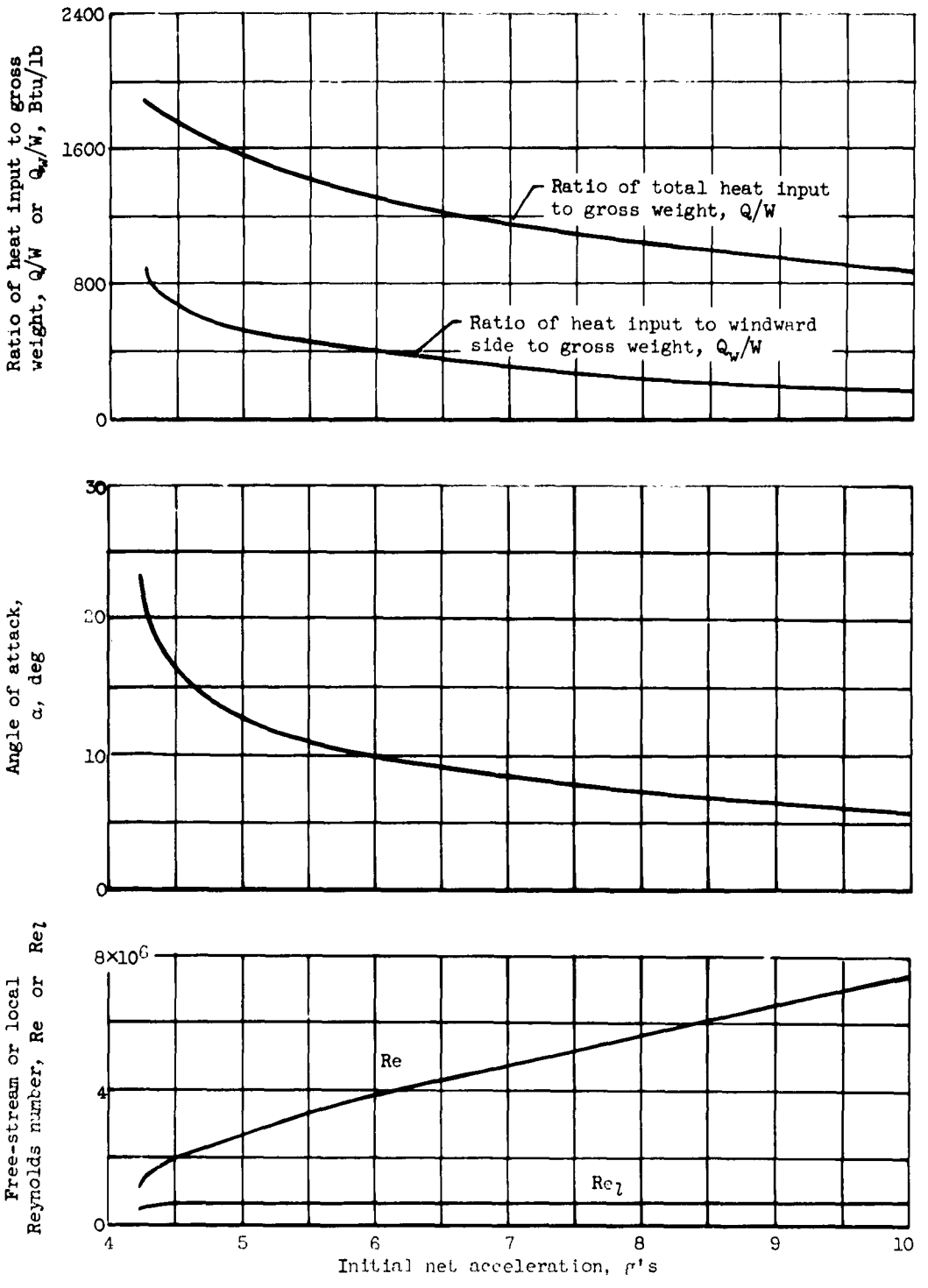

Figure 14. - Total heat input for constant-angle-of-attack flight path for Earth atmosphere. Initial velocity ratio, 3.0; maximum lift-drag ratio, 1.0; entry vehicle gross weight, 10,000 pounds; average entry vehicle density, 20 pounds per cubic foot; geometric leading-edge sweep angle, 60°.

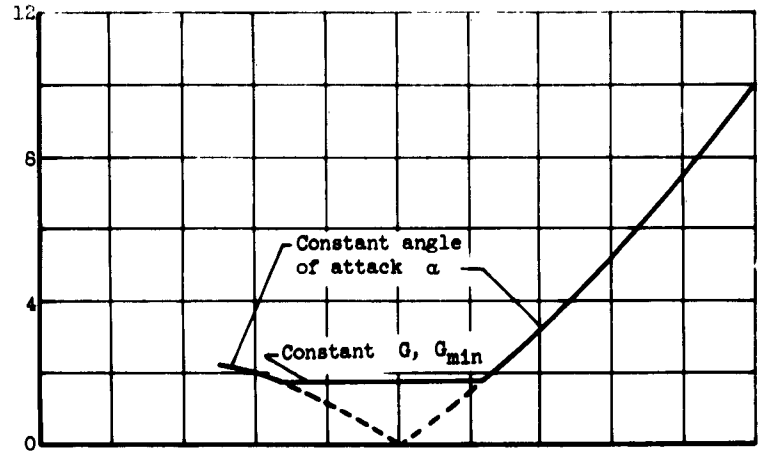

(a) Modified constant-angle-of-attack flight path.

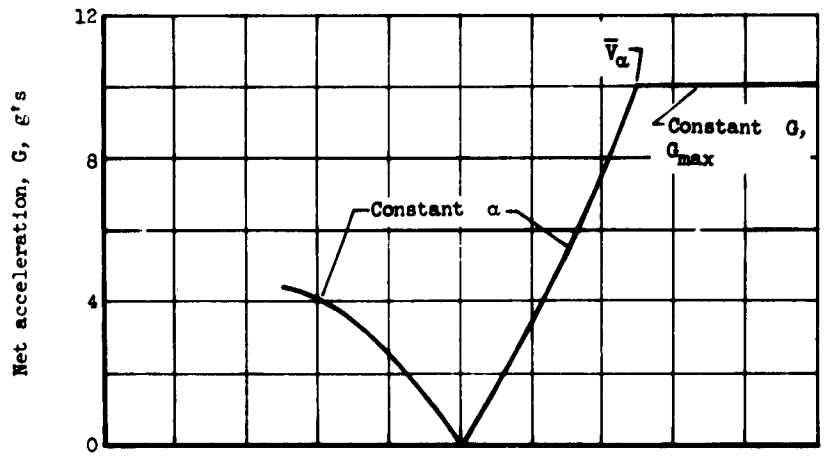

(b) Modified constant-net-acceleration-flight path.

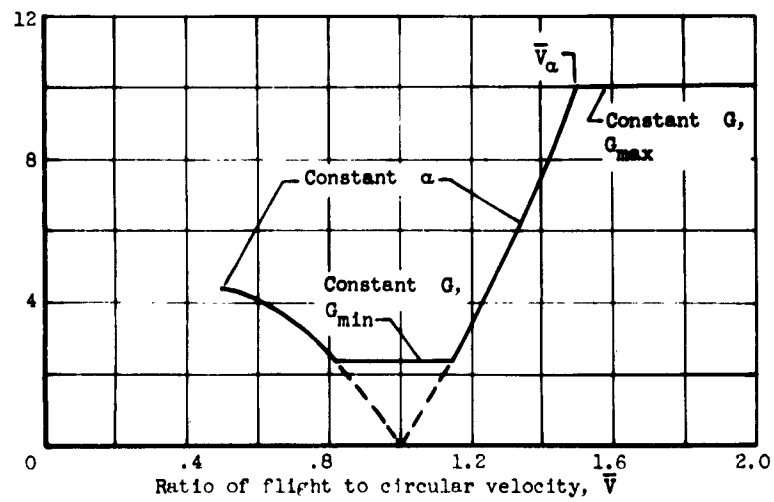

(c) Composite flight path.

Figure 15. - Flight paths with control of landing location.

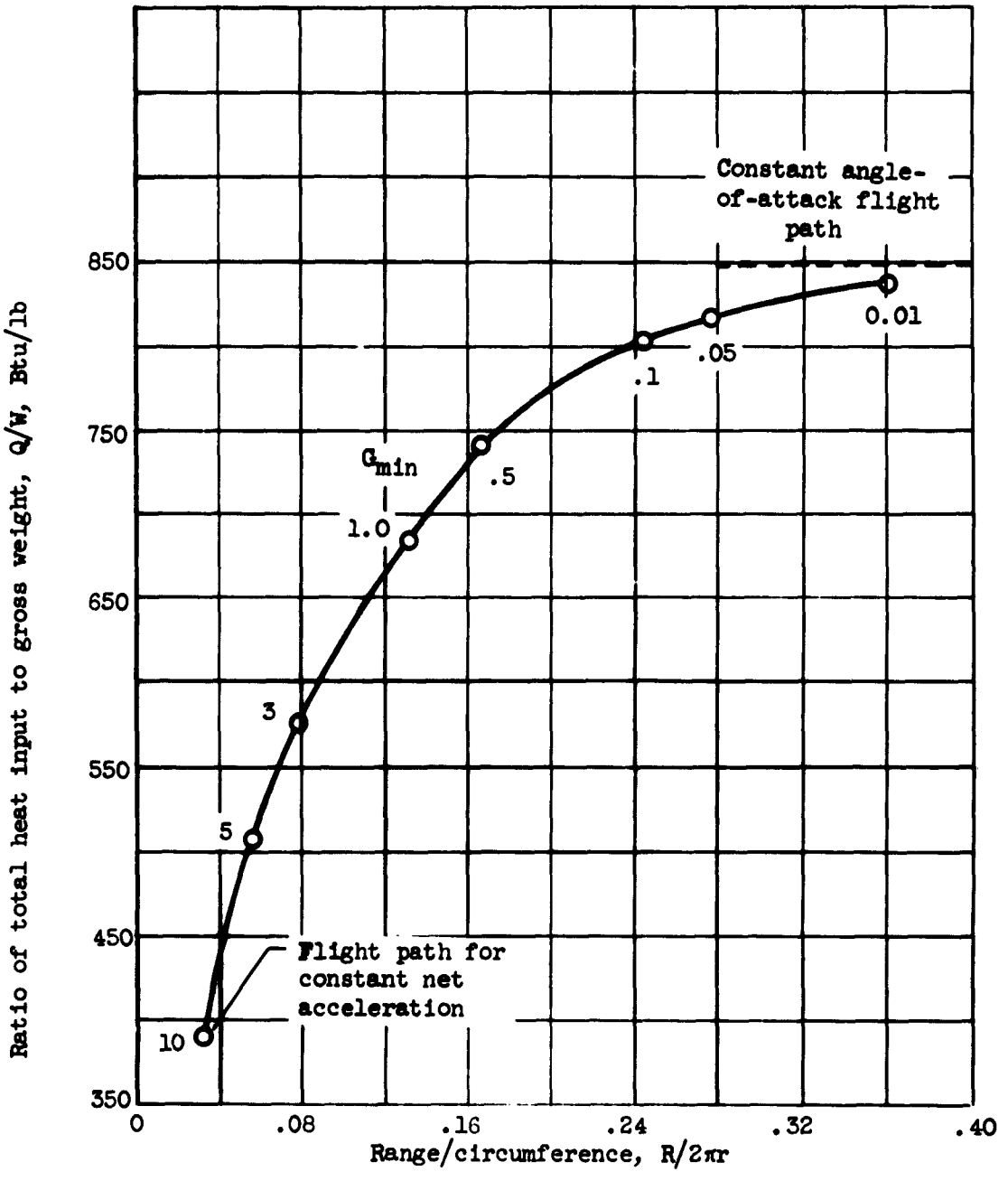

Figure 16. - Total heat input at Earth for modified constant-angle-of-attack flight path (fig. 15(a)). Initial net acceleration, 10 g's; initial velocity ratio, 2.0; maximum lift-drag ratio, 1.0; entry vehicle gross weight, 10,000 pounds; average entry vehicle density, 20; geometric leading-edge sweep angle, 60°.

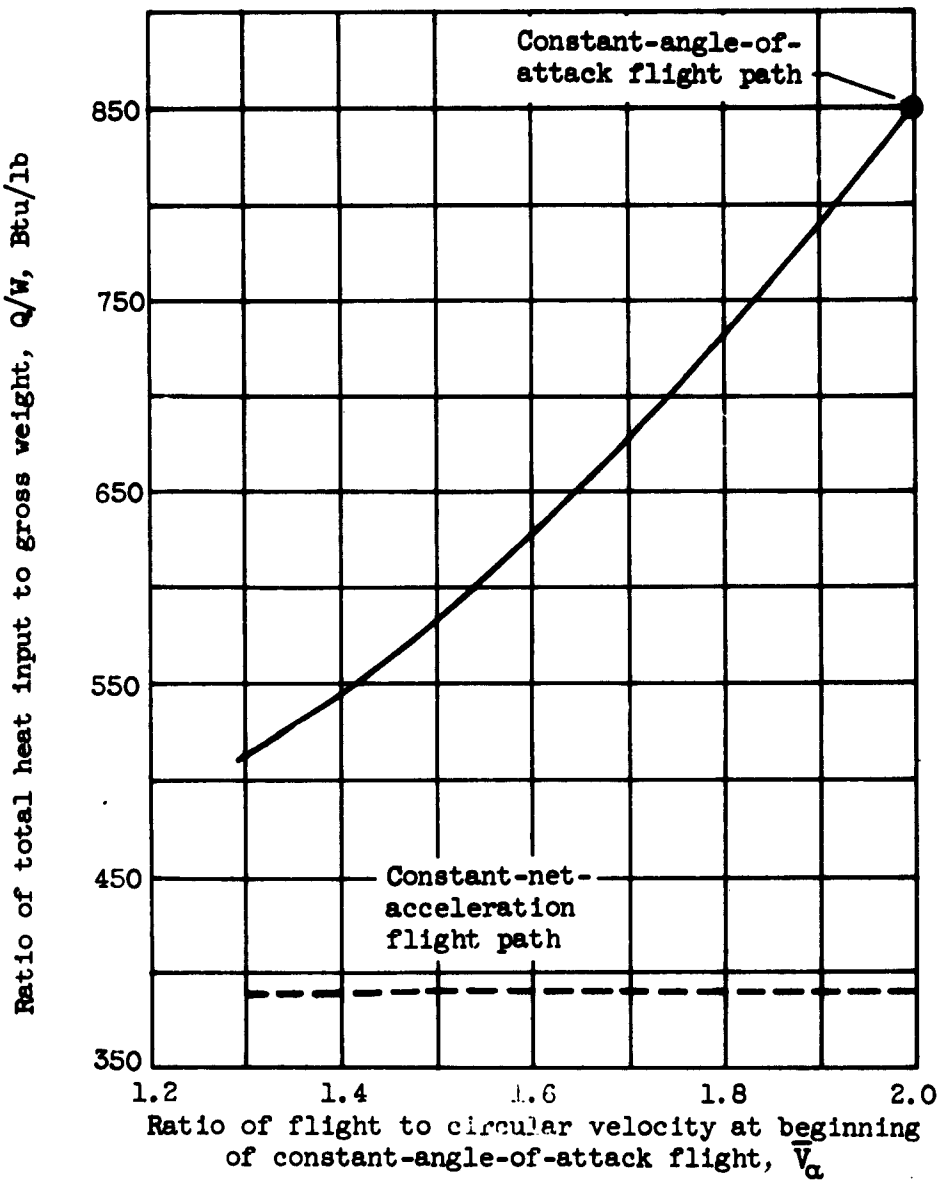

Figure 17. - Total heat input at Earth for modified constant-net-acceleration flight path (fig. 15(b)) and infinite range. Initial net acceleration, 10 g's; initial velocity ratio, 2.0; maximum lift-drag ratio, 1.0; entry vehicle gross weight, 10,000 pounds; average entry vehicle density, 20; geometric leading-edge sweep angle, 60°.

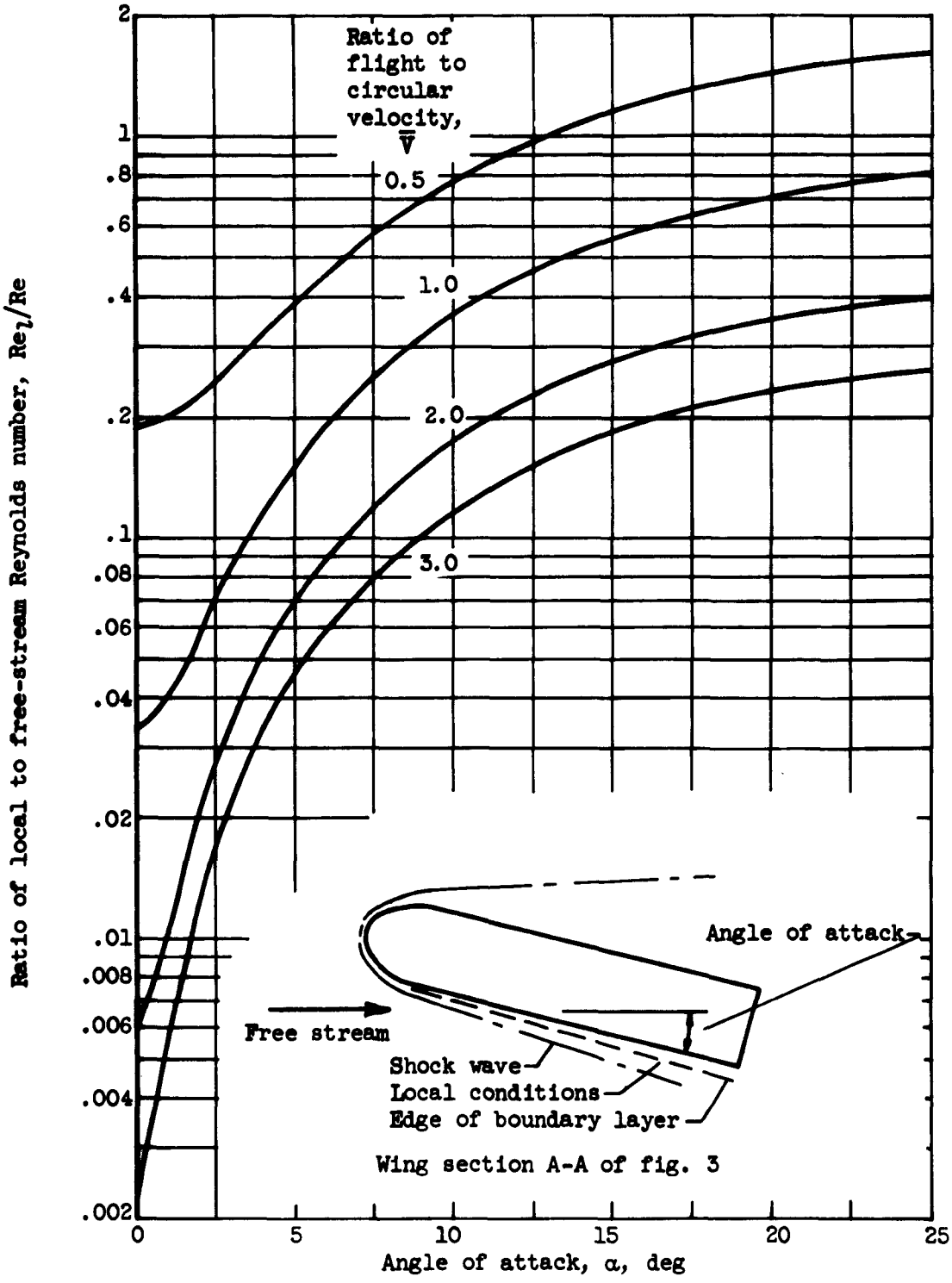

Figure 18. - Ratio of local to free-stream Reynolds number for swept blunt leading edge for Earth atmosphere. Leading-edge sweep angle, 60; specific-heat ratio, 1.2.

NASA TN D-1091
National Aeronautics and Space Administration.
FLIGHT-PATH CHARACTERISTICS FOR DECELERATING FROM SUPERCIRCULAR SPEED. Roger W. Luidens. December 1961. 92p. OTS price, $2.25. (NASA TECHNICAL NOTE D-1091)

Characteristics of six types of flight paths for the deceleration from circular and supercircular speeds are developed in closed form. The heating rate, heat input per square foot obtained from an integration over the flight path, the total heat input obtained from an integration over the vehicle, and the flight-path histories in terms of path angle, altitude, lift coefficient, net acceleration, angle of attack, and Reynolds number are discussed as a function of type of flight plan, initial net acceleration, and initial velocity. A flight plan with essentially a "point landing" capability is suggested.

Copies obtainable from NASA, Washington

I. Luidens, Roger W.
II. NASA TN D-1091

(Initial NASA distribution: 5, Atmospheric entry.)

NASA

NASA TN D-1091
National Aeronautics and Space Administration.
FLIGHT-PATH CHARACTERISTICS FOR DECELERATING FROM SUPERCIRCULAR SPEED. Roger W. Luidens. December 1961. 92p. OTS price, $2.25. (NASA TECHNICAL NOTE D-1091)

Characteristics of six types of flight paths for the deceleration from circular and supercircular speeds are developed in closed form. The heating rate, heat input per square foot obtained from an integration over the flight path, the total heat input obtained from an integration over the vehicle, and the flight-path histories in terms of path angle, altitude, lift coefficient, net acceleration, angle of attack, and Reynolds number are discussed as a function of type of flight plan, initial net acceleration, and initial velocity. A flight plan with essentially a "point landing" capability is suggested.

Copies obtainable from NASA, Washington

I. Luidens, Roger W.
II. NASA TN D-1091

(Initial NASA distribution: 5, Atmospheric entry.)

NASA

NASA TN D-1091
National Aeronautics and Space Administration.
FLIGHT-PATH CHARACTERISTICS FOR DECELERATING FROM SUPERCIRCULAR SPEED. Roger W. Luidens. December 1961. 92p. OTS price, $2.25. (NASA TECHNICAL NOTE D-1091)

Characteristics of six types of flight paths for the deceleration from circular and supercircular speeds are developed in closed form. The heating rate, heat input per square foot obtained from an integration over the flight path, the total heat input obtained from an integration over the vehicle, and the flight-path histories in terms of path angle, altitude, lift coefficient, net acceleration, angle of attack, and Reynolds number are discussed as a function of type of flight plan, initial net acceleration, and initial velocity. A flight plan with essentially a "point landing" capability is suggested.

Copies obtainable from NASA, Washington

I. Luidens, Roger W.
II. NASA TN D-1091

(Initial NASA distribution: 5, Atmospheric entry.)

NASA

NASA TN D-1091
National Aeronautics and Space Administration.
FLIGHT-PATH CHARACTERISTICS FOR DECELERATING FROM SUPERCIRCULAR SPEED. Roger W. Luidens. December 1961. 92p. OTS price, $2.25. (NASA TECHNICAL NOTE D-1091)

Characteristics of six types of flight paths for the deceleration from circular and supercircular speeds are developed in closed form. The heating rate, heat input per square foot obtained from an integration over the flight path, the total heat input obtained from an integration over the vehicle, and the flight-path histories in terms of path angle, altitude, lift coefficient, net acceleration, angle of attack, and Reynolds number are discussed as a function of type of flight plan, initial net acceleration, and initial velocity. A flight plan with essentially a "point landing" capability is suggested.

Copies obtainable from NASA, Washington

I. Luidens, Roger W.
II. NASA TN D-1091

(Initial NASA distribution: 5, Atmospheric entry.)

NASA